STUDIA
UNIVERSITATIS BABEȘ-BOLYAI

PHYSICA

2

1979

CLUJ-NAPOCA

ANUL XXIV 1979

STUDIA

UNIVERSITATIS BABEŞ-BOLYAI

PHYSICA

2

Redacţia: 3400 CLUJ-NAPOCA, str. M. Kogălniceanu, 1 ● Telefon 1 34 50

SUMAR — CONTENTS — SOMMAIRE — INHALT

Note — Notes — Notizen

Recenzii — Books — Livres parus — Bucherbesprehung

STUDIA UNIV BABEŞ-BOLYAI, PHYSICA, XXIV, 2, 1979

CONSECUTIVE METASTABLE DISSOCIATION OF TRIATOMIC IONS. THE SH_2^+ MOLECULAR ION

I. MASTAN, A. PAMULA*, V. MERCEA

1. **Introduction.** The process of consecutive metastable dissociation in two steps has been observed for the first time in 1966 by K. R. Jennings [1] in the mass spectra of some heavy molecular ions. The finding of these processes was performed when the double-focussing mass spectrometry has been used for the study of metastable dissociations. In toluene mass spectrum the sequence $C_7H_7^+ \rightarrow C_5H_5^+ \rightarrow C_3H_3^+$ was observed. Other consecutive metastable transitions observed by this method are the sequence $C_6H_5F^+ \rightarrow C_4H_3F^+ \rightarrow C_4H_2^+$ in the mass spectrum of fluorobenzene and the sequence $C_3H_7^+ \rightarrow C_3H_5^+ \rightarrow C_3H_3^+$ in the mass spectrum of n-butane. It was estimated that all the three transitions are spontaneous processes and that they take place with a rate constant lies in the range $10^5 - 10^6\ s^{-1}$. In the next years have been published a few papers [2—4] which prove the consecutive metastable dissociation of heavy molecular ions. Quantitative computations concerning to rate constants of spontaneous dissociations are given for the first time in the paper [4]. The results obtained in this last paper have been discussed in terms of QET of mass spectra [4—9]. A new improved method for the investigation of consecutive metastable dissociations was reported by J. M. Miller et al. [10]. In the main, the improvement consists in the following. Between collector and magnetic analyzer of a doublefocussing Nier-Johnson geometry mass spectrometer a supplementary electrostatic deflector was introduced. It was underlined the fact that with the help of this improved experimental technique might be investigated consecutive metastable dissociations in three steps. However, the apparatus testing has only been made on consecutive metastable dissociations in two steps.

So far consecutive metastable dissociations of triatomic ions were not reported. In the present paper we shall report some results concerning to consecutive metastable dissociation of the SH_2^+ triatomic ion.

2. **Apparatus and method.** *Apparatus.* The investigation of consecutive metastable dissociations requires employment of double-focussing or tandem mass spectrometers. We have used two magnetic mass spectrometers in tandem. The schematic representation of the apparatus is given in Fig. 1. The two magnetic analyzers are of sector type having the angle $\Phi = 90°$. They have a symmetrical arrangement. The distances between the object and image slits of the ion source and magnetic field limits of the first analyzer are both equal to 10 cm. The geometry of the second magnetic analyzer is identical with that of the first one (see Fig. 1). On the trajectory portion $0 \rightarrow 1$ the ions are accelerated up to their maximum energy. Generally, on the trajectory portion $1 \rightarrow 8$ the ions will fly with a constant velocity corresponding to maximum energy

* Institute of Isotopic and Molecular Technology, Cluj-Napoca.

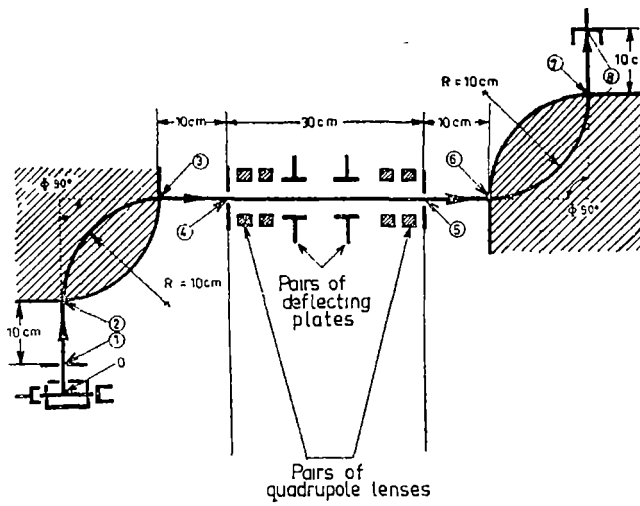

Fig. 1.

gained at point 1 of the trajectory. The trajectory portions 1→2, 3→6, and 7→8 are respectively the first, second and third field-free regions. For the investigation of simple and consecutive metastable dissociations are of interest the first and the second field — free regions. In the second field-free region the ions may be decelerated in the neighbourhood of point 4 of the trajectory. The retarding voltage V_r may be continuously changed from zero to 1500 volts. In the neighbourhood of point 5 of the trajectory the ions are reaccelerated up to the maximum energy corresponding to the point 1 of the trajectory, i.e. 2 000 eV. Our results which will be presented here were obtained without retarding on the trajectory portion 4→5. The others parameters of interest in the present paper are given on Fig. 1.

Apparent masses. Let us consider the following consecutive metastable dissociation

$$m_0^+ \rightarrow m^+ \rightarrow m_1^+ \tag{1}$$

If the metastable dissociation (1) takes place on either first and second field-free regions, then the m^+ and m_1^+ fragment ions will be respectively recorded at the apparent masses m^2/m_0 and m_1^2/m_0. Concerning to the origin of the m_1^+ fragment ion it is impossible to distinguish between the process (1) and „short" transition $m_0^+ \rightarrow m_1^+$. This is a serious disadvantage of the method.

Let us now assume that the first analyzer is transparent for the apparent mass m^2/m_0. This means that the second field-free region will be crossed only by the m^+ fragment ions which were born from the m_0^+ ions on the first field-free region, i.e. the first step of the dissociation (1). Now, if the second step of the transition (1) takes place on the second field-free region, then the m_1^+ fragment ion will be collected at the apparent mass m_1^2/m_0. Thus the following conclusion can be drawn. If the first analyzer is transparent for the apparent mass m^2/m_0 and at collector are recorded metastable peaks at the apparent

masses m^2/m_0 and m_1^2/m_0, it means that the consecutive metastable dissociation (1) takes really place.

Method. Consecutive metastable dissociation (1) can be written under the following form

$$m_0^+ \begin{array}{c} \xrightarrow{\lambda_1} m^+ \\ \xrightarrow{\sigma_1} m^+ \end{array} \longrightarrow (m^+) \begin{array}{c} \xrightarrow{\lambda_2} m_1^+ \\ \xrightarrow{\sigma_2} m_1^+ \end{array} \longrightarrow (m_1^+) \tag{2}$$

Here by λ_1 and λ_2 are denoted rate constants of the spontaneous dissociations, while σ_1 and σ_2 characterize collision- induced dissociations and represent the cross-sections of the process. In order to avoid any confusions the ionic currents corresponding to m_0^+, m^+ and m_1^+ will be respectively doneted by I, I', and I''. In this paper only those mathematical reasons will be given that are necessary for the understanding of experimental results. A detailed description of the method is elsewhere given [11—14].

Let us assume that the first analyzer is transparent for the m_0^+ ions. If the consecutive metastable dissociation (2) takes really place, then by I'_{8s} and I_8 we will respectively denote the ionic currents m^+ and m_0^+ which are recorded at mass spectrometer collector. Starting from I'_{8s} and I_8 it is defined the function $R[\lambda_1, \lambda_2, p(N)] = I'_{8s}/I_8$ for which one can obtain

$$R[\lambda_1, \lambda_2\, p(N)] = \frac{(\lambda_1 + \sigma_1 N k_0) \cdot \exp\{(\lambda_1 + \sigma_1 N k_0)(t_8 - t_3)\}}{[(\lambda_2 + \sigma_2 N k_0) - (\lambda_1 + \sigma_1 N k_0)]} \cdot$$
$$\cdot [\exp\{-(\lambda_1 + \sigma_1 N k_0)(t_6 - t_3)\} \cdot \exp\{-(\lambda_2 + \sigma_2 N k_0)(t_8 - t_6)\} - \tag{3}$$
$$- \exp\{-(\lambda_2 + \sigma_2 N k_0)(t_8 - t_3)\}]$$

Let us now consider that the first analyzer is transparent for the apparent mass m^2/m_0. Then, the trajectory portion 3→6 will be crossed only by the m^+ ions which have been born from the m_0^+ ions on the trajectory portion 1→2. Now, if the second analyzer is transparent for the apparent mass m_1^2/m_0, then at collector will be recorded only the m_1^+ ions which are born from the m^+ ions on the trajectory portion 3→6. On this trajectory portion the ionic current m_1^+ is described by the differential equation

$$\frac{dI''_{t \geq t_3}}{dt} = (\lambda_2 + \sigma_2 N k_0) \cdot I'_{t \geq t_3} \tag{4}$$

which is integrated taking in account that $I''_{6f} = I''_{8f}$ and one obtains

$$I''_{8f} = \frac{I_0 \cdot (\lambda_1 + \sigma_1 N k_0) \cdot \exp\{-(\lambda_1 + \sigma_1 N k_{0m} \cdot t_1\}}{[(\lambda_2 + \sigma_2 N k_0) - (\lambda_1 + \sigma_1 N k_0)]} \cdot$$
$$\cdot [\exp\{-(\lambda_1 + \sigma_1 N k_0)(t_2 - t_1)\} - \exp\{-(\lambda_2 + \sigma_2 N k_0)(t_2 - t_1)\}] \cdot$$
$$\cdot [\exp\{-(\lambda_2 + \sigma_2 N k_0)(t_3 - t_2)\} - \exp\{-(\lambda_2 + \sigma_2 N k_0)(t_6 - t_2)\}] \tag{5}$$

On the other hand, starting from I''_{8f} and I_8 one can define the function $M[\lambda_1, \lambda_2, p(N)] = I''_{8f}/I_8$ for which is finally obtained

$$M[\lambda_1, \lambda_2, p(N)] = \frac{(\lambda_1 + \sigma_1 N k_0)}{[(\lambda_2 + \sigma_2 N k_0) - (\lambda_1 + \sigma_1 N k_0)]} \cdot \exp\{(\lambda_1 + \sigma_1 N k_0)(t_8 - t_1)\} \cdot$$
$$\cdot [\exp\{-(\lambda_1 + \sigma_1 N k_0)(t_2 - t_1)\} - \exp\{-(\lambda_2 + \sigma_2 N k_0)(t_2 - t_1)\}] \cdot \tag{6}$$
$$\cdot [\exp\{-(\lambda_2 + \sigma_2 N k_0)(t_3 - t_2)\} - \exp\{-(\lambda_2 + \sigma_2 N k_0)(t_6 - t_2)\}]$$

The rate constants λ_1 and λ_2 of spontaneous dissociations can be obtained if is solved the following system of two transcendental equations

$$R[\lambda_1, \lambda_2, 0] = \frac{\lambda_1 \cdot \exp\{\lambda_1(t_8 - t_3)\}}{(\lambda_2 - \lambda_1)} \cdot$$
$$\cdot [\exp\{-\lambda_1(t_6 - t_3)\} \cdot \exp\{-\lambda_2(t_8 - t_6)\} - \exp\{-\lambda_2(t_8 - t_3)\}] \tag{7}$$
$$M[\lambda_1, \lambda_2, 0] = \frac{\lambda_1 \cdot \exp\{\lambda_1(t_8 - t_1)\}}{(\lambda_2 - \lambda_1)} \cdot$$
$$\cdot [\exp\{-\lambda_1(t_2 - t_1)\} - \exp\{-\lambda_2(t_2 - t_1)\}] \cdot [\exp\{-\lambda_2(t_3 - t_2)\} - \exp\{-\lambda_2(t_6 - t_2)\}]$$

Here by $R[\lambda_1, \lambda_2, 0]$ and $M[\lambda_1, \lambda_2, 0]$ we have denoted the values of functions $R[\lambda_1, \lambda_2, p(N)]$ and $M[\lambda_1, \lambda_2, p(N)]$ for pressure $p(N) \to 0$. On the basis of functions (3) and (6) one can obtain a second system of two transcendental equations. This is the system (3), (6) whose solutions are just the cross-sections σ_1 and σ_2 characterizing collision-induced dissociations. But in order to solve the system (3), (6) we must know numerical values of rate constants λ_1 and λ_2. If in the system of transcendental equations (7) the substitution

$$\lambda_2 = \lambda_1 + \alpha \tag{8}$$

is introduced, then to solve the system is reduced to the finding of that α value which is a solution for the next transcendental equation

$$M[\lambda_1, \lambda_2, 0] = \frac{R[\lambda_1, \lambda_2, 0]}{[\exp\{-\alpha(t_8 - t_6)\}\{-\exp\{-\alpha(t_8 - t_3)\}]} \cdot$$
$$\cdot \exp\left\{\frac{\alpha \cdot R[\lambda_1, \lambda_2, 0]}{[\exp\{-\alpha(t_8 - t_6)\} - \exp\{-\alpha(t_8 - t_3)\}]} \cdot (t_8 - t_3)\right\} \cdot [1 - \exp\{-\alpha(t_2 - t_1)\}] \cdot$$
$$\cdot \Big[\exp\{-\alpha(t_3 - t_2)\} - \exp\{-\alpha(t_6 - t_2)\} \cdot \tag{9}$$
$$\cdot \exp\left\{-\frac{\alpha \cdot R[\lambda_1, \lambda_2, 0]}{[\exp\{-\alpha(t_8 - t_6)\} - \exp\{-\alpha(t_8 - t_3)\}]} \cdot (t_6 - t_3)\right\}\Big]$$

Here it is understood that $R[\lambda_1, \lambda_2, 0] = R[\lambda_1, \lambda_1 + \alpha, 0]$ and also $M[\lambda_1, \lambda_2, 0] = M[\lambda_1, \lambda_1 + \alpha, 0]$. Now the λ_1 and λ_2 values which are solutions for

the system (7) can respectively be obtained introducing that α value which is solution for equation (9) in

$$\lambda_1 = \frac{\alpha \cdot R[\lambda_1, \lambda_2, 0]}{[\exp\{-\alpha(t_8 - t_6)\} - \exp\{-\alpha(t_8 - t_3)\}]} \tag{10}$$

and taking into account the substitution (8).

If in the system of transcendental equations (3), (6) besides the substitution (8) the following one

$$\sigma_2 = \sigma_1 + \beta \tag{11}$$

is also introduced, then to solve the system is reduced to the finding of that β value which is solution for the next transcendental equation

$$\begin{aligned} M[\lambda_1, \lambda_2, p(N)] = & \left[\frac{R[\lambda_1, \lambda_2, p(N)]}{[\exp\{-(\alpha + \beta Nk_0)(t_8 - t_6)\} - \exp\{-(\alpha + \beta Nk_0)(t_8 - t_3)\}]}\right] \cdot \\ & \cdot \exp\left\{\frac{(\alpha + \beta Nk_0) \cdot R[\lambda_1, \lambda_2, p(N)]}{[\exp\{-(\alpha + \beta Nk_0)(t_8 - t_6\} - \exp\{-(\alpha + \beta Nk_0)(t_8 - t_3)\}]} \cdot (t_8 - t_3)\right\} \cdot \\ & \cdot [1 - \exp\{-(\alpha + \beta Nk_0)(t_2 - t_1)\}] \cdot \Big[\exp\{-(\alpha + \beta Nk_0)(t_3 - t_2)\} - \\ & - \exp\{-(\alpha + \beta Nk_0)(t_6 - t_2)\} \cdot \\ & \cdot \exp\left\{-\frac{(\alpha + \beta Nk_0) \cdot R[\lambda_1, \lambda_2, p(N)]}{[\exp\{-(\alpha + \beta Nk_0)(t_8 - t_6)\} - \exp\{-(\alpha + \beta Nk_0)(t_8 - t_3)\}]} \cdot (t_5 - t_3)\right\}\Big] . \end{aligned} \tag{12}$$

Here it is also understood that $R[\lambda_1, \lambda_2, p(N)] \equiv R[\lambda_1, \lambda_1 + \alpha, p(N)]$ and $M[\lambda_1, \lambda_2, p(N)] \equiv M[\lambda_1, \lambda_1 + \alpha, p(N)]$ Those values of cross-sections σ_1 and σ_2 that are solutions for the system (3), (6) can respectively be computed introducing that β value which is solution for equation (12) in

$$\sigma_1 = \frac{1}{Nk_0} \cdot \left[\frac{(\alpha + \beta Nk_0) \cdot R[\lambda_1, \lambda_2, p(N)]}{[\exp\{-(\alpha + \beta Nk_0)(t_8 - t_6)\} - \exp\{-(\alpha + \beta Nk_0)(t_8 - t_3)\}]} - \lambda_1\right] \tag{13}$$

and taking in account the substitution (11).

3. Experimental results and discussions. *Experimental results.* The results concerning to the metastable dissociation of the SH_2^+ ion have been published for the first time by V. H. Diebeler et al. [15]. In the hydrogen sulfide mass spectrum the following simple metastable dissociations have been observed

$$SH_2^+ \rightarrow S^+ + H_2 \qquad (m^* = 30{,}12) \tag{14}$$

$$SH^+ \rightarrow S^+ + H \qquad (m^* = 31{,}0) \tag{15}$$

But till now were not published none results concerning to consecutive metastable dissociation of the SH_2^+ ion, or generally, of a triatomic one. The triatomic molecular ion is the smallest one which can undergo a consecutive metastable dissociation. The investigation of these processes might be useful for

the knowledge of excited states of triatomic molecular ions and for the understanding of metastable dissociation mechanisms.

The purpose of the present paper is to commite a first investigation concerning to consecutive metastable dissociation of the SH_2^+ ion. Our experimental results are shown on Figs. 2 and 3.

From the analysis of these results one can draw the following conclusion. The SH_2^+ molecular ion undergoes a consecutive metastable dissociation which can schematically be presented as follows

$$SH_2^+ \begin{array}{l} \xrightarrow{\lambda_1} SH^+ \\ \xrightarrow{\sigma_1} SH^+ \end{array} \longrightarrow (SH^+) \begin{array}{l} \xrightarrow{\lambda_2} S^+ \\ \xrightarrow{\sigma_2} S^+ \end{array} \longrightarrow (S^+) \qquad (16)$$

In Fig. 3 we have actually the proof of consecutive metastable dissociation of the SH_2^+ ion. Experimental results presented here were obtained in the following conditions. The first mass spectrometer analyzer has been made transparent for the apparent mass 32,03. This means that the trajectory portion 3→6 is crossed by the SH^+ ions which have been born from the SH_2^+ ions on the trajectory portion 1→2. Together with the SH^+ ions enter the S^+ ones from hydrogen sulfide normal mass spectrum. The second analyzer was scanned so that to cover a sufficient large mass range. As a result at the collector were recorded two peaks: the first at the apparent mass 30,12 and the second at the mass 32. At the mass 32 are actually superposed two peaks: the normal peak from the mass 32 and metastable peak from the apparent mass 32,03. Metastable peak from the apparent mass 30,12 corresponds to the S^+ ions which have been born from the SH^+ ions on the trajectory portion 3→6. But, in their turn, the SH^+ ions have been born from the SH_2^+ ions on the trajectory portion 1→2. Therefore, the SH^+ ions are daughters for the SH_2^+ ions and parents for the S^+ ions or, that is to say, the SH_2^+ ions undergo a consecutive metastable dissociation. In Fig. 3 we have also shown pressure dependence of the mixed peak from the mass 32 which was denoted by I_{32}^{*n}. It can be observed that the peak I_{32}^{*n} is independent of pressure in mass spectrometer tube. From this behaviour the following conclusions might be frawn. (a) The contribution of the SH^+ metastable ions in the peak I_{32}^{*n} is negligible in comparison with that of the S^+ ions from normal mass spectrum. This is a natural result. (b) In that pressure range where the measurements were performed the diffusion of molecular ions on residual gas is negligible with regard to collision-induced metastable dissociations.

Experimental results which are shown on Fig. 2 were obtained as follows. The first mass spectrometer analyzer has been made transparent for the SH_2^+ ions from hydrogen sulfide normal mass spectrum. The second analyzer was scanned between the masses 30 and 34. As a result at the collector were recorded two metastable peaks at the apparent masses 30,12 and 32,03 and the parent peak at normal mass 34.

The systems of transcendental equations (7) and (3), (6). were solved using experimental results shown in Figs. 2 and 3. From these results were drawn out

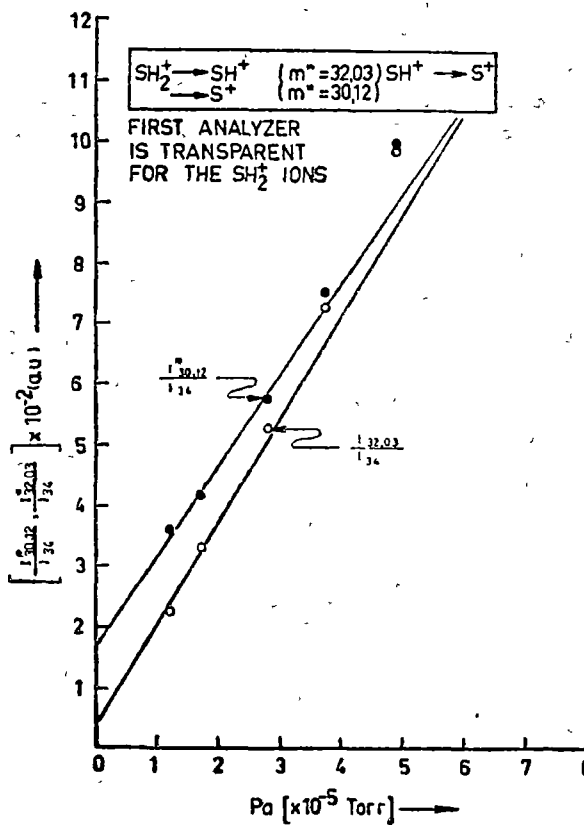
SH$_2^+$ → SH$^+$ (m* = 32,03) SH$^+$ → S$^+$
→ S$^+$ (m* = 30,12)
FIRST ANALYZER
IS TRANSPARENT
FOR THE SH$_2^+$ IONS
8
$\frac{I^*_{30,12}}{I_{34}}$
$\frac{I_{32,03}}{I_{34}}$
$\left[\frac{I^*_{30,12}}{I_{34}}, \frac{I^*_{32,03}}{I_{34}}\right] \times 10^{-2}$ (a.u.)
Pa [$\times 10^{-5}$ Torr]
0
1
2
3
4
5
6
7
8
9
10
11
12

Fig. 2.

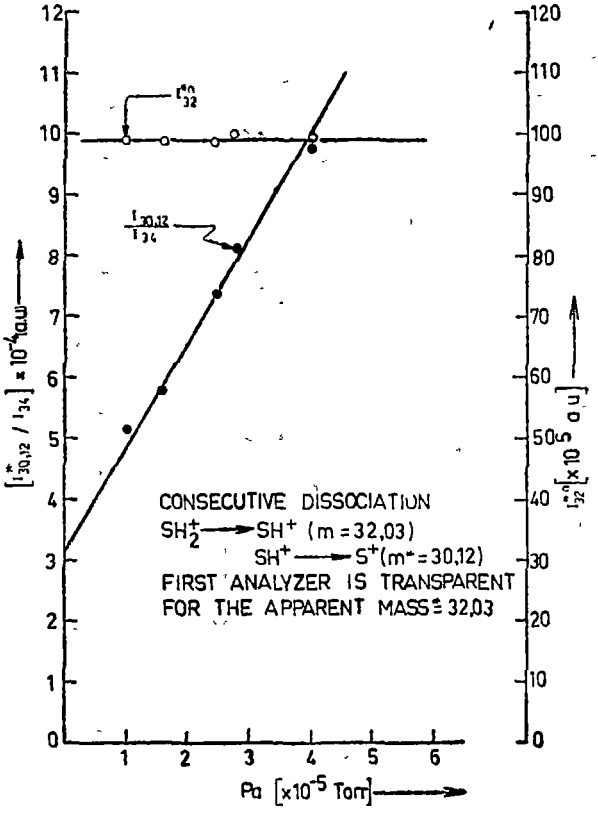
I^{*n}_{32}
$\frac{I_{30,12}}{I_{34}}$
CONSECUTIVE DISSOCIATION
$SH_2^+ \longrightarrow SH^+$ (m = 32,03)
$SH^+ \longrightarrow S^+$ (m* = 30,12)
FIRST ANALYZER IS TRANSPARENT
FOR THE APPARENT MASS ≙ 32,03
$[I^*_{30,12} / I_{34}] \times 10^{-4}$ a.u.
$[I^{*n}_{32}] \times 10^{5}$ a.u.
Pa [$\times 10^{-5}$ Torr]
0
1
2
3
4
5
6
7
8
9
10
11
12
10
20
30
40
50
60
70
80
90
100
110
120

Fig. 3.

several numerical values on the basis of the following identification relations

$$I_{34} = I_8; \qquad I^*_{32,03} = I'_{8s}; \qquad I^*_{30,12} = I''_{8f};$$

$$R[\lambda_1, \lambda_2, p(N)] = I^*_{32,03}/I_{34}; \; M[\lambda_1, \lambda_2, p(N)] = I^*_{30,12}/I_{34};$$

$$R[\lambda_1, \lambda_2, 0] = [I^*_{32,03}/I_{34}]_{p(N)\to 0}; \; M[\lambda_1, \lambda_2, 0] = [I^*_{30,12}/I_{34}]_{p(N)\to 0}$$

As a result, for the consecutive metastable dissociation of the SH ion the lifetimes $\tau_1 = (1/\lambda_1) = 5{,}54 \cdot 10^{-4}s$ and $\tau_2 = (1/\lambda_2) = 2{,}27 \cdot 10^{-5}s$ and the cross-sections $\sigma_1 = 9{,}58 \cdot 10^{-1}$ cm^2 and $\sigma_2 = 3{,}75 \cdot 10^{-1}$ cm^2 were obtained.

Discussions. In our paper was clearly established the following channel for the metastable dissociation of the SH_2^+ ion

$$SH_2^+ \rightarrow SH^+ + H \qquad (m^* = 32{,}03) \tag{17}$$

The investigation of this process is useful for the dissociation mechanism understanding of the SH_2^+ molecular ion. An analogous metastable dissociation of the $H_2O_2^+$ molecular ion has already been observed [16].

The knowledge of the SH_2^+ molecular ion electronic states is necessary for producing mechanism understanding of the SH^+ and S^+ fragment ions as a result of normal and metastable dissociations. Ionization of the SH_2 and H_2O triatomic molecules was the subject of numerous papers [15, 17—34]. Electron impact ionization [15, 17—19, 22, 34], photoionization [20, 21, 23, 24, 26, 29, 32] and photoelectron spectroscopy [25, 27, 28, 30, 31, 33] have alike been used for the investigation of electronic states of these relatively simple molecular ions, i.e. of the SH_2^+ and H_2O^+ ions. With the development of high resolution photoelectron spectroscopy the knowledges concerning to electronic states of these two and of many others molecular ions have been greatly increased. It is known that the fundamental electronic state of the SH_2 molecule is the $^1A_1$ state. As a result of the hydrogen sulfide ionization by electronic and photonic impact there are well enough known the first three electronic states of the SH_2^+ molecular ion. These three electronic states are $^2B_1$, $^2A_1$ and $^2B_2$ and they appear respectively for the ionizing energies of 10,45 eV, 12,9 eV and 14,8 eV. By photoelectron spectroscopy [33] has been found the fourth electronic state of the SH_2^+ molecular ion, i.e. the state $^2A_1$ appearing at 22,2 eV. It seems that this electronic state of the SH_2^+ ion has also been observed by electron impact ionization [34] at 22,6 eV.

The dissociation mechanism of the SH_2^+ molecular ion has been studied for the first time by F. Fiquet-Fayard et al. [35]. In this basic paper have constructed the correlation diagrams of the first electronic excited states of the SH_2^+ ion. From the examination of correlation diagrams it was drawn the conclusion that the SH^+ and S^+ fragment ions are produced only as a result of electronic predissociation of the $^2B_2$ state. The yielding of the S^+ ions is much less likely than that of the SH^+ ions, i.e. the electronic predissociation to the S^+ fragment ions is negligible in comparison with that of SH^+ fragment ions. In another paper [36] it has been suggested that the SH^+

ions are initially formed by predissociation from $^2A_1$ state and when it is energetically possible from $^2B_2$ state.

In two more recent papers [37, 38] the electronic states of the H_2O^+ molecular ion have theoretically been investigated. In connection with these electronic states the yielding mechanisms of the OH^+, H^+ and O^+ fragment ions in normal and metastable mass spectrum have been discussed. As a result of these investigations the following important conclusions were drawn. The vibrational levels of the H_2O^+ molecular ion above the first dissociation asymptote are totally predissociated owing to strong anharmonicity and vibronic couplings. These states produce either OH^+ and H^+ fragment ions, sometimes metastable, and not molecular ions. The predissociation channels leading to the O^+ fragment ions are in competition with that leading to ionic fragments OH^+ and H^+ but the first ones are very unlikely. Since the crossing electronic states are of different multiplicity, the aforesaid results draw attention to the following fact. For the electronic predissociation processes, even in the case of some light molecular ions such as H_2O^+, the spin conservation rule is a weak selection rule [39]. The violation of this selection rule only decreases the dissociation rate constant by three orders of magnitude, let us say from 10^{13} s^{-1} to 10^{10} s^{-1}. Further lowering of rate constant, i.e. the appearance of metastable dissociation, is due to the predissociation by a tunneling process.

Our experimental results were obtained for 70 eV as energy of ionizing electrons. Consequently, the first step of consecutive metastable dissociation (16) cannot directly be assigned to aforesaid discussed predissociation processes However, it is known that the autoionization constitues a major mechanism in the production of charged species and very likely of parent molecular ions Thus, it might be assumed that the first step of consecutive metastable dissociation is due to the autoionization of some Rydberg states finally leading at the known electronic states of the SH_2^+ molecular ion. Further on, metastable dissociation mechanism would be the predissociation by tunneling effect from these electronic states. Only a tunneling process might explain so long lifetimes as that obtained in our paper. It might also be assumed that the first step of consecutive metastable dissociation is due to predissociative autoionization by tunneling effect of some Rydberg states. The last two mechanisms, i.e. autoionization and predissociative autoionization by tunneling effect of some Rydberg states, might be both or/and in competition responsible for the first step of consecutive metastable dissociation. Unfortunately, these Rydberg states are not well-known.

Second step of consecutive metastable dissociation (16) might be due to the predissociation by tunneling effect from one or several electronic states of the SH^+ ion. From correlation diagrams presented in paper [35] follow that the SH^+ fragment ions can be produced in the following electronic states: $^3\Sigma^-$, $^1\Delta$, $^1\Sigma^+$ and $^3\Pi$. It is very likely that one or several of these electronic states are predissociated by tunneling effect giving rise to the second step of consecutive metastable dissociation of the SH_2^+ molecular ion. Only a tunneling process might lead to so long lifetimes as that obtained in our paper for the second step of metastable transition.

(Received November 10, 1978)

REFERENCES

1. K. R. Jennings, Chem. Comm., 283 (1966).
2. J. Seibl, Helv. Chim. Acta, **50**, 263 (1967).
3. C. H. Ottinger, paper presented at the 17 th Annual Conference on Mass Spectrometry, Dallas, Texas, 1969.
4. L. P. Hills, J H. Furtell, A. L. Wahrhafting, J. Chem. Phys., **51**, 5255 (1969)
5. A. Kropf, E. M. Eyring, A. L. Wahrhafting, H. Eyring, J. Chem. Phys., **32**, 149 (1960).
6. M. Vestal, A. L. Wahrhafting, W. H. Johnston, J. Chem. Phys., **37**, 1276 (1962).
7. M. Vestal, J. Chem. Phys., **43**, 1356 (1965).
8. J. C. Tou, L. P. Hills, A. L. Wahrhafting, J. Chem. Phys., **45**, 2129 (1966).
9. M. Vestal, J. Chem. Phys., **41**, 3997 (1964).
10. J. M. Miller, G. L. Wilson, Int. J. Mass Spectrom. Ion Phys., **12**, 225 (1973).
11. I. Mastan, A. Toderean, Contract 201/1975.
12. I. Mastan, A. Toderean, V. Mercea, Studia Univ. Babeş-Bolyai, Phys., 1, 12 (1977).
13. I. Mastan, A. Toderean, N. Palibroda, Studia Univ. Babeş-Bolyai, Phys., 2, 45 (1977).
14. I. Mastan, A. Toderean, V. Mecea, Studia Univ. Babeş-Bolyai, Phys., 2, 3 (1977).
15. V. H. Dibeler, H. M. Rosenstock, J. Chem. Phys., **39**, 3106 (1963).
16. J. Momigny, H. Wankenne, private communication.
17. D. C. Frost, C. A. McDowell, Can. J. Chem., **36**, 39 (1958).
18. M. Cottin, J. Chim. Phys., **56**, 1024 (1960).
19. A. Skerbele, E. N. Lassettre, J. Chem. Phys., **42**, 395 (1965).
20. P. H. Metzger, G. R. Cook, J. Chem. Phys., **41**, 642 (1964).
21. K. Watanabe, A. S. Jursa, J. Chem. Phys., **41**, 1650 (1964).
22. H. Sjogren, Ark. Fys., **33**, 597 (1967).
23. A. J. C. Nicholson, J. Chem. Phys., **43**, 1171 (1965).
24. V. H. Dibeler, J. A. Walker, H. M. Rosenstock, J. Res. Nat. Bur. Stand., 70a, 459 (1966).
25. M. I. Al-Jobury, D. W. Turner, J. Chem. Soc., 4434 (1964).
26. V. H. Dibeler, S. K. Liston, J. Chem. Phys., **49**,, 482 (1968).
27. C. R. Brundle, D. W. Turner, Proc. Roy. Soc. (London), **A307**, 27 (1968).
28. A. D. Baker, C. R. Brundle, D. W. Turner, Int. J. Mass Spectrom. Ion Phys., **1**, 443 (1968).
29. L. de Reilhac, N. Damany, Spectrochim. Acta, **26 A**, 801 (1970).
30. J. Delwiche, P. Natalis, Chem. Phys. Lett., **5**, 564 (1970).
31 J. Delwiche, P. Natalis, J. E. Collin, Int. J. Mass Spectrom. Ion Phys., **5**, 443 (1970).
32. R. B. Cairns, H. Harrison, R. I. Schoen, J. Chem. Phys., **55**, 4886 (1971).
33. A. W. Potts, W. C. Price, Proc. Roy. Soc. (London), **A 326**, 181 (1972) .
34. J. D. Morrison, J. C. Traeger, Int. J. Mass Spectrom. Ion Phys., **11**, 77 (1973).
35. F. Fiquet-Fayard, P. M. Guyon, Mol. Phys., **11**, 17 (1966).
36. D. W. Turner, C. Baker, C. R. Brundle, Molecular Photoelectron Spectroscopy, Wiley-Interscience, London-New York, 1970.
37. J. C. Leclerc, J. A. Horsley, J. C. Lorquet, Chem. Phys., **4**, 337 (1974).
38. A. J. Lorquet, J. C. Lorquet, Chem. Phys., **4**, 353 (1974).
39. A. J. Lorquet, J. C. Lorquet, H. Wankenne, J. Momigny, J. Chem. Phys., **55**, 4053 (1971).

DISOCIEREA METASTABILĂ CONSECUTIVĂ A IONILOR TRIATOMICI. IONUL MOLECULAR SH_2^+

(Rezumat)

Folosind două spectrometre de masă magnetice în tandem a fost pusă în evidență pentru prima dată disocierea metastabilă consecutivă a unui ion molecular triatomic. S-a stabilit că ionul molecular SH_2^+ suferă disocierea metastabilă consecutivă $SH_2^+ \xrightarrow{\lambda_1, \sigma_1} SH^+ \xrightarrow{\lambda_2, \sigma_2} S^+$. Pentru vieţile medii şi secţiunile eficace ale acestui proces au fost respectiv obţinute valorile $\tau_1 = (1/\lambda_1) = 5{,}54 \cdot 10^{-4}$s, $\tau_2 = (1/\lambda_2) = 2{,}27 \cdot 10^{-5}$s şi $\sigma_1 = 9{,}58 \cdot 10^{-16}$ cm^2, $\sigma_2 = 3{,}75 \cdot 10^{-15}$ cm^2.

Sînt discutate mecanismele posibile ale disocierii metastabile consecutive. Pentru primul pas sînt propuse două mecanisme: autoionizarea şi/sau autoionizarea predisociativă prin efect tunel a unor stări Rydberg. Pentru pasul al doilea mecanismul cel mai probabil este predisocierea prin efect tunel a uneia sau mai multor stări electronice ale ionului SH^+.

STUDIA UNIV BABEŞ-BOLYAI, PHYSICA, XXIV, 2, 1979

COMPUTER SIMULATIONS OF THE BEHAVIOUR OF THE OPTICAL DICHROISM OF PARTIALLY ORIENTED FIBRE SPECIMENS.

T. PORUMB and H. PORUMB*

The paper presents a preliminary note on computer simulations of the linear dichroism of biological polymer fibres, which were performed within a model in which the internal misalignment of the specimen was described by a Gaussian function.

The linear dichroism is introduced in relation to fibres of complexes of polynucleotides with drugs and the results are presented in the form of plots of the dichroic ratio as function of the orientation of the drug chromophore or of the electric transition moment relative to the polymer axis, for different degrees of Gaussian misalignment of the polymers.

1. **Theoretical considerations.** A large number of biological specimens are linear polymers, organized in essentially cylindrical structures (fibres). The optical linear dichroism of such specimens may be defined as the ratio of the absorptions of the light polarized perpendicular and parallel to the fibre axis.

The study was undertaken in an attempt to describe explicitly the dependence of these properties of the fibres on the secondary structure of the polynucleotide helices and the orientation of the drug chromophore, on one hand, and on the degree of internal ordering of the specimens, on the other hand. Two fields that could draw benefits from the present simulations are the infra-red dichroism of partially oriented specimens and the optical dichroism of fibres obtained from complexes of DNA with dyes or drugs (in which the polynucleotide chains are preferentially aligned parallel to the fibre axis), the dichroism being observed at wavelengths that correspond to the absorption band of the dye or drug chromophore. Molecules of this kind, which include the biologically useful agents proflavine [1] or ethidium bromide [2] usually posses planar aromatic chromophores, with the electric transition moments responsible for their visible absorption bands lying in the planes of the chromophores.

2. **Computer simulations.** In the theoretic simulations of the fibre dichroism it was assumed that the drug molecules were rigidly bound onto the polynucleotide molecules, which were considered to have a Gaussian distribution of orientations about the fibre axis. The absorption of plane polarized light by a chromophore is proportional to the square of the cosine of the angle between the direction of polarization of the light and the relevant electric transition moment [3]. The computer program operated cylindrical averaging routines at the level of both the fibre and the polymer molecule, in which the individual contributions of each drug molecule to the absorptions of light polarized perpendicular and parallel to the fibre axis were accumulated separately and the two quantities thus obtained were divided into one another to yield the dichroic ratio D.

* Departament of Biophysics, Institute of Medicine and Pharmacy, Cluj-Napoca.

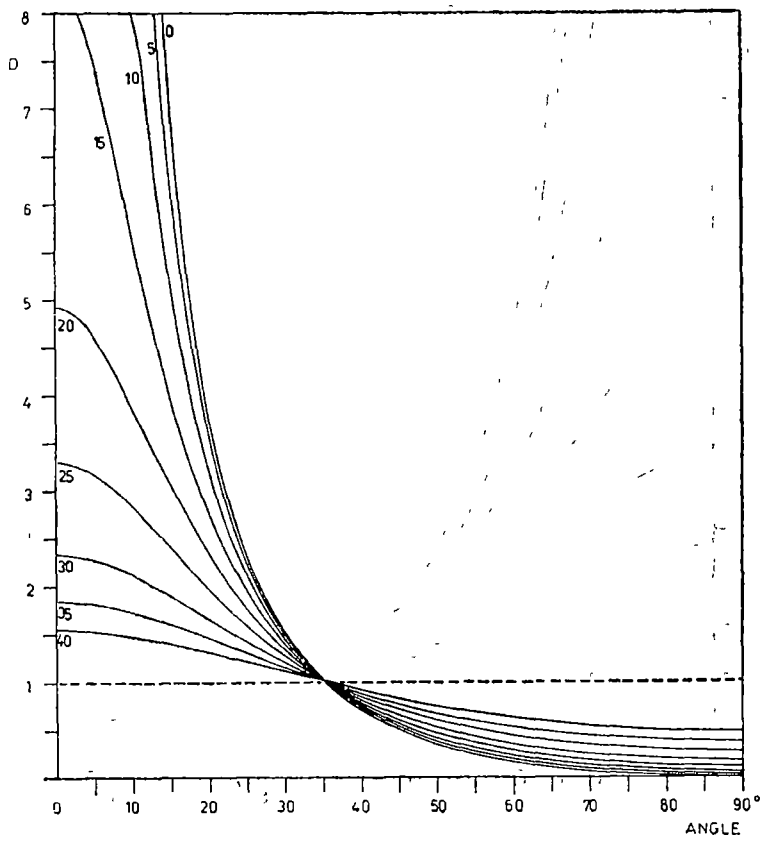

Fig. 1. Computer simulations of the dichroic ratios of partially oriented fibre specimens as a function of the orientation of the transition moment relative to the plane perpendicular to the polymer axis. The Gaussian misalignment parameters are indicated on the curves

Fig. 1 represents the dichroic ratios calculated for fibres of various degrees of misalignment, as a function of the angle between the transition moment and the plane perpendicular to the polymer axis. The dichroic ratios vary between O and infinity and all the curves cross over on the D = 1 line, for an angle equal to 35°16′. The curve referring to a perfectly oriented fibre reproduces the features of the theoretical calculations previously performed by Fraser [3]. Each point of the graph was obtained by running the computer program once.

The practical use of this simulation requires that the orientation of the electric transition moment in the chromophore is known; an information which is frequently not available. For convenience, in such cases the absorption of light can be considered to be isotropic in the plane of the chromophore. It turns out that this is a reasonable approximation, especially for small angles of tilt.

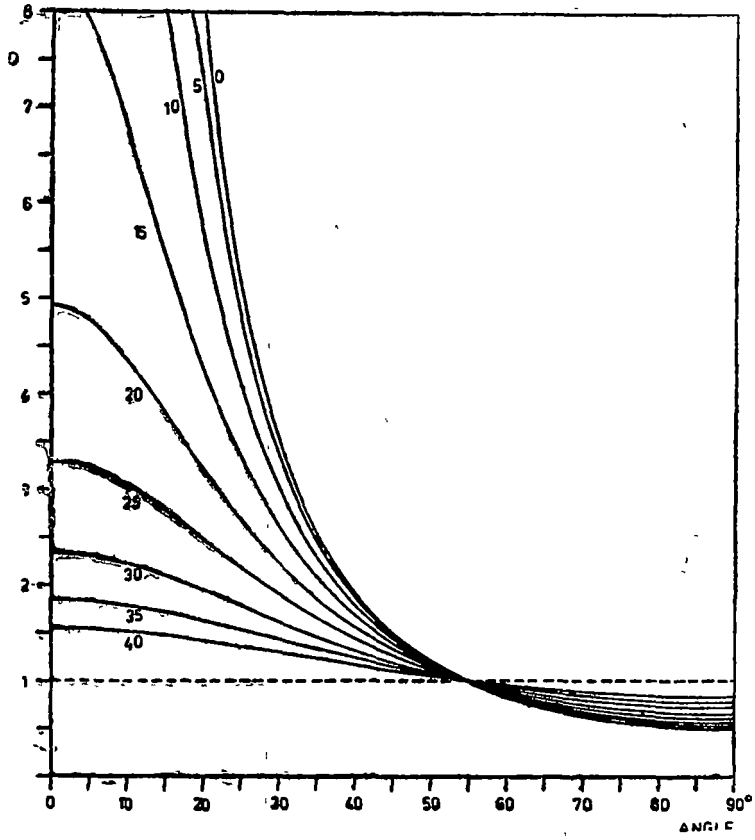

Fig. 2. Computer simulations of the dichroic ratios of partially oriented fibre specimens as a function of the orientation of the chromoph ore, assuming that the absorption of light was isotropic in the plane of the chromophore.

Fig. 2 shows the dichroic ratios calculated on the basis of this assumption, as a function of the angle of tilt of the chromophore (the angle between the normal to the plane of the chromophore and the polymer axis). The crossover point occurs on the D = 1 line at 54°44′ of tilt, and D varies between 0.5 and infinity. The vertical axis is intercepted at the same values as in Fig. 1, which means that for small angles of tilt, the results predicted by both models would be similar. Thus an important conclusion which emerges from this study is that for the molecules bound with their chromophores approximately perpendicular to the polymer axis the dichroic ratios are determined primarily by the degree of ordering of the polymers in the fibre, and are not sensitive to the particular orientation of the transition moment in the planar chromophore.

3. Discussion and relevance to experiment. In previous studies [4], the departures from perfect alignment were treated in terms of a model according to which a fraction of the polymer chains were perfectly oriented, while the

Table 1

Optical dichroism data obtained from fibres of complexes of DNA with drugs

Drug	Experimental dichroic ratio	Corresponding misalignment parameter*	Misalignment parameter deduced by ESR
Chlorpromazine (small drug content)	3–5	20–27°	27°
Chlorpromazine (large drug content)	1.5	40°	40°
Ethidium bromide, anthracyclines	3–6	15–25°**	–

*assuming the attachment of the drug with its general plane perpendicular to the DNA helical axis
**account was taken of the existence of a fraction of externally bound molecules [6].

others were randomly disordered. The present simulations were carried out within a model which assumed that the fibre consisted of bunches of polymers distributed in a Gaussian fashion about the fibre axis, such that the probability of a polymer bunch lying along the generator of a cone of semiangle θ is proportional to exp $(-\theta^2/2s^2)$, where s, the "misalignment parameter", is the half width of the distribution.

The application of the simulations is illustrated in Table 1 with data obtained from fibres of DNA complexed with the cation form of the drug chlorpromazine [5] A previous study by electron spin resonance techniques indicated a misalignment parameter of 27–40°. The values of the misalignment parameter obtained on the basis of the optical dichroism data are in very good agreement with the results of the ESR investigation and are also consistent with the appearance of the X-ray diffraction patterns obtained from the same fibres The slightly smaller value for the misalignment parameter obtained using the optical dichroism method may arise from the fact that the measurement was taken from a selected area closer to the centre of the fibre, which probably had a better orientation than the average of the whole fibre. Table 1 also includes results obtained from fibres of DNA complexed with the "intercalating" drugs ethidium bromide and anthracyclines [6].

(Received January 13, 1979)

REFERENCES

1. L. L. Ingraham, H Johansen, Arch. Biochem. Biophys., **132**, 205 (1969).
2. P. U. Giacomoni, M. Le Bret, FEBS Letters, **27**, 227 (1973).
3. R. D. B. Fraser, J. Chem. Phys, **21**, 1511 (1953).
4. J. Pilet, J. Brahms, Biopolymers, **12**, 307 (1973).
5. T. Porumb, E. F. Slade, J. Magn Reson, **22**, 216 (1967).
6. H. Porumb, T. Porumb, Clujul Medical, **LI**, 3, 259 and 263 (1978).

SIMULĂRI ALE COMPORTAMENTULUI DICROISMULUI OPTIC AL UNOR FIBRE PARŢIAL ORIENTATE

(R e z u m a t)

Comunicarea prezintă simulări, obţinute folosind calculatorul, ale dicroismului liniar al unor fibre de polimeri biologici, efectuate în cadrul unui model în care ordinea internă este descrisă de o funcţie gausiană Se fac referinţe la fibre obţinute din complexe ale acizilor nucleici cu unele medicamente, iar rezultatele sînt prezentate sub formă de familii de curbe ale raportului dicroic în funcţie de orientarea cromoforului sau a momentului tranziţiei electronice faţă de axa polimerului, pentru diferite grade de dezorientare gausiană a polimerilor

STUDIA UNIV BABEŞ-BOLYAI, PHYSICA, XXIV, 2, 1979

THE DESIGN OF A MICROSPECTROPHOTOMETER SYSTEM WITH PHASE-SENSITIVE DETECTION

HOREA PORUMB*

Introduction. The construction of a microspectrophotometer was undertaken because of the need for an apparatus capable of measuring the absorbance and the linear optical dichroism of small areas, less than 100 μm across, of highly absorbant drug-nucleic acid fibres, which were used in parallel with an X-ray investigation [1]. As with microscopic specimens there is nothing such as a 'matched' reference sample, the possibility of constructing a double beam system was rejected from the start.

The absorbance at a given wavelength is expressed in terms of the 'transmitted' (I) and 'background' (I_0) light intensities by the following formula:

$$A = -\log_{10}(I/I_0) = \log I_0 - \log I. \tag{1}$$

In a single-beam spectrophotometer the two light intensities (in the presence and in the absence of the specimen) are recorded consecutively. Wavelength-dependent factors such as the detector sensitivity, the output of the lamp, the reflectance of the diffraction grating have the same multiplying effect of both intensities and their ratio (hence, the absorbance) remains a property of the specimen alone. For the difference of the two terms in eqn (1) to be meaningful, the mechanic and electronic parameters of the spectrophotometer have to remain unaltered during the time taken to make the two recordings. From these considerations it emerges that stability is an essential requirement for a single beam system.

The basic design. The basic design of the microspectrophotometer may be understood by reference to Fig. 1, showing the optical diagram of the system and Fig 2, which presents the layout of the optical and electronic moduli. The system was based on a Zeiss Universal polarizing microscope.

White light from the 12 V, 100 W quartz-iodine lamp, S, is focused onto the entrance slit of the diffraction-grating monochromator, MC. The emergent monochromatic beam, interrupted at the frequency of 110 Hz by a vibrating-vane chopper, CH, illuminates a rectangular aperture, F, which is equivalent to the field aperture F_1 of the conventional microscope and determines the area in the object plane, OP, which will be illuminated (Fig. 1). An aluminium front-surfaced mirror at 45° joins up the optical axis of the monochromator section with the optical axis of the microscope. The vertical tube of the microscope, carrying the eyepiece E, is extended with the detector column having the photomultiplier PM at the top end (RCA type 931 A).

A part of the main light beam branches off at the level of the triple mirror T, enabling the observation of the specimen through the viewer V. The

* Department of Biophysics, Institute of Medicine and Pharmacy, Cluj-Napoca.

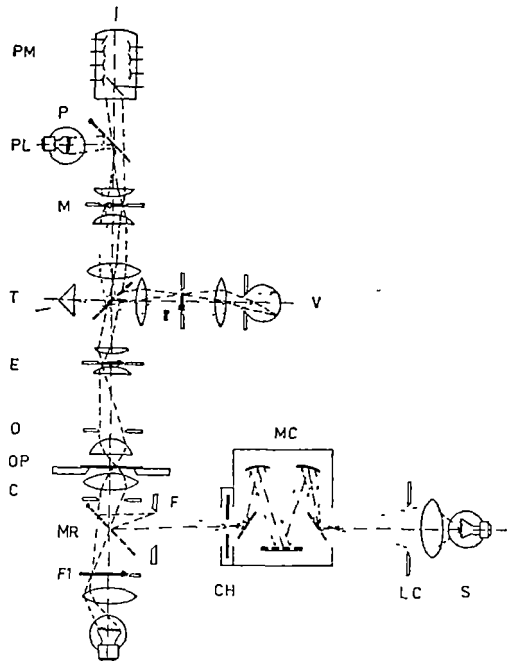

Fig 1. Optical diagram of the microspectrophotometer

object plane is imaged midway up the column at the level of the measuring aperture M. The role of M is to isolate from the image of the specimen only the area the transmittance of which is to be measured, light from a pilot lamp, PL, can be projected through M and directed by the triple mirror towards the viewer, where the image of the measuring aperture becomes superimposed onto the field of view.

The phase-sensitive detector (Brookdeal 9501 lock-in amplifier), which acts in synchronization with the light chopper, will convert the squared-wave signal from the photomultiplier into a low-noise DC voltage proportional to the light intensity incident on it (Fig. 2). Note that the use of chopped light and phase-sensitive detection enables the spectra to be recorded in full daylight.

The output of the phase-sensitive detector is displayed either directly, or after logarithmic amplification, as the Y-deflection on a two-dimensional graph plotter. The X-deflection is linear with the wavelength and is produced by a ramp voltage generated by a ten-turn potentiometer rigidly coupled at right angles to the shaft of the monochromator. A stepping motor is flexibly coupled at the end of that shaft and the range-control unit, based on two voltage comparators controls the scanning of the wavelengths between pre-selected values.

The curves plotted or recorded in digital form on punched paper tape (Fig. 2) represent light intensity (or its logarithm) as a function of wavelength. In order to obtain an absorption spectrum, two consecutive scans are required, one for the 'transmitted', the other for the 'background' intensity. The absorbance is then calculated at every wavelength according to eqn. (1), either manually, or with the aid of a computer. In order to obtain the linear dichroism, two such spectra are obtained for light polarized parallel and perpendicular to the optical axis of the same specimen [2].

The performance of the system. The features of the absorption spectra of standard filters compared favourably with the spectra of the same filters recorded on a commercial spectrophotometer. Consistent absorbance values were obtained for neutral density filters for any orientation of the polarizer and irrespective of the microscope magnification employed, provided the background intensities were recorded under the same conditions.

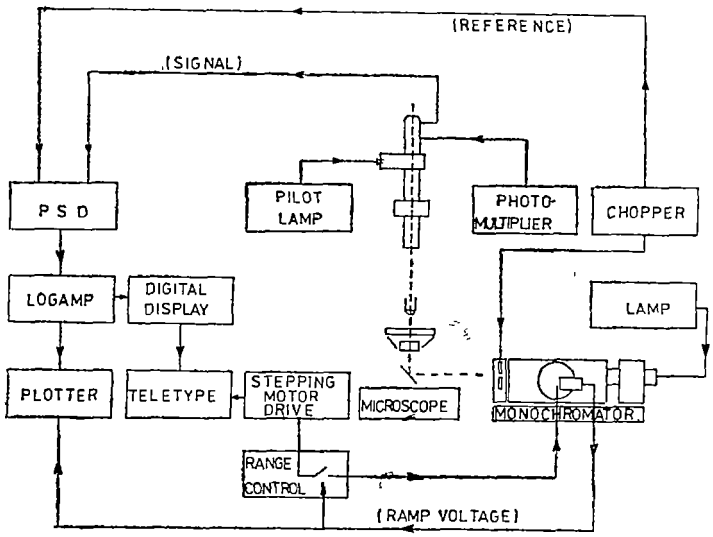

Fig. 2. The full microspectrophotometer system.

The dynamic range of the sensitivity was tested with neutral density filters superimposed over a blue filter. With an averaging time of three seconds, the features of the spectrum could still be identified up to a total optical density of 5, although the electronic noise started to be troublesome for optical densities greater than 4.

(Received January 13, 1979)

REFERENCES

1. H. Porumb, T. Porumb, Clujul Medical, LI, 3, 259 (1978)
2. H. Porumb, T. Porumb, Clujul Medical, LI, 3, 263 (1978).

UN SISTEM MICROSPECTROFOTOMETRIC CU DETECȚIE SENSIBILĂ LA FAZĂ

(Rezumat)

Este descrisă construcția unui microspectrofotometru cu lumină polarizată cu o singură cale optică Sistemul, bazat pe un microscop Zeiss Universal, servește la obținerea spectrelor de absorbție în domeniul vizibil ale unor arii selectate din preparate microscopice

STUDIA UNIV BABEŞ-BOLYAI, PHYSICA, XXIV, 2; 1979

RHEOLOGIC PROPERTIES MODIFICATION OF SOME SUSPENSIONS IN ULTRASONIC FIELD

D. AUSLÄNDER, I. IVAN, LIA ONIŢIU

Introduction. The rheologic characteristics of kaolin suspensions are determinant of the properties of slips used in the ceramic technologies, their moulding conditions being the better so as the viscosity and tixotropy have lower values.

Taking into account that the slips prepared with kaolin from Aghireş have rheologic properties needing improvements for their use in moulding technologies [2] we carried out investigations concerning the effects of ultrasound upon some rheological properties.

Experiment. Two types of kaolin slip samples from E.M. Aghireş were analysed; the results are presented in tables 1, 2, 3, 4.

Table 1

Nr	Sample name	Chemical analysis (%)								
		P C	SiO_2	Al_2O_3	Fe_2O_3	CaO	MgO	K_2O	Na_2O	TiO_2
1.	Sample E	10.98	54 49	31 00	1 37	0 56	0 15	0 80	0 50	0 52
2.	Sample D	12.37	51 43	31 27	1.15	0 75	0.25	0.90	0 50	0 46

Table 2

Nr.	Sample name	Structural Rontgen analysis (%)		
		Kaolinite	Quartz	Illit-Hidrom.
1	Sample E	71	16	13
2	Sample D	70	14	16

Table 3

Nr	Sample name	Value of tixotropic index		
		Addition 0 4% Na_2CO_3	Addition 0.5% Na_2CO_3	Addition 0.6% Na_2CO_3
1	Sample E (r = 1180 g/l)	2.20	1 91	1.95
2	Sample D (r = 1170 g/l)	Undeterm	Undeterm.	Undeterm.

Table 4

Nr	Sample name	(%) Particles (μ)										
		14 01	9 91	8.09	5 72	4 67	4 04	3 62	3 30	3.06	2.86	1.65
1	Sample E	13 83	21.28	23 93	29 26	33 51	36 17	37 24	39 36	41.49	42.55	61.17
2	Sample D.	21.28	25.00	29.26	32 98	35.64	37 77	39 89	40.96	42.55	44.15	60.64

The sonications were made at 16 kHz, 20 kHz, 1 MHz and 2 MHz at different intensities, with treatment times between 30 seconds and 30 minutes.

The viscosity of the control and sonicated samples was determined by means of a "Rotovisko" type rheoviscosimeter at 22 °C under thermostat conditions, and the tixotropic index was measured with a Stormer viscosimeter on suspensions prepared according to the kaolin standard.

Results and discussion. The effect of ultrasound upon the rheology of kaolin suspensions with floculant addition (hydrolyzed polyacryleamide) increases with the decrease of frequency and with the sonication time up to a limit value.

In the case of sample E, with a determinable tixotropic index, the suspension formed from the kaolin resulting after filtration maintains its improved values of the tixotropic index shown in table 5.

Table 5

Nr.	Ultrasound frequency	Value of tixotropic index		
		T_1(s)	T_2(s)	I.T
1	Control sample E (floculated)	127	242	1 91
2	20 kHz	128	165 2	1.28
3	1 MHz	170	306	1 80
4	2 MHz	184	—	Undeterm

In sample D, with undeterminable tixotropic index the modifications similar to sample E are present only in the sonicated suspensions, the preparation of the suspension from the kaolin resulting through filtration does not present discernible modifications.

In the suspensions with sodium carbonate and silicate in different percentage, the effect of ultrasound manifests itself by the decrease of plasticity, viscosity and tixotropy.

The decrease of ultrasound effect with the increase of electrolyte addition amount, and its strengthening with the frequency decrease are found.

The results obtained through sonication at 20 kHz frequency, shown in tables 6 and 7, demonstrate the favourable contribution of sodium carbonate to the tixotropy decrease.

Table 6

Nr	Sample	Na_2CO_3 addition (%)	Value of tixotropic index		
			T_1(s)	T_2(s)	I.T.
1	E_a—control	0 05	38 4	62 2	1 62
2	E_a—sonicated	0 05	144 2	185 2	1.28
3	E_b— control	0 10	42 2	70 0	1 67
4	E_b—sonicated	0 10	136 8	176.2	1.30
5	E_c—control	0 15	36 0	55 0	1 53
6	E_c—sonicated	0 15	78 4	99 0	1 26
7	E_d—control	0 20	35 0	48 4	1 37
8	E_d—sonicated	0.20	69.3	83 3	1.20

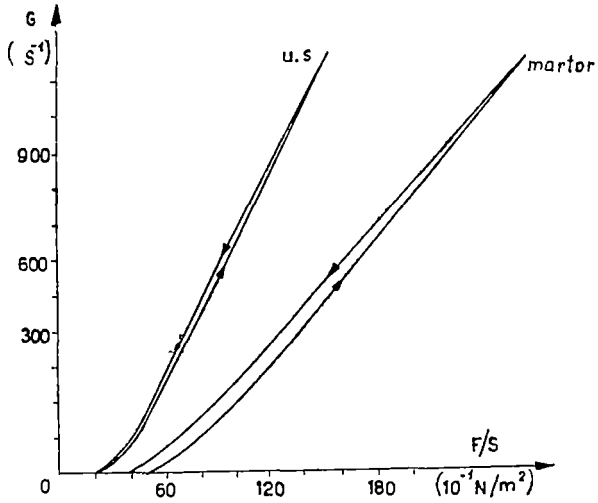

Fig. 1. Rheogram of the suspension with floculants addition, control suspension and sonicated suspension at 20 kHz.

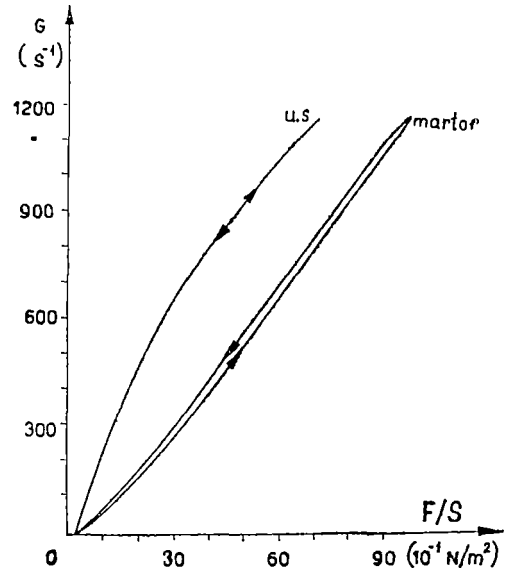

Fig 3 Rheogram of suspension with electrolyte addition (Na_2SiO_3), control suspension and sonicated suspension at 20 kHz.

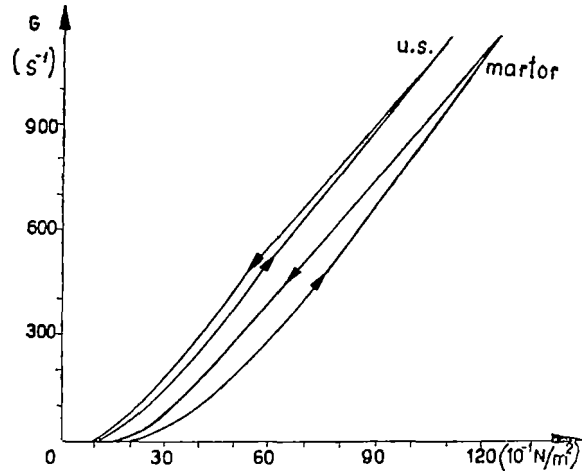

Fig. 2. Rheogram of suspension with electrolyte addition (Na_2CO_3), control suspension and sonicated suspension at 20 kHz.

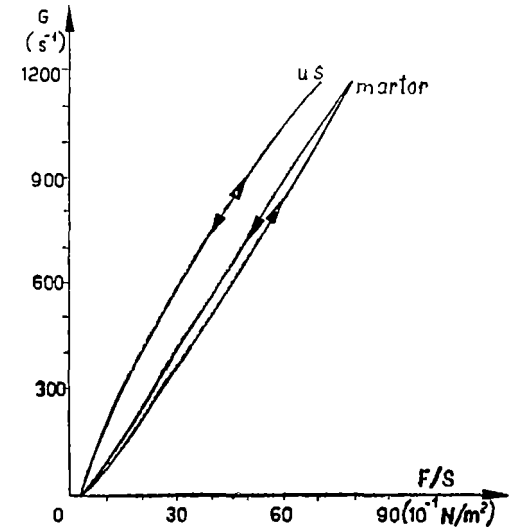

Fig. 4 Rheogram suspension with electrolyte addition ($Na_2CO_3 + Na_2SiO_3$), control suspension and sonicated suspension.

The figures 1, 2, 3 and 4 show the rheograms of the control samples and respectively of the sonicated ones at 20 kHz on different additions.

The experimental results and the explanation of the behaviour of tixotropic system in ultrasonic field — rather little studied in the literature — deprived of a unitary theoretical substantiation, are characterized by a series of disagreements [3], [4], [5], [6].

Table 7

Nr.	Sample	Na_2SiO_3 (%)	Value of tixotropic index		
			T_1(s)	T_2(s)	I.T
1	E_e—control	0 5	105 2	139.8	1 33
2	E_e—sonicated	0 5	115 2	200.0	1 73
3	E_f—control	1.0	134 4	271 0	2 01
4	E_f—sonicated	1 0	167 4	325 2	1 93
5	E_g—control	1.5	273	656	2.4
6	E_g—sonicated	1 5	100.8	201.2	1.96
7	E_h—control	2 0	163 2	180.4	1.10
8	E_h—sonicated	2.0	278	320	1.15

The effect of ultrasounds upon the kaolin suspensions manifests itself by the reduction of Binghamian flow limit, with a tendency towards a Newtonian behaviour; the increase of acoustic field intensity and respectively the frequency decrease, act in the direction of the effect intensification. These results plead for a cavitational hypothesis of the perturbation mechanism of the structure with tixotropic behaviour.

The modification of the effect due to the addition of different floculants is explained by the absorbing of the hydraulic shock of cavitational bubble implosion by the layer of hydrated colloidal micelles, respectively by the adsorbtion processes at the particles surfaces, with implications upon the values of interfacial tensions which have repercussions on the cavitational process intensity.

(Received February 2, 1979)

REFERENCES

1. G. Bandet, M. Mairo, Rev. Ind. Min., dec., 163 (1974).
2. I Magda, P. Piso, I Ivan, Rev. Minelor. **7**, 362 (1972).
3. D. Hums, R. Bruckner, Tonindustrie-Z, **95**, 10, 294 (1971).
4. R. Bruckner, Glass-Email-Keramo-Technik, **22**, 1, 9, (1971)
5. U. Hoffmana, Ber. Deutsch Keram. Ges., **46**, 109 (1969).
6. L. I. Kulchitsky, Colloid. J., **32**, 4, 344 (1970).

MODIFICAREA PROPRIETĂŢILOR REOLOGICE ALE UNOR SUSPENSII ÎN CÎMP ULTRASONIC

(Rezumat)

În vederea îmbunătăţirii proprietăţilor reologice ale suspensiilor ceramice industriale, s-au studiat două tipuri de barbotină caolinoasă de la E M. Aghireş, urmărindu-se efectul intensităţii cîmpului ultrasonic, al frecvenţei şi al timpului de ultrasonare asupra viscozităţii şi indicelui tixotropic, cercetările s-au extins şi asupra suspensiilor cu adaus de floculant şi de diferiţi electroliţi.

STUDIA UNIV BABEŞ-BOLYAI, PHYSICA, XXIV, 2, 1979

WEIBEL INSTABILITY OF A RELATIVISTIC ELECTRON BEAM

J. KARÁCSONY

It has long been known that streaming charged particles are unstable with respect to the transverse electromagnetic perturbations propagating perpendicular to the streaming direction [1]. This is named the "Weibel-type" instability. It has been extensively investigated, in the nonrelativistic regime, by many authors [2—7].

The purpose of this paper is to study the "Weibel-type" instability of a relativistic electron beam propagating in a magnetized plasma using the cold-fluid equations. Unlike the other papers concerned with the study of electron beam-plasma interaction and which neglect the self-magnetic field of the beam, in our paper, to avoid any contradiction with Maxwell's equations, arising from the omission of this self-magnetic field, we will assume that in the plasma there is a homogeneous return current. It is well-known that an intense relativistic electron beam can propagate in the presence of a dense plasma by inducing a plasma return current which is approximately equal and opposite to the beam current [8—11]. In this way the self-magnetic field of the system is nearly zero, but on the other hand in the unperturbed state the plasma electrons are no longer at rest, so the plasma contains a current flow.

In our model, we will consider a relativistic electron beam having the number density of electrons n_{b0} and the average velocity of electrons $\vec{v}_0$ oriented parallel to the external magnetic field $\vec{B}_0$. This magnetic field is assumed to be oriented along the positive Oz axis, $\vec{B}_0 = B_0 \vec{e}_z$ ($\vec{e}_z$ is the basic vector of Oz axis.) The unperturbed plasma electron mean velocity $\vec{v}_1$, producing the return current, is oriented in opposite direction to the beam electron velocity and it is equal with $-(n_{b0}/n_0)\,\vec{v}_0$. (n_0 is the plasma electron density and it satisfies the condition $n_0 \gg n_{b0}$.) The last expression for plasma electron mean velocity results from the current neutralization condition:

$$\vec{j}_{b0} + \vec{j}_{p0} = 0 \tag{1}$$

where $\vec{j}_{b0}$ and $\vec{j}_{p0}$ denote the unperturbed beam current density and plasma current density, respectively. Since we are concerned with high frequency oscillations we will assume the positive ion at rest, they only forming a stationary background of charge which neutralizes the unperturbed electron gas at each point.

The instability of the beam can be investigated by means of dispersion relation that we will obtain further.

The linearized equation of motion is

$$\left(\frac{\partial}{\partial t}+\vec{v}_0\cdot\nabla\right)\left[\frac{\vec{v}'}{\sqrt{1-v_0^2/c^2}}+\frac{\vec{v}_0(\vec{v}_0\cdot\vec{v}')}{c^2(1-v_0^2/c^2)^{3/2}}\right]=-\frac{e}{m}\left[\vec{E}'+\frac{1}{c}(\vec{v}'\times\vec{B}_0)+\frac{1}{c}(\vec{v}_0\times\vec{B}')\right] \quad (2)$$

for the beam electrons, and

$$\left(\frac{\partial}{\partial t}+\vec{v}_1\cdot\nabla\right)\vec{v}_1'=-\frac{e}{m}\left[\vec{E}'+\frac{1}{c}(\vec{v}_1'\times\vec{B}_0)+\frac{1}{c}(\vec{v}_1\times\vec{B}')\right]. \quad (3)$$

for the plasma electrons. In these equations the perturbed electric field, magnetic field and velocities are denoted by $\vec{E}'$, $\vec{B}'$, $\vec{v}'$ and $\vec{v}'_1$, respectively. For plane waves of the form exp $[i\ (\omega t-kx)]$ the perturbed velocities for the beam and plasma are:

$$v_x'=i\frac{e\omega\gamma_0}{m(\omega^2-\omega_c^2\gamma_0^2)}E_x'-\frac{e\omega_c\gamma_0^2}{m(\omega^2-\omega_c^2\gamma_0^2)}E_y'+i\frac{ekv_0\gamma_0}{m(\omega^2-\omega_c^2\gamma_0^2)}E_z' \quad (4)$$

$$v_y'=\frac{e\omega_c\gamma_0^2}{m(\omega^2-\omega_c^2\gamma_0^2)}E_x'+i\frac{e\omega\gamma_0}{m(\omega^2-\omega_c^2\gamma_0^2)}E_y'+\frac{ekv_0\omega_c\gamma_0^2}{m\omega(\omega^2-\omega_c^2\gamma_0^2)}E_z' \quad (5)$$

$$v_z'=\frac{ie\gamma_0^2}{m\omega}E_z' \quad (6)$$

$$v_{1x}'=i\frac{e\omega}{m(\omega^2-\omega_c^2)}E_x'-\frac{e\omega_c}{m(\omega^2-\omega_c^2)}E_y'-i\frac{ekv_1}{m(\omega^2-\omega_c^2)}E_z' \quad (7)$$

$$v_{1y}'=\frac{e\omega_c}{m(\omega^2-\omega_c^2)}E_x'+i\frac{e\omega}{m(\omega^2-\omega_c^2)}E_y'-\frac{ekv_1\omega_c}{m\omega(\omega^2-\omega_c^2)}E_z' \quad (8)$$

$$v_{1z}'=i\frac{e}{m\omega}E_z' \quad (9)$$

In the above expressions $\omega_c=eB_0/mc$ is the cyclotron frequency and

$$\gamma_0=\sqrt{1-v_0^2/c^2}=\sqrt{1-\beta^2}$$

From Maxwell's equations we obtain the wave equation

$$\frac{\partial^2\vec{E}'}{\partial t^2}+c^2\nabla\times(\nabla\times\vec{E}')=-4\pi\frac{\partial}{\partial t}(\vec{j}_b'+\vec{j}_p') \quad (10)$$

which becomes

$$(k^2c^2-\omega^2)\vec{E}'-\vec{k}c^2(\vec{k}\cdot\vec{E}')=-4\pi i\omega(\vec{j}_b'+\vec{j}_p') \quad (11)$$

for plane waves. The perturbed currents $\vec{j}_b'$ and $\vec{j}_p'$ are of the form:

$$\vec{j}_b'=-e(n_{b0}\vec{v}'+n_b'\vec{v}_0) \quad (12)$$

$$\vec{j}_p'=-e(n_0\vec{v}_1'+n'\vec{v}_1) \quad (13)$$

From the continuity equations, the perturbed beam density n'_b and the perturbed plasma density n' are:

$$n'_b = n_{b0} k v'_x / \omega \tag{14}$$

and

$$n' = n_0 k v'_{1x} / \omega \tag{15}$$

respectively.

Combining equations (4)—(15), we then obtain:

$$\begin{pmatrix} D_{xx} & D_{xy} & D_{xz} \\ D_{yx} & D_{yy} & D_{yz} \\ D_{zx} & D_{zy} & D_{zz} \end{pmatrix} \cdot \begin{pmatrix} E_x \\ E_y \\ E_z \end{pmatrix} = 0 \tag{16}$$

where

$$D_{xx} = \frac{\omega^2}{k^2c^2} - \frac{\omega^2}{k^2c^2} \frac{\omega_{b\perp}^2}{\omega^2 - \omega_c^2\gamma_0^2} - \frac{\omega^2}{k^2c^2} \frac{\omega_p^2}{\omega^2 - \omega_c^2} \tag{17}$$

$$D_{xy} = -D_{yx} = -i \frac{\omega\omega_c}{k^2c^2} \left(\frac{\omega_{b\perp}^2 \gamma_0}{\omega^2 - \omega_c^2\gamma_0^2} + \frac{\omega_p^2}{\omega^2 - \omega_c^2} \right) \tag{18}$$

$$D_{xz} = D_{zx} = -\frac{\beta\omega}{kc} \left(\frac{\omega_{b\perp}^2}{\omega^2 - \omega_c^2\gamma_0^2} - \varepsilon \frac{\omega_p^2}{\omega^2 - \omega_c^2} \right) \tag{19}$$

$$D_{yy} = \frac{\omega^2}{k^2c^2} - 1 - \frac{\omega^2}{k^2c^2} \frac{\omega_{b\perp}^2}{\omega^2 - \omega_c^2\gamma_0^2} - \frac{\omega^2}{k^2c^2} \frac{\omega_p^2}{\omega^2 - \omega_c^2} \tag{20}$$

$$D_{yz} = -D_{zy} = i \frac{\beta\omega_c}{kc} \left(\frac{\omega_{b\perp}^2 \gamma_0}{\omega^2 - \omega_c^2\gamma_0^2} - \varepsilon \frac{\omega_p^2}{\omega^2 - \omega_c^2} \right) \tag{21}$$

$$D_{zz} = \frac{\omega^2}{k^2c^2} - 1 - \frac{\omega_{b\|}^2 + \omega_p^2}{k^2c^2} - \beta^2 \frac{\omega_{b\perp}^2}{\omega^2 - \omega_c^2\gamma_0^2} - \varepsilon^2 \frac{\beta^2\omega_p^2}{\omega^2 - \omega_c^2} \tag{22}$$

In the above expressions the electron plasma frequency, transverse beam frequency and longitudinal beam frequency are $\omega_p^2 = 4\pi n_0 e^2/m$, $\omega_{b\perp}^2 = 4\pi n_{b0} e^2 \gamma_0/m = \varepsilon\gamma_0\omega_p^2$ and $\omega_{b\|}^2 = 4\pi n_{b0} e^2 \gamma_0^3/m = \varepsilon\gamma_0^3 \omega_p^2$, respectively. With ε we denoted the ratio $\varepsilon = n_{b0}/n_0 \ll 1$.

For a system of two identical electron plasmas, counterstreaming nonrelativistically along an external uniform magnetic field, the terms D_{xz}, D_{yz}, D_{zx} and D_{zy} exactly cancel [4—7]. Therefore the electromagnetic wave propagating perpendicular to $\vec{B}_0$ decomposes into the ordinary and extraordinary waves. The ordinary wave can become unstable with its electric field $\vec{E}'$ linearly polarized $\vec{E}' \parallel \vec{B}_0$, as it is usual for a Weibel-type instability. For a relativistic electron beam propagating in a magnetized plasma this does not happen. However, since the beam is weak ($\varepsilon \ll 1$) and if we consider the case when $\omega \ll ck$, the above decomposition remains true to a good approximation. Then to the lowest significant

order, the term $D_{zz} = 0$ describes the ordinary electromagnetic mode. Thus we have:

$$\frac{\omega^2}{k^2c^2} - 1 - \frac{\omega_{b\parallel}^2 + \omega_p^2}{k^2c^2} - \frac{\beta^2\omega_{b\perp}^2}{\omega^2 - \omega_c^2\gamma_0^2} - \varepsilon^2\frac{\beta^2\omega_p^2}{\omega^2 - \omega_c^2} = 0 \tag{23}$$

Neglecting ω^2/c^2k^2 compared with 1, $\omega_{b\parallel}^2$ compared with ω_p^2 and the term of order ε^2, we obtain:

$$1 + \frac{\omega_p^2}{k^2c^2} + \frac{\beta^2\omega_{b\perp}^2}{\omega^2 - \omega_c^2\gamma_0^2} = 0 \tag{24}$$

This dispersion relation gives for the growth rate the following expression:

$$\omega_i = \left[\beta^2\omega_{b\perp}^2\left(1 + \frac{\omega_p^2}{k^2c^2}\right)^{-1} - \omega_c^2\gamma_0^2\right]^{1/2} \tag{25}$$

The instability is purely growing, the axial magnetic field having a stabilizing effect, as in the nonrelativistic regime.

In the dispersion relation (23) the effect of return current is represented by the last term. This term is of order ε^2 and therefore the effect of the return current in Weibel-instability of a relativistic electron beam is negligible. A similar result has been obtained by I. Nebenzahl [12] in his analysis of the role of return currents in the transverse instability of a relativistic electron beam-plasma system, but this has been done in the absence of the external magnetic field.

(Received February 3, 1979)

REFERENCES

1 E. S. Weibel, Phys Rev. Letters, **2**, 83 (1959)
2. B. D. Fried, Phys. Fluids, **2**, 337 (1959).
3 H. Momota, Progr. Theor. Phys, **35**, 380 (1966)
4. K. F. Lee, Phys Rev., **181**, 447 (1969).
5. K. F. Lee, Phys. Rev., **181**, 453 (1969).
6 M. Bornatici and K F. Lee, Phys. Fluids **13**, 3007 (1970).
7. K. E. Zayed and A. B. Kitsenko, Plasma Phys ,**10**, 673 (1968).
8. J. L. Cox and W. H. Bennett, Phys. Fluids, **13**, 182 (1970).
9. D A. Hammer and N. Rostoker, Phys. Fluids, **13**, 1831 (1970).
10. R. Lee and R. N. Sudan, Phys. Fluids, **14**, 1213 (1979).
11. K. R Chu and N. Rostoker, Phys. Fluids, **16**, 1472 (1973).
12. I. Nebenzahl, Phys. Fluids, **15**, 311 (1972).

INSTABILITATEA WEIBEL A UNUI FASCICUL RELATIVIST DE ELECTRONI

(Rezumat)

Se studiază instabilitatea transversală în sistemul fascicul relativist de electroni-plasmă în prezența unui cîmp magnetic exterior. Rezultatele obținute arată că instabilitatea este absolută, cîmpul magnetic exterior are efect de stabilizare și că efectul curentului invers indus de fasciculul relativist este neglijabil.

STUDIA UNIV BABEŞ-BOLYAI, PHYSICA, XXIV, 2, 1979

FINITE AMPLITUDE DRIFT WAVES IN A TWO ION SPECIES PLASMA

M. CRISTEA

Introduction. The linear theory of drift waves is well established, whereas the study of nonlinear drift waves is more difficult, because of their multi-dimensional propagation. Drift waves transform into ion acoustic waves as the angle between the direction of propagation and the magnetic field decreases; moreover if the density gradient is sufficiently small the linear dispersion relation for drift waves reduces to that for ion acoustic waves This suggests that, at least in some cases, the propagation of nonlinear drift waves can be governed by a nonlinear equation similar to the Korteweg-de Vries (KdV) equation, which describes the one dimensional propagation of small but finite amplitude ion acoustic wave in a collisionless plasma [1, 2].

With the help of the usual reductive perturbation method, a multi-dimensional modified KdV equation describing the weakly nonlinear propagation of drift waves in a collisionless plasma was derived, and a special solution in the form of a solitary wave was obtained [3, 4].

Goswami and Buti [5] derived a modified multi-dimensional KdV equation for the propagation of nonlinear drift waves in a collisional plasma where both parallel resistivity and perpendicular viscosity are important. The nonlinear term of this equation is essentially the same as that for ion acoustic waves.

Recently, Tagare [6] has shown that the propagation of electrostatic drift waves of small but finite amplitude in a collisionless multi-component plasma is described by a modified KdV equation in a two dimensional space comprising the external magnetic field and the direction normal to a density gradient.

In this paper we want to extend Tagare's study of electrostatic drift waves in a multi-component plasma, considering the effect of ionic temperature on propagation of these waves.

Basic equations. We consider an inhomogeneous collisionless plasma consisting of hot isothermal electrons with temperature T_e and two ion species with masses m_1 and m_2 ($m_1 < m_2$) and temperatures T_1 and T_2 Plasma is located in a nearly homogeneous magnetic field $\vec{B} = B\vec{e}_z$ and a density gradient exists in the x-direction. If the magnetic field is sufficiently strong, the electrons drift in the y-direction with a velocity

$$v_0 = -\frac{T}{eB}\frac{1}{n_0}\frac{dn_0}{dx},$$

where e is the magnitude of the electronic charge and n_0 is the unperturbed plasma density which depends on x. Neglecting the induced magnetic field and the elec-

tron inertia, the basic equations which describe the system are given by

$$\frac{\partial n_1}{\partial t} + \nabla(n_1 v_1) + A n_1 v_{1x} = 0 \tag{1}$$

$$\frac{\partial v_{1x}}{\partial t} + (\vec{v}_1 \cdot \nabla) v_{1x} = \mu \left(\Omega v_{1y} - \frac{\partial \Phi}{\partial x} - \frac{\gamma_1 \theta_1}{n_1} \frac{\partial n_1}{\partial x} - A \gamma_1 \theta_1 \right) \tag{2}$$

$$\frac{\partial v_{1y}}{\partial t} + (\vec{v}_1 \cdot \nabla) v_{1y} = - \mu \left(\Omega v_{1x} + \frac{\partial \Phi}{\partial y} + \frac{\gamma_1 \theta_1}{n_1} \frac{\partial n_1}{\partial y} \right) \tag{3}$$

$$\frac{\partial v_{1z}}{\partial t} + (\vec{v}_1 \cdot \nabla) v_{1z} = - \mu \left(\frac{\partial \Phi}{\partial z} + \frac{\gamma_1 \theta_1}{n_1} \frac{\partial n_1}{\partial z} \right) \tag{4}$$

$$\frac{\partial n_2}{\partial t} + \nabla(n_2 \vec{v}_2) + A n_2 v_{2x} = 0 \tag{5}$$

$$\frac{\partial v_{2x}}{\partial t} + (v_2 \cdot \nabla) v_{2x} = \Omega v_{2y} - \frac{\partial \Phi}{\partial x} - \frac{\theta_2 \gamma_2}{n_2} \frac{\partial n_2}{\partial x} - A \gamma_2 \theta_2 \tag{6}$$

$$\frac{\partial v_{2y}}{\partial t} + (v_2 \cdot \nabla) v_{2y} = - \Omega v_{2x} - \frac{\partial \Phi}{\partial y} - \frac{\gamma_2 \theta_2}{n_2} \frac{\partial n_2}{\partial y} \tag{7}$$

$$\frac{\partial v_{2z}}{\partial t} + (\vec{v}_2 \cdot \nabla) v_{2z} = - \frac{\partial \Phi}{\partial z} - \frac{\gamma_2 \theta_2}{n_2} \frac{\partial n_2}{\partial z} \tag{8}$$

$$\Delta \Phi = n_e - n_1 - n_2 \tag{9}$$

$$\frac{\partial n_e}{\partial z} = n_e \frac{\partial \Phi}{\partial z} \tag{10}$$

$$\frac{\partial n_e}{\partial t} + \frac{1}{\Omega} \left[\frac{\partial n_e}{\partial y} \frac{\partial \Phi}{\partial x} - \frac{\partial n_e}{\partial x} \frac{\partial \Phi}{\partial y} - A n_e \frac{\partial \Phi}{\partial y} \right] + \frac{\partial}{\partial z} (n_e v_{ez}) = 0 \tag{11}$$

where

$$A = \frac{1}{n_0} \frac{dn_0}{dx}, \quad \Omega = \frac{\omega_i}{\omega_p} = \frac{eB}{m_2} \left(\frac{\varepsilon_2 m_0}{n_0 e^2} \right)^{1/2}, \quad \theta_i = \frac{T_i}{T_e}, \quad \mu = \frac{m_1}{m_2}$$

and the constants γ_i have the values. $\gamma_i = 1$ if the ions are isothermal, and $\gamma_i = 3$ if they are described by an adiabatic equation of state.

In these equations spatial distances are measured in Debye length unit $(\varepsilon_0 T_e / n_0 e^2)^{1/2}$, velocities in a characteristic velocity unit $(T_e/m_2)^{1/2}$, times are normalized to $(\varepsilon_0 m_2 / n_0 e^2)^{1/2}$, densities to unperturbed plasma density n_0 and electric potential to T_e/e.

Derivation of the modified KdV equation. We now consider an electrostatic drift wave of small but finite amplitude propagating in the yz-plane. Following [3] we take the stretched variables for the wave in the form

$$\zeta = \varepsilon^{1/2}(z - \lambda t), \quad \eta = \varepsilon^{1/2} y, \quad \tau = \varepsilon^{3/2} t, \tag{12}$$

while the variable for the inhomogeneity is

$$\zeta = \varepsilon x. \tag{13}$$

Here λ is a phase velocity of the wave and ε is a small parameter. The stretching (13) implies that the density gradient approaches zero faster than the wavenumber of the perturbation does [5].

The vector

$$U = (n_1,\ n_2,\ n_e,\ v_{1x},\ v_{2x},\ v_{ex},\ \Phi)$$

is expanded in powers of ε around

$$U^{(0)} = (\alpha,\ 1-\alpha,\ 1,\ 0,\ 0,\ 0,\ 0)$$

as

$$U = U^{(0)} + \varepsilon U^{(1)} + \varepsilon^2 U^{(2)} + \ldots$$

whereas the vectors

$$V = (v_{1x},\ v_{2x}) \text{ and } W = (v_{1y},\ v_{2y})$$

have the expansions

$$V = \varepsilon^{1/2}(\varepsilon V^{(1)} + \varepsilon^2 V^{(2)} + \ldots)$$
$$W = \varepsilon(\varepsilon W^{(1)} + \varepsilon^2 W^{(2)} + \ldots).$$

As $A \ll 1$ we put $A = \varepsilon^2 A^{(1)}$, where $A^{(1)}$ is of order unity. The concentration of light ions α is defined as $\alpha = n_1^{(0)}/(n_1^{(0)} + n_2^{(0)})$.

Having specified the stretching for the independent variables and the expansions for the dependent variables we can now derive the nonlinear partial differential equation which governs one of the first order quantities, for example Φ^1. Using the reductive perturbation method [3] we substitute the mentioned expansions into (1) — (11) and equate coefficients of different powers of ε to zero. Then, one has

$$n_1^{(1)} = \frac{\alpha}{\lambda} v_{1x}^{(1)} = \frac{\mu\alpha}{\lambda^2 - \mu\gamma_1\theta_1} \Phi^{(1)} \tag{14}$$

$$n_2^{(1)} = \frac{1-\alpha}{\lambda} v_{2x}^{(1)} = \frac{1-\alpha}{\lambda^2 - \gamma_2\theta_2} \Phi^{(1)} \tag{15}$$

$$n_e^{(1)} = \frac{1}{\lambda} v_{ex}^{(1)} = \Phi^{(1)} = n_1^{(1)} + n_2^{(1)} \tag{16}$$

$$v_{1x}^{(1)} = -\frac{\lambda^2}{\Omega(\lambda^2 - \mu\gamma_1\theta_1)} \frac{\partial\Phi^{(1)}}{\partial\eta} \tag{17}$$

$$v_{1y}^{(1)} = \frac{1}{\Omega}\left[\frac{\lambda^3}{\mu\Omega(\lambda^2 - \mu\gamma_1\theta_1)} \frac{\partial^2\Phi^{(1)}}{\partial\eta\partial\zeta} + \frac{\lambda^2}{\lambda^2 - \mu\gamma_1\theta_1} \frac{\partial\Phi^{(1)}}{\partial\xi} + A^{(1)}\gamma_1\theta_1\right] \tag{18}$$

Form (14) — (16) it follows

$$\frac{\mu\alpha}{\lambda^2 - \mu\gamma_1\theta_1} + \frac{1-\alpha}{\lambda^2 - \gamma_2\theta_2} = 1\,. \tag{19}$$

Equation (19) allows us to find the phase velocity λ. We notice that for a cold ion plasma ($\theta_1 = \theta_2 = 0$), equation (19) gets

$$\lambda^2 = 1 - \alpha + \mu\,\alpha,$$

which is just T a g a r e's result [6]. In the case of a warm ion plasma, two different values of λ^2 can be obtained, hence there are two important modes in this plasma, which propagate with different phase velocities A similar situation was theoretically predicted [7] and experimentally confirmed [8] for the one dimensional propagation of ion acoustic waves in a multi-component plasma with warm ions

Making use of (14) — (18) and then eliminating second order quantities, we finally get the modified KdV equation in two dimensional space

$$\frac{\partial \Phi^{(1)}}{\partial \tau} + P\Phi^{(1)}\frac{\partial \Phi^{(1)}}{\partial \zeta} + R\,\frac{\partial^3 \Phi^{(1)}}{\partial \eta^2 \partial \zeta} + S\left(\frac{\partial^3}{\partial \eta^2 \partial \zeta} + \frac{\partial^3}{\partial \zeta^3}\right)\Phi^{(1)} = 0 \tag{20}$$

where $P = B/A$, $R = C/A$, $S = D/A$ and

$$A = \frac{\mu\alpha}{(\lambda^2 - \mu\gamma_1\theta_1)^2} + \frac{1-\alpha}{(\lambda^2 - \gamma_2\theta_2)^2}$$

$$B = \frac{1}{2\lambda}\left[\frac{\mu^2\alpha(3\lambda^2 - \mu\gamma_1\theta_1)}{(\lambda^2 - \mu\gamma_1\theta_1)^3} + \frac{(1-\alpha)(3\lambda^2 - \gamma_2\theta_2)}{(\lambda^2 - \gamma_2\theta_2)^3} - 1\right]$$

$$C = \frac{\lambda^3}{2\Omega^2}\left[\frac{\mu\alpha}{\mu^2(\lambda^2 - \mu\gamma_1\theta_1)^3} + \frac{1-\alpha}{(\lambda^2 - \gamma_2\theta_2)^2}\right]$$

$$D = \frac{1}{2\lambda}$$

If $\theta_1 = \theta_2 = 0$, equation (20) reduces to equation (2 15) from [6], except the coefficient of the nonlinear term, where a misprint can be easily observed. It is worth noticing that in the case of a cold ion plasma [6], the coefficient of the nonlinear term is positive for any values of plasma parameters, whereas in the case considered here, the quantity B can become negative, so that P in (20) can be either positive or negative.

Stationary solutions of the modified KdV equation. Let us now consider the propagation of the drift wave in a particular direction such that the propagation direction makes an angle φ with the magnetic field. Therefore, the two space variables are now related through $\psi = \zeta \cos\varphi + \eta \sin\varphi$. In order to obtain the stationary solution of (20), we introduce into it the variable $\chi = \psi - U\tau$ (going over to a wave frame moving with velocity U, such that $\Phi^{(1)}$ depends on ψ and τ only through χ). Integrating the resulting equation and using the boundary conditions

$$\Phi^{(1)} \to 0, \frac{d\Phi^{(1)}}{d\chi} \to 0, \quad \frac{d^2\Phi^{(1)}}{d\chi^2} \to 0 \text{ as } (\chi) \to \infty$$

we obtain the intermediate integral

$$\left(\frac{d^2\Phi^{(1)}}{d\chi^2}\right)^2 = \frac{2d\,\Phi^{(1)2}}{\Delta^2}\left(1 - \frac{\Phi^{1)}}{\Phi_0}\right) \tag{21}$$

where

$$\Phi_0 = \frac{3U}{P\cos\varphi}, \qquad \Delta^2 = \frac{4\cos\varphi}{U}(R\sin^2\varphi + S).$$

The solitary wave solution of (20) and (21) is

$$\Phi^{(1)}(\chi) = \Phi_0 \operatorname{sech}^2(\chi/\Delta) \tag{22}$$

where Φ_0 is the amplitude of the drift solitary wave, and Δ is the width of this wave. As we have already mentioned, for a given set of plasma parameters, the coefficient P of the nonlinear term can be negative, consequently, in this case, the amplitude of the drift solitary wave will be negative too. This means that in a two ion species plasma with unequal ion temperatures, rarefactive drift solitary waves with negative amplitude can propagate.

Conclusions. The propagation of a small but finite amplitude drift wave in a collisionless, two ion species plasma can be described by means of a modified KdV equation. Such an equation has been derived by Tagare [6] for a cold ion plasma. Taking into account the finite ion temperatures, we have found two new features, namely:

a) in the linear approximation, there are two important modes propagating with different phase velocities given by (19);

b) the nonlinear equation admits stationary solutions in the form of solitary waves, whose amplitude can be negative, therefore rarefactive drift solitary waves can exist.

(Received February 20, 1979)

REFERENCES

1 R C. Davidson, *Methods in nonlinear plasma theory*, Academic Press, New York, 1972
2 M Washimi, T Taniuti, Phys Rev. Lett, **17**, 996 (1966).
3 K. Nozaki, T Taniuti, J Phys Soc Japan, **36**, 267 (1974)
4 N. Asano, Suppl Progr Theor Phys, No **55**, 52 (1974)
5 B N Goswami, B Buti, Plasma Phys, **19**, 53 (1977).
6. S. G Tagare, Canad J Phys, **55**, 861 (1977)
7. B. D Fried, R B. White, T. K. Samec, Phys Fluids, **14**, 2388 (1971).
8 M. Q Tran, S Coquerand, Phys Rev., **14 A**, 2301 (1976).

UNDE DE DRIFT CU AMPLITUDINE FINITĂ ÎNTR-O PLASMĂ CU DOUĂ SPECII DE IONI

(Rezumat)

Cu ajutorul unei metode perturbaţionale reductive s-a dedus o ecuaţie neliniară care descrie propagarea undelor de drift cu amplitudine finită într-o plasmă cu două specii de ioni, cu temperaturi diferite Această ecuaţie admite soluţii staţionare de forma undelor solitare, a căror amplitudine poate fi negativă.

STUDIA UNIV BABEŞ-BOLYAI, PHYSICA, XXIV, 2, 1979

SUR L'ÉQUATION DE DISPERSION D'UN MODÈLE DE PLASMA COMPOSÉ (II)

MIRCEA VASIU

1. **Introduction.** Le but de ce travail est de généraliser l'équation de dispersion obtenue antérieurement [1] Dans ce travail nous nous proposons d'étudier un modèle de plasma cosmique consitué d'un *composant ionique*, compressible, viqueux, doué d'une conductivité électrique finie et d'une pression anisotrope, en *mouvement de rotation* avec la vitesse angulaire $\vec{\Omega}$, dirigée d'après l'axe Oz $(\vec{\Omega}(0, 0, \Omega))$, sous l'action d'un champ magnétique uniforme et de son propre champ gravifique et d'un *composant neutre*, compressible, visqueux, en *mouvement de rotation* avec la vitesse angulaire $\vec{\Omega}_n$, dirigée d'après l'axe Oz $(\vec{\Omega}_n(0, 0, \vec{\Omega}_n))$, sous l'action du même champ gravifique. Nous admettons que les vitesses angulaires ont des valeurs distinctives. Nous choisirons comme système de référence le système de coordonnées cartésiennes Oxyz.

À l'intérieur du plasma le champ magnétique $\vec{B}_0$ possède une composante dirigée d'après l'axe Ox.

Nous utilisons les resultats obtenus par nous [1] et par Chhonkar, Bhatia [2]. À la différence des travaux cités nous prenons en considération l'action simultanée des vitesses angulaires des composants du plasma

2. **Equations magnétohydrodynamiques pour l'état perturbé du plasma.** En tenant compte de toutes ces suppositions, le système d'équations magnétohydrodynamiques pour l'état perturbé du plasma s'écrit de la manière suivante:

$$\rho_0 \frac{\partial \vec{u}}{\partial t} = -\nabla(\delta \overleftarrow{P}) - \rho_0 \nabla(\delta V) + 2\rho_0 \vec{u} \times \vec{\Omega} + \rho_0 \nu_c(\vec{u}_n - \vec{u}) + \tilde{\mu} \Delta \vec{u} + \frac{\vec{\mu}}{3} \nabla(\nabla \cdot \vec{u}) + \frac{1}{4\pi}(\nabla \times \delta \vec{B}) \times \vec{B}_0, \tag{1}$$

$$\rho_{n0} \frac{\partial \vec{u}_n}{\partial t} = -\nabla(\delta p_n) - \rho_{n0} \nabla(\delta V) - \rho_0 \nu_c(\vec{u}_n - \vec{u}) + 2\rho_{n0} \vec{u}_n \times \vec{\Omega}_n + \tilde{\mu}_n \Delta \vec{u}_n + \frac{\mu_n}{3} \nabla(\nabla \cdot \vec{u}_n), \tag{2}$$

$$\frac{\partial(\delta \rho)}{\partial t} = -\rho_0 \nabla \cdot \vec{u}, \tag{3}$$

$$\frac{\partial(\delta \rho_n)}{\partial t} = -\rho_{n0} \nabla \cdot \vec{u}_n, \tag{4}$$

$$\frac{\partial(\delta\vec{B})}{\partial t} = \nabla \times (\vec{u} \times \vec{B}_0) + \nu_m \Delta(\delta\vec{B}), \tag{5}$$

$$\Delta(\delta V) = 4\pi G(\delta\rho + \delta\rho_n), \tag{6}$$

où la signification des notations utilisées est donnée dans le travail [1]. Admettons que de petites perturbations se propagent dans le plasma sous la forme des ondes planes transversales [1]

$$\delta\varphi = \varphi^* exp[i(kz - \omega t)]. \tag{7}$$

En remplaçant (7) dans les équations (1)—(6), écrites en projection sur les axes Oxyz, on parvient au système d'équations pour les amplitudes des perturbations

$$[\tilde{\rho}_n\omega^2 + i\omega(\nu_c + \tilde{\nu}_n k^2)]\xi^*_{nx} = i\nu_c\omega\xi_x + 2\tilde{\rho}_n i\omega\Omega_n\xi^*_{ny}, \tag{8}$$

$$[\tilde{\rho}_n\omega^2 + i\omega(\nu_c + \tilde{\nu}_n k^2)]\xi^*_{ny} = i\nu_c\omega\xi_y - 2\tilde{\rho}_n i\omega\Omega_n\xi^*_{nx}, \tag{9}$$

$$\left[\tilde{\rho}_n(\omega^2 - k^2 v^2_{ns} + 4\pi G\rho_{n0}) + i\omega\left(\nu_c + \frac{4}{3}k^2\tilde{\nu}_n\right)\right]\xi_{nz} = (i\nu_c\omega - 4\pi G\rho_{n0})\xi_z, \tag{10}$$

$$[\omega^2 + i\omega(\nu_c + k^2\tilde{\nu})]\,\xi_x - 2i\omega\Omega\xi_y = i\nu_c\omega\xi_{nx}, \tag{11}$$

$$2i\omega\Omega\xi_x + [\omega^2 + i\omega(\nu_c + k^2\tilde{\nu})]\xi_y + i\nu k^2\omega\xi_z = i\nu_c\omega\xi_{ny} \tag{12}$$

$$\begin{aligned} -i\omega\nu k^2\xi_y + \left[\omega^2 + i\omega\left(\nu_c + \frac{4}{3}k^2\tilde{\nu}\right) - (k^2 v_s^2 - 4\pi G\rho_0) + \frac{ik^2 v_A\omega^2}{\nu_m k^2 - i\omega}\right]\xi_z = \\ = (i\nu_c\omega - 4\pi G\rho_{n0})\xi_{nz}, \end{aligned} \tag{13}$$

$$i\delta\rho = k\rho_0\xi_z, \tag{14}$$

$$i\delta\rho_n = k\rho_{n0}\xi_{nz}, \tag{15}$$

$$(\nu_m k^2 - i\omega)\delta B_x = -B_0 k\omega\xi_z, \tag{16}$$

$$\delta V = -\frac{4\pi G}{k^2}(\delta\rho + \delta\rho_n). \tag{17}$$

Introduisant les notations utilisées dans le travail [1] et aussi la notation

$$A_n = 2i\Omega_n\omega, \tag{18}$$

où Ω_n est la composante de la vitesse angulaire $\vec{\Omega}_n$ (du composant neutre du plasma), employant une méthode analogue avec celle du travail [1], finalement nous obtenons le système d'équations pour les grandeurs ξ_x, ξ_y, ξ_z

$$(D_n^2 D^2 - \Omega_c^2 - A_n A)\xi_x - (AD_n^2 + A_n D^2)\xi_y - CA_n\xi_z = 0, \tag{19}$$

$$(AD_n^2 + A_n D^2)\xi_x + (D_n^2 D^2 - \Omega_c^2 - A_n A)\xi_y + CD_n^2\xi_z = 0, \tag{20}$$

$$-C(E_n^2 - \Omega_{In}^2)\xi_y + [(E^2 - \Omega_I^2 + \Omega_A^2)(E_n^2 - \Omega_{In}^2) - \Omega_G^2]\xi_z = 0. \tag{21}$$

3. **L'équation de dispersion.** L'équation de dispersion s'obtient par l'annulation du déterminant formé par les coefficients des grandeurs ξ_x, ξ_y, ξ_z:

$$\begin{vmatrix} D^2D_n^2 - \Omega_c^2 - A_nA & -AD_n^2 - A_nD^2 & -CA_n \\ AD_n^2 + A_nD^2 & D^2D_n^2 - \Omega_c^2 - A_nA & CD_n^2 \\ 0 & -C(E_n^2 - \Omega_{In}^2) & K^2(E_n^2 - \Omega_{In}^2) \end{vmatrix} = 0 \tag{22}$$

où $K^2 = E^2 - \Omega_I^2 + \Omega_A^2 - \dfrac{\Omega_G^2}{E_n^2 - \Omega_{In}^2}$.

Faisant les calculs on obtient l'équation de dispersion cherchée:

$$\begin{aligned} &[(E^2 - \Omega_I^2 + \Omega_A^2)(E_n^2 - \Omega_{In}^2) - \Omega_G^2][(D_n^2D^2 - \Omega_c^2 - AA_n)^2 + \\ &+ (AD_n^2 + A_nD^2)^2] + (E_n^2 - \Omega_{In}^2)[(D_n^2D^2 - \Omega_c^2 - \\ &-AA_n)C^2D_n^2 + (AD_n^2 + A_nD^2)C^2A_n] = 0. \end{aligned} \tag{23}$$

Cas particuliers 1. En l'absence du mouvement de rotation pour le composant neutre du plasma ($A_n = 0$; $\Omega_n = 0$) l'équation de dispersion (23) se réduit à l'équation de dispersion obtenue par nous [1], 2. En l'absence du mouvement de rotation du composant neutre ($A_n = 0$) et aussi en l'absence du mouvevement de rotation du composant ionique du plasma ($A = 0$), l'équation de dispersion (23) se réduit à l'équation de dispersion obtenue par Chhonkar, Bhatia [2] (pour le cas de la propagation transversale des perturbations).

(Manuscrit reçu le 19 février 1979)

BIBLIOGRAPHIE

1 M. Vasiu, Studia Univ Babeş-Bolyai, Phys., 1, 54 (1979)
2. R. Chhonkar, P Bhatia, J Plasma Phys, **18**, 273 (1977).

ASUPRA ECUAŢIEI DE DISPERSIE A UNUI MODEL DE PLASMĂ COMPUSĂ (II)

(Rezumat)

În lucrarea de faţă se obţine ecuaţia de dispersie pentru un model de plasmă analog cu cel analizat în lucrarea [1], cu deosebirea că şi componenta neutră a plasmei se găseşte în mişcare de rotaţie Aplicînd un procedeu de calcul analog cu cel utilizat în lucrarea [1], autorul obţine ecuaţia de dispersie pentru modelul de plasmă studiat

În cazurile particulare ale absenţei mişcării de rotaţie pentru componenta neutră şi respectiv pentru componenta neutră şi pentru componenta ionică ale plasmei se obţine· ecuaţia de dispersie obţinută de autor în lucrarea [1] şi respectiv ecuaţia de dispersie obţinută de Chhonkar, Bhatia [2] (pentru cazul propagării transversale a perturbaţiilor)

STUDIA UNIV BABEŞ-BOLYAI, PHYSICA, XXIV, 2, 1979

A DEVICE MEANT FOR MEASUREMENT OF CRITICAL FLICKER FREQUENCY

E. ŢIGĂRA, M. O. IONESCU, C. IONESCU, E. TĂTARU

In the paper we describe a device meant to measure eye weariness; it presents the following advantages in comparison with the classical ones: they make use of integrated circuits and Light Emitting Diodes, the consume of energy is diminished, small cost and dimensions, long-lasting functioning.

The block-diagram of the device is illustrated in the following figure 1. The block-diagram contains a rectangular impulse generator (G) tension controlled, two logical portals AND-NO (P_1 and P_2) and other two power portals AND—NO (P_3 and P_4) that lead the LED-s bill-sticking (LED_1 and SED_2) (1)(4)(2). When building the device for the P_1 and P_2 portals we made use of CDB400E integrated circuit, and for the P_2 and P_4 portals — a CDB440E integrated circuit. The block-diagram contains two 5 K potentiometers by which the light — intensity provided by the two LED-s, is controlled. We have also used a 100Ω potentiometer meant to control flickering frequency of the two LED-s (3). The frequency band is limited between 20...90 Hz As the rectangular impulse generator that is tension controlled gives linear information, the scale of the potentiometer will be linear too. For the building of the generator (G) we used a CDB400E integrated circuit. The block-diagram of the

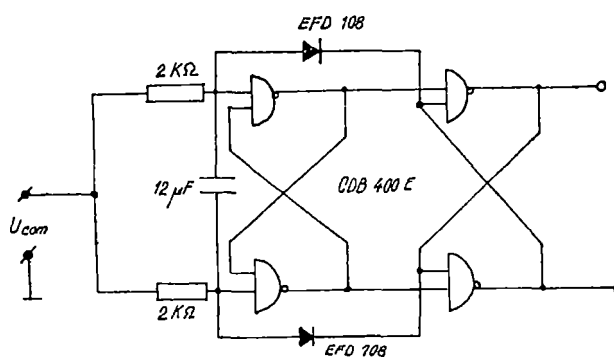

Fig 1 The block-diagram of the device meant for measurement of eye weariness

generator is given below (fig. 2). The commutator K permits consecutive or simultaneous supply with energy of two LED-s The energy supply is provided by a voltage stabilized rectifier that gives a 5 V voltage. The block diagram of the feeder is the one in fig. 3. The two LED-s are fit up in a viewfinder which is connected to the device by an elastic cable. The viewfinder we used ensures a good isolation of the two eyes against the light of the environment. In order to utilize the device we lay the viewfinder on the head of the subject

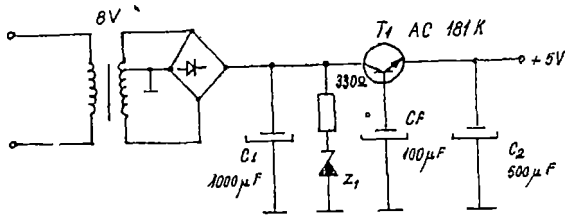

Fig. 2 The block-diagram of the generator

of the examination; after a delay necessary to the adaptation to the dark we begin the experiment The experiment consists in testing the critical point of the fusion by: stimuli of increasing or decreasing frequency, the changing of the colour we use; measurement of the dependence of the critical frequency of fusion upon the intensity of the stimuli. All these measurements will be

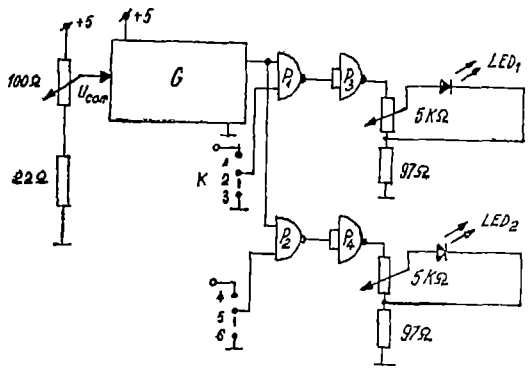

Fig 3. The block-diagram of the feeder.

correlated in time with different states of weariness of the subject and their age. A relaxed subject perceives the flickering of the LED up 50...55 Hz. For a weary subject or who presents psychic disorders, brain injuries, sight disorders, and so on, the critical frequency of fusion represents the frequency with which the flickering disappears, the subject seeing continuous light. Another aim of the device is to discover daltonism with subjects. The present device was built and tested. Subjects working in different fields and of different ages were examined. The results were registered in a tabel indicating a decrease of the fusion point depending on the age weariness of the subjects and on light intensity

The present device is recommended in work psychology in different fields of activity such as: shipping, motor and air-transport, railways, in optical and electronic industry, fine mechanics, automatized electric power stations and generally in fields where eye is highly solicited.

(Received February 10, 1979)

REFERENCES

1 D. Vasiliu, *Iniţiere în dispozitive semiconductoare*, Ed tehnică, Bucureşti, 1968
2. M. Săvescu, Al Popovici, M Popescu, *Circuite electronice*, Ed tehnică, Bucureşti, 1974.
3 A. Vătăşescu, *Circuite cu semiconductoare în industrie*, Ed. tehnică, Bucureşti, 1963.
4. A M Bonici-Bruievici, *Folosirea tuburilor electronice în fizica experimentală*, Ed. tehnică, Bucureşti, 1958
5. Al Roşca, *Psihologia experimentală*, Ed. didactică şi pedagogică, Bucureşti, 1962
6. S S Stevens, *Handbook of Experimental Psychology*, vol 1, Academic Press, New York, 1958, p 642–685
7 S. Bartley, B Howard, J. Exp Psychology, **21**, 338 (1938)
8 W. I. Crozier, E Wolf and G Zarrahn, J Gen Psychology, **23**,, 203 (1937)

APARAT PENTRU MĂSURAREA PRAGULUI CRITIC DE FUZIUNE A LICĂRIRILOR

(Rezumat)

În lucrare noi descriem un aparat destinat măsurării oboselii, ce are următoarele avantaje faţă de cele clasice utilizează circuite integrate şi diode electroluminiscente, consum de energie redus, gabarit şi preţ de cost mic, durată mare de funcţionare

STUDIA UNIV BABEŞ-BOLYAI, PHYSICA, XXIV, 2, 1979

REGULATOR PROPORŢIONAL DE TEMPERATURĂ

V. IONCU, GH. ILONCA şi I. POP

Introducere. Pentru diferite practici experimentale în domeniul temperaturilor joase este necesar să se menţină o temperatură constantă. Această cerinţă este asigurată de regulatorul de temperatură realizat, de obicei, electronic Lucrarea descrie un astfel de regulator proporţional pentru domeniul cuprins între 77—350 K.

În lucrarea [1] este efectuată o analiză teoretică a caracteristicilor regulatoarelor criotehnice de temperatură. Lucrarea [2] descrie un regulator de temperatură utilizînd un termistor ca element sesizor. Regulatorul este cu două game (seturi de piese interschimbabile), funcţionînd în intervalul de 77—273 K şi permiţînd, de asemenea, utilizarea şi a altor elemente sesizoare: platină, sesizor cu cărbune, germaniu etc., a căror caracteristici generale sînt descrise în [3].

Regulatorul descris în [4] foloseşte ca element sesizor joncţiunea bază-colector a unui tranzistor cu siliciu Pe acelaşi principiu funcţionează şi regulatorul descris în lucrarea [5]. În [6] sînt prezentate regulatoare de temperatură digitale, programabile, înzestrate cu sesizor de platină

Controlorul de temperatură porporţional acţionează după principiul „totul sau nimic". Potrivit acestui principiu de fiecare dată cînd temperatura sarcinii, detectată de sesizor, este inferioară temperaturii consemnate, energia totală este furnizată sarcinii. Cînd se atinge punctul de consemn, energia este tăiată complet şi nu este restabilită decît atunci cînd temperatura revine la valoarea determinată de sensibilitatea regulatorului. Schema regulatorului este prezentată în figura 1.

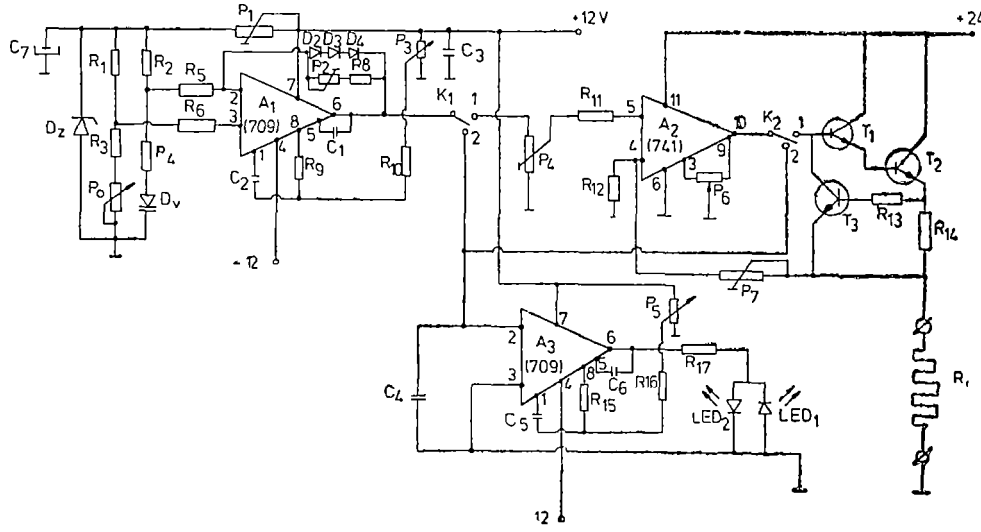

Fig. 1 Schema regulatorului proporţional de temperatură

Descrierea aparatului. Blocurile funcţionale ale regulatorului sînt puntea cu elementul sesizor de temperatură, comparatorul — realizat cu amplificatorul operaţional A_1 —, amplificatorul operaţional A_2 care, împreună cu tranzistoarele T_1, T_2 lucrază în regim de convertor tensiune-curent, amplificatorul operaţional A_3 care realizează, împreună cu cele două diode electroluminiscente LED_1, LED_2, un galvanometru electronic, precum şi dispozitivul de protecţie la supracurent, realizat cu tranzistorul T_3.

Traductorul în punte. Traductoarele care utilizează o punte Wheatstone pot să detecteze cele mai mici schimbări de impedanţă cu o foarte înaltă precizie. Această modificare de impedanţă este produsă de fenomenul de măsurat pe funcţia de transfer a traductorului. Cum circuitul punţii este un circuit static este necesară o sursă de excitaţie pentru a obţine un semnal electric funcţie de variaţia impedanţei.

La realizarea practică s-a optat pentru utilizarea unei diode varicap ca element sesizor de temperatură din considerente de realizare tehnologică, dependenţă cu linearitate bună de temperatură a tensiunii pe diodă, precum şi reproductibilitate foarte bună.

Puntea este realizată cu ajutorul grupului R_1, R_2, R_3, R_4, P_0, D_v, pe care se aplică o tensiune stabilizată cu ajutorul diodei Zenne D_z, pe una din diagonalele punţii. De pe cealaltă diagonală se alege tensiunea apărută ca urmare a variaţiei de temperatură cu influenţă asupra diodei varicap D_v. Tensiunea pe diodă s-a ales astfel încît curentul prin diodă să fie aproximativ 100μA.

Alegerea temperaturii se face cu ajutorul potenţiometrului P_0.

Comparatorul. Este realizat cu ajutorul amplificatorului A_1 (βA 709), al cărui coeficient de amplificare este determinat de grupul R_5, R_8, P_2, putînd fi ajustat cu ajutorul potenţiometrului P_2. Corecţia caracteristicii de frecvenţă s-a realizat cu ajutorul grupului C_1, C_2, R_9 Pentru reglajul „offset"-ului s-a prevăzut grupul P_3, R_{10}. Alimentarea operaţionalului A_1 se face de la o sursă stabilizată, simetrică. Grupul de diode D_2, D_3, D_4 a fost prevăzut pentru protecţia operaţionalului la apariţia de supratensiuni.

Convertorul tensiune-curent. Reprezintă un transformator tensiune-curent, cu sarcina la masă. Amplificatorul operaţional utilizat este un βA 741, a cărui amplificare este fixată cu ajutorul grupului R_{12}, P_7, P_4. Reglajul „offset"-ului se realizează cu ajutorul potenţiometrului P_6

Semnalul de la amplificatorul operaţional A_2 este preluat de tranzistorul compus T_1, T_2 care modifică tensiunea la bornele rezistenţei R , respectiv curentul prin rezistenţă. Cu ajutorul potenţiometrului P_4 se fixează valoarea tensiunii de ieşire, iar cu ajutorul potenţiometrului P_7 se fixează valoarea maximă a tensiunii de ieşire. T_3 se deschide la o valoare determinată a curentului prin rezistenţa de sarcină, valoare fixată cu ajutorul rezistorului R_{14} ($R_{14} = 0{,}7/I_{max}$).

Galvanometrul electronic. Este realizat cu ajutorul unui circuit integrat βA 709 funcţionînd în buclă deschisă, nepunîndu-se probleme de stabilitate şi urmărindu-se realizarea unui cîştig maxim.

Compensarea în frecvenţă se realizează cu ajutorul grupului C_5, C_6, R_{15}, iar reglajul „offset"-ului cu ajutorul potenţiometrului P_5. La ieşirea amplificatorului operaţional sînt legate două diode electroluminiscente LED_1 şi LED_2,

astfel încît la schimbarea polarităţii tensiunii de ieşire să emită semnal luminos numai acea diodă care este polarizată în sens direct.

Pentru diferenţă de tensiune, între cele două intrări, care tinde la zero, strălucirea luminii se micşorează, iar cînd această diferenţă este nulă, ambele diode vor fi stinse. Ţinînd cont de amplificarea mare a lui A_3 precizia de funcţionare a galvanometrului electronic este bună (pînă la 300 μV la ieşirea lui A_1 şi A_2).

Alimentarea. Se folosesc două surse de tensiune, stabilizate, una simetrică ± 12 V şi una pentru 24 V/5A.

Principiul de funcţionare. Alegerea temperaturii se face cu ajutorul potenţiometrului P_0. Acesta dezechilibrează puntea de rezistenţe, punte care cuprinde şi elementul traductor D_v.

Tensiunii de dezechilibru, proporţională cu temperatura dorită, i se opune tensiunea pe diodă, diferenţa între aceste două tensiuni fiind amplificată de amplificatorul operaţional βA 709 (A_1). Semnalul de la ieşirea lui A_1 este preluat de amplificatorul A_2, ce lucrează în regim de transformator tensiune-curent şi amplificat, apoi comandă curentul prin rezistenţa de încălzire R în sensul anulării diferenţei de tensiune menţionate mai sus. La atingerea temperaturii dorite puntea se găseşte din nou în stare de echilibru, diferenţa de tensiune pe cele două intrări ale amplificatorului A_1 este egală cu zero. Orice scădere a temperaturii sub valoarea prestabilită se traduce prin dezechilibrarea punţii şi intrarea în lucru a sistemului conform modelului menţionat mai sus. Vederea generală a aparatului este redată în figura 2.

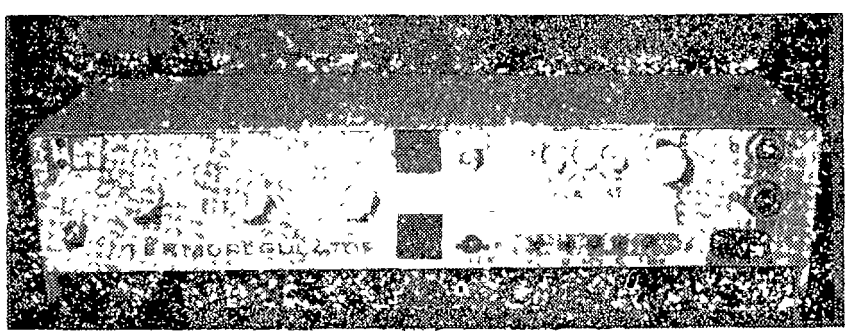

Fig 2. Vederea de ansamblu al aparatului

Modul de lucru. Sonda D se introduce în incinta de termostatare, se cuplează cele două surse (± 12V şi 24 V); se reglează „offset"-ul galvanometrului electronic punîndu-i intrările în scurtcircuit şi la masă, apoi se ajustează potentiometrul P pînă cînd ambele diode LED nu mai luminează; se reglează „offset"-ul lui A_1 şi A_2 comutînd K_1 şi respectiv K_2 pe poziţia 2 şi reglînd corespunzător P_3 şi P_6 pînă la stingerea celor două LED-uri. Cu ajutorul potenţiometrului P_0 se alege temperatura dorită (pentru mediul criogenic), cu comu-

tatorul K_1 şi K_2 în poziţia 1, moment în care dispozitivul este în stare de funcţionare. În acest moment galvanometrul electronic poate fi decuplat.

Caracteristici. Stabilitatea temperaturii în incintă pentru $-150\,°C$ a fost mai bună ca $\pm 0{,}02$ C, iar pentru $+10\,°C$ ea a fost mai bună ca $\pm 0{,}01\,°C$.

Concluzii. Utilizarea diodelor varicap ca element sesizor în regulatoarele de temperatură permite soluţionări simple, fără circuite asociate complicate, datorită marii lor sensibilităţi şi a liniarităţii foarte bune. Dimensiunile geometrice mici ale sondei permit utilizarea regulatorului pentru reglarea, mai ales, a incintelor mici care pot fi, de exemplu, criostate optice, dispozitive criochirurgicale etc. Cu ajutorul acestui termoregulator simplu şi cu fiabilitate ridicată se poate face o reglare precisă a temperaturii, cu minim de oscilaţii în jurul valorii de menţinut, deriva de temperatură în timp fiind practic nulă.

(Intrat în redacţie la 21 februarie 1979)

BIBLIOGRAFIE

1 E M Forgan, Cryogenics, **14**, 4, 207 (1974).
2 J. Veprek, Sloboproudy obroz, **35**, 12, 562 (1974)
3 J Veprek, *Electricka mereni nizkych teplot*, SNTL, Praha, 1977.
4 J. Sthanapati, S. N Bhattacharyya, Cryogenics, **16**, 12, 735 (1976)
5 P. V Kucinskij, V. M. Lomaka, Pribori i tehnika experimenta, **4**, 261 (1976)
6 Katalog firmy Planar Products LTD

TEMPERATURE PROPORTIONAL REGULATOR

(Summary)

The paper presents a simple temperature regulator in the range about 77 — 350 K, which provides temperature stability with accuracy of 0 02 K

As the sesisor a BB109 varicap diode was used.

The regulator was made using the principle of proportional regulator

STUDIA UNIV BABEŞ-BOLYAI, PHYSICA, XXIV, 2, 1979

A THERMOMETER AND LEVELMETER FOR CRYOGENIC LIQUIDS

GH. CRISTEA, V. IONCU, D. STĂNILĂ

Introduction. In research laboratories as well as in industrial frigotechniques it is often felt the need for rapid and accurate measurement of temperature. It also arises the necessity for location and controlling of the level of cryogenic liquids in closed containers. There are a number of devices reported in literature designed both for temperature measurement [1, 2, 3, 4] as well as for locating and control of cryogenic liquids [5, 6, 7]. However, for high reproducibility thermometers some very severe requirements are imposed which can only be fulfilled in highly specialized laboratories. That is why we have tested [8] the p-n junction of some Romanian made varicap diode as temperature sensors. In this paper we propose a simple apparatus designed for the measurement of temperature between 173 and 373 K, as well as for location and control of the level of liquid nitrogen, which uses as temperature sensors varicap diodes. In figure 1, the electronic diagram of the double function-thermometer and levelmeter-apparatus is shown.

The thermometer. The main components of the thermometer are: two 9V batteries, an usual μA-741 operational amplifier, an 100 μA microampermeter and the temperature sensor element — the varicap diode D_{v1} — of BB105 type. For operating as thermometer the K and K_1 switches should be in the position 1.

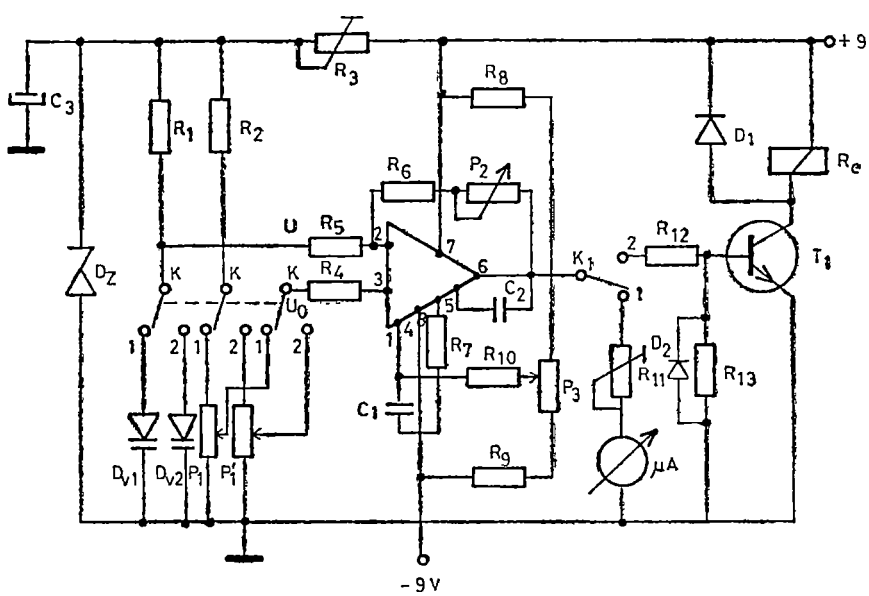

Fig. 1 The common electronic circuit of the thermometer and nivelmeter.

The diode D_{v1}, connected in one of the branches of the bridge, and positioned at the place where the temperature is to be measured, is powered with stabilized voltage by means of a Zenner diode The current through the directly biassed diode is set at a value below 300 μA by means of R_3, in order to avoid the selfheating effects. Initially the bridge is balanced by means of P_1 for a given temperature (usually the temperature corresponding to the beginning of the measurement), so that the output signal of the operational amplifier is zero. Any temperature change of the diode environment causes a change of the diode resistance, which in turns leads to the unbalance of the bridge. The appeared voltage is amplified by the operational amplifier and displayed on the microampermeter scale, calibrated previously in temperature degrees.

The frecquency compensation of the circuit is done with the group C_1, C_2 and R_7, while the amplification (sensitivity) is adjusted by means of the group R_5, R_6 and P_2 The off-set of the apparatus, when the input signal is zero, is established by P_3. To compensate any drift caused by disymetric wear of the batteries the P_3 potentiometer is accessibly placed. This adjustment should be checked up periodically.

The calibration of the microampermeter scale in temperature degrees has been done as follows. For each range of 10 K the instrument is set at „zero" by means of P_1 and at „100" (the end of the scale) by means of P_2. For each 10 K range of temperature there is a pair of P_1 and P_2; the change from one range to the next one is done by a multichannel switch (not shown in the diagram). The above procedure is correct only if the temperature dependence of the diode voltage is absolutely linear [8]. If this is not the case, the circuit must be completed with a „feed-back" reaction, which will ensure a linear output signal. In fact, the use of the varicap diodes as temperature sensors is possible in a much wider range of temperature than that mentioned above. The only limiting factors (in our case) were the length of the microampermeter scale and the linearity of the temperature characteristic of the diode voltage. For the future we intend to widen the range of measurement by using a digital instrument.

The levelmeter. The main components of the levelmeter are common with those of the thermometer. But, if we wish not only to locate the level of the cryogenic liquid but also to maintain it at a certain value, then an intermediary transistor T_1 and a driving relay R_e should be added.

The levelmeter works as follows: The switches K and K_1 are put in to position 2 By doing this the thermometer diode D_{v1} is replaced by the levelmeter diode D_{v2}, which is placed at the line where the level of the liquid nitrogen is to be kept At the same time, the transistor T_1 takes the places of the microampermeter.The transistor is necessary because the output signal of the operational amplifier is too weak (5—10 mA) to drive the relay R_e. To avoid the selfinduction currents the diode D_1 was also added.

The voltage on the diode D_{v2} varies from 0.7 V, at the room temperature, to 1.05 V at 77 K. We set the voltage $U_0 = 1.05$ V on the potentiometer P_1. Let U be the diode voltage on D_{v2}, at a temperature $T > 77$ K. When the level of the liquid nitrogen in the container reaches the diode D_{v2}, then $U = U_0$ and output signal of the amplifier is zero. The unbiassed transistor T_1 is blocked

and the relay commands the closing of the inlet electrovalve. When the level of nitrogen falls, then $U < U_0$, the output signal of the amplifier opens the transistor and the relay opens the inlet electrovalve. Thus the level of the liquid nitrogen is automatically kept at the position of the D_{v2} diode. The sensitivity of the apparatus can be adjusted by means of P_2.

To visualize the liquid nitrogen reaching the desired level it is enough to switch K_1 back in position 1. As long as the microampermeter shows a signal different from zero, the voltage on the diode is different from U_0, which means that the liquid nitrogen level is still below the desired level.

Conclusions. The apparatus is simple, cheap, low consuming and portable. As a thermometer it is about 40 times more sensitive than thermocouples and therefore it can easily read temperature with an accuracy of 10^{-3} K. The temperature characteristic of the diode voltage is linear within the above-mentioned range of temperature and free of histeresis effects against repeated coolings. As levelmeter the apparatus can successfully replace other equipment designed to this purpose. It can be useful in research laboratory and industrial frigotechniques.

(Received February 22, 1979)

REFERENCES

1. D I. Marchidan, A Ciopec, *Temperatura, scări, metode si mijloace de măsurare*, Ed ştiinţifică şi enciclopedică, Bucureşti, 1977.
2 R. L. Rosenbaum, Rev Scient Instrum, **40**, 577 (1969).
3. C. M. Herzfeld and A I Dahl, *Temperature-Its Measurement and Control in Science and Industry*, vol 3, part 2, p 383, 1962.
4. M. H Edlow and H H. Plumb, Nat Bur. Stand., **71C**, 29 (1967).
5 M Sauzade et al, Cryogenics, **5**, 42 (1965).
6 E. A. Davies and D. S. Gosling, J. Scient. Instrum., **40**, 249 (1963).
7 Yu. I. Nechaev, Cryogenics, **2**, 175 (1962)
8. Gh. Cristea, V. Ioncu, D. Stănilă, Studia Univ Babeş-Bolyai, Phys., **XXV**, 1, (1980).

TERMOMETRU ŞI NIVELMETRU PENTRU LICHIDE CRIOGENICE

(Rezumat)

S-a realizat un aparat destinat măsurării temperaturii între 173 şi 373 K şi pentru reperarea şi controlul nivelului lichidelor criogenice în containere închise Atît pentru termometru cît şi pentru nivelmetru senzorul de temperatură este o diodă varicap BB105, de fabricaţie românească. Aparatul, portabil, are largi aplicaţii în laboratoarele de cercetare şi în instalaţiile criogenice industriale.

STUDIA UNIV BABEŞ-BOLYAI, PHYSICA, XXIV, 2, 1979

ON A METHOD FOR CALCULATION THE SHEAR-VISCOSITY OF A BINARY LIQUID METAL ALLOY

SPERANŢA COLDEA

1. **Introduction.** The first kinetic equation for pure fluids which employed the hard-sphere potential was derived and solved by Enskog [1]—[2]. Introducing the obtained distribution function into the mass, momentum and energy flux vectors, analytic expressions were achieved for the diffusion, viscosity and thermal conductivity coefficients

The hard-sphere potential model provides the simplest mathematical formalism of a kinetic theory for liquids. This potential was used by Thorne and Tham-Gubbins to develop a transport theory for binary liquids [2] and for a m-component liquid mixture, respectively [3].

Dymond and Alder were the first to use implementation of Enskog mathematical formalism of hard-sphere potential with diameters shrinking with increasing temperature [4], i. e, the implementation of the kinetic theory of hard-spheres with „effective" soft spheres. The physical picture of soft spheres is a more realistic description of the real liquid than one of hard spheres.

Ascarelli and Paskin applied the Dymond-Alder theory [4] to pure liquid metals and obtained very good numerical results for the self-diffusion of such liquids [5].

Protopapas, Andersen and Parlee developed a corresponding states principle for the temperature dependence of the hard sphere diameters of liquid metals [6]. With the formula for this temperature-dependence and the Enskog's theory corrected on the basis of molecular dynamics calculations [7] they obtained excellent numerical results for the temperature-dependence of self-diffusion coefficients of pure liquid metals for which experimental data were available.

The proposed model was tested, too, on the calculation of the structure factors of 71 binary liquid metal alloys of different temperatures and compositions [8]; the results are in good agreement with both theoretical results and available experimental data [8].

In the present work, to predict the shear viscosities of several binary alloys, the previous proposed simulation of a binary liquid metal alloy by a hypothetical single-component hard-sphere liquid is used [6], [8].

2. **The theoretical model of shear-viscosity calculations.** Our model is based on several important assumptions. first, that a real binary liquid metal alloy may be treated as a binary hard-sphere fluid, second, that this fluid can be simulated by a hypothetical single-component hard-sphere liquid, the overall molecular interactions of which are described by the „effective" soft-sphere potential previously established for pure liquid metals [6], [10]. This „effective" potential was extended to the treatment of binary liquid metal alloys [8], [9]. It is postulated that the temperature dependent hard-sphere potential for pure

liquids [6], also accurately describes all three kinds of intermolecular interactions in a binary alloy

The considered single-component hard-sphere liquid has four parameters of identity completely determining its structural and transport behaviour. Their analytic expressions used by us are presented below.

a) *The hard-sphere mass* The mass of a hypothetical sphere of the single component liquid is of the form [8]:

$$m_a = \frac{x_1 M_1 + x_2 M_2}{N} \tag{1}$$

where x_i are the respective atom fractions of the real binary liquid alloy, N is Avogadro's number and M_i are the atomic weights of the two metals in the mixture.

b) *The number-density* The mass-density of a binary alloy is defined as:

$$\rho_a = \frac{M_a}{V_a} = \frac{(x_1 M_1 + x_2 M_2)}{V_a} \tag{2}$$

where V_a is the volume of one mole of alloy:

$$V_a = x_1 V_1^P + x_2 V_2^P \tag{3}$$

with V_i^P — the molar volume of the component liquid metal „i" in the pure state ($i = 1, 2$).

Thus, the number-density of the alloy is related to the mass-density through the following expression.

$$m_a = \frac{\rho_a}{m_a} = \frac{\rho_a N}{M_a} = \frac{N}{(x_1 M_1/\rho_1^P + x_2 M_2/\rho_2^P)} \tag{4}$$

ρ_i^P being the mass-density of the component „i" in the pure state. The number densities of the two components in the alloy can be taken from the relation:

$$n_i = x_i \cdot n_a \tag{5}$$

c) *The hard-sphere diameter* In this theory it is also taken into account the real shrinking of the hard-sphere diameters with the increasing temperature Thus, the previously hard-sphere expression for a pure liquid metal [6], [10] is also applicable to the considered hypothetical single-liquid. The hard-sphere diameter σ, at any absolute temperature T, is related to the hard — sphere diameter σ_m and to melting point T_m, through the relation:

$$\sigma \cong \sigma_m \left[1 - 0{,}112 \left(\frac{T}{T_m}\right)^{1/2}\right] \Big/ 0{,}888 \tag{6}$$

where the hard-sphere diameter at T_m is written as.

$$\sigma_m = 1{,}288 \left(\frac{M_a}{\rho_m}\right)^{1/3} \tag{7}$$

In the above expression ρ_m is the melting point density of the alloy.

Table 1

The shear—viscosity values calculated on the relation (10) (the Protopapas' method for σ' and η')

Composition of liquid alloy	46,4% Na — —53,6% K	12,2% Na— —87,8% K	65,1% Na— —34,9% K	93,4% Na— —6,6% K	78,4%Na —21,6%K	49,6%Ag— —50,4%Sn	31,8%Ag— —68,2%Sn	75%Ag— —25%Sn	70%Al— —30%Sn
T(°K)	388	388	388	388	388	853	803	1043	873
μ_1 (cP)	0,542	0,5482	0,5733	0,6799	0,6133	3,245	2,975	3,967	2,5624
Composition of liquid alloy	90% Al— —10% Sn	97% Al— —3% Sn	22% Cu— —88%Sn	55% Cu— —45%Sn	80%Cu— —20%Sn	45%Cu— —55%Sn	65%Cu— —35%Sn	70% In— —30%Hg	5%Tl— —95%Hg
T(°K)	933	933	793	1373	1073	903	1373	413	298
μ_1(cP)	2,775	2,13	3,172	3,3593	3,967	3,3512	3,32	2,95	2,327
Composition of liquid alloy	28,6%Tl— —71,4% Hg	3,42%Ga— —96,6%Hg	98%Ga— —2% Hg	60%Pb— —40% Hg	20%Pb— —80%Mg	80%Pb— —20%Mg	5%Pb— —95%Mg	31%Pb— —69%Mg	
T(°K)	298	298	323	323	755	845	576	901	
μ_1(cP)	2,52	2,667	1,91	2,67	2,175	2,869	1,8167	2,5783	
Composition of liquid alloy	50%Pb— —50% Bi	10%Pb— —90% Bi	80%Pb— —20%Bi	40%Pb— —60%Bi	90%Pb— —10%Bi				
T(°K)	427	593	539	427	603				
μ_1(cP)	2,655	3,12	3,001	2,62	3,84				

d) *The packing fraction.* We consider that all hypothetical liquids at their respective melting points T_m, have the same value of packing fraction. This is defined as:

$$\eta = \frac{\pi}{6} n_a \sigma_a^3 \tag{8}$$

where

$$\sigma_a = \left(\frac{6}{\pi} n_a \cdot \eta\right)^{1/3} \tag{9}$$

is the hard-sphere diameter of alloy Thus, the melting point packing fraction is:

$$\eta_m = \frac{\pi}{6} n_m \cdot \sigma_m^3 = 0{,}472 \tag{8'}$$

Having so precised these structural and transport properties of the considered single-component liquid, we can calculate the shear-viscosity coefficient of such a liquid using the formula deduced from the Enskog's theory [2], [9]:

$$\mu_1 = \frac{1{,}25}{\sigma'^2}\left(\frac{M_a k T}{N}\right)^{1/2} \cdot \left[\frac{4\eta'}{g(\sigma')} + 0{,}8 + 3{,}0456\, \eta' g(\sigma')\right] \tag{10}$$

The input data needed in this expression are: the melting point T_m, the absolute temperature T of the alloy, the atomic fractions of the two components x_i, the densities ρ_m and ρ_T, the atomic weight of the binary alloy, M_a, the computed hard-sphere diameter σ' and the packing fraction η' for the studied liquid. All these quantities are presented in tables 1 and 2.

We have estimated the shear-viscosity coefficients of 9 binary liquid metal alloys, at different compositions and temperatures, considered as single-component liquids: Na-K, In-Hg, Tl-Hg, Ga-Hg, Pb-Mg, Pb-Bi, Ag-Sn, Al-Sn, and Cu-Sn.

We used the corrected hard-sphere diameters σ' and packing fractions η' computed by Protopapas' and Enderby-North' methods [8], [11].

The calculated shear-viscosity values of the nine considered binary liquid alloys are not tested with the corresponding experimental data, because such data are not available to us up to the present. The obtained binary alloy viscosities results are given in tables 1 and 2, too.

In all cases under consideration, the viscosity values computed by us, using the two sets of input data, are in good agreement one with the other. We hope to obtain the necessary data and to make a more detailed discussion of the binary alloys viscosity behaviour. It is expected that the proposed theoretical method will succeed in predicting the viscosity of many other binary liquid alloys.

(Received February 23, 1979)

REFERENCES

1. D. Enskog and K Svensk, Vet —Akad. Hand., **63**, no. 4 (1921)
2. S Chapman and T.G. Cowling, *The mathematical theory of nonuniform Gases*, Cambridge Univ Press, London, 1954
3. M K Tham and K E Gubbins, J Chem Phys, **17**, 988 (1949)
4. J H. Dymond and B J. Alder, J. Chem. Phys, **45**, 2061 (1966).
5. P. Ascarelli and A Paskin, Phys. Rev, **165**, 222 (1967)
6. Protopapas, H. C Andersen and N A D Parlee, J Chem Phys, **59**, 15 (1973).
7. B. J Alder, D M Gass and T E Wainwright, J Chem Phys, **53**, 3813 (1970)
8. P. Protopapas and N A D Parlee, High. Temp. Sciences, **7**, 259 (1975)
9. S. Coldea, Revue Roum. Phys, **24**, 5, 459 (1979)
10. S Coldea, Studia Univ Babeş-Bolyai, ser Physica, fasc 2, 28, (1974), 1, 20 (1978)
11. J E Enderby and D M. North, Phys Chem. Liquids, **1**, 1 (1968)

ASUPRA UNEI METODE DE CALCUL A VISCOZITĂŢII LAMINARE ÎNTR-UN ALIAJ BINAR LICHID

(Rezumat)

Pentru a estima valorile viscozităţilor laminare ale unor aliaje binare lichide, se foloseşte în această lucrare metoda simulării amestecurilor binare lichide printr-un lichid ipotetic unicomponent ,precum şi modelul Enskog al fluidului de sfere rigide S-au calculat astfel coeficienţii de viscozitate laminară pentru 9 aliaje binare lichide (pe bază de mercur, plumb şi staniu), la diferite temperaturi şi compoziţii

STUDIA UNIV BABEŞ-BOLYAI, PHYSICA, XXIV, 2, 1979

EINE VELIMPULSMETHODE ZUR MESSUNG DER T_1—RELAXATIONSZEIT DER PROTONEN IN ThH_x—ZWEIPHASIGEN WASSERSTOFFKONZENTRATIONEN*

P. MAXIM, R. MÜLLER, B. SCHNABEL****

Eine der wichtigsten Eigenschaften der Metallhydride ist die sehr haufige hohe Beweglichkeit der Wasserstoffatome im Metallgitter Die umfangreichesten Informationen bezuglich dieser Beweglichkeit liefern die NMR-Methoden, unter diesen in erster Reihe die Analyse der Temperaturanderung der T_1 —, $T_{1\rho}$ — oder T_{2e} —Relaxationszeit.

Die einfachste Methode zur Messung der T_1 —Relaxationszeiten, die mit Hilfe eines Impulsspektrometers durchzufuhren ist, ist die $\pi - \frac{\pi}{2}$ Nulldurchgangsmethode. Die Messung der T_1 —Relaxationszeit erfolgt dadurch, dass die Magnetisierung, die im Gleichgewichtszustand paralel zu $H_0 \mid\mid z$ steht, infolge der Einstrahlung eines π—Impulses in die $-z$ Richtung umgekippt wird Zur Messung der Zeit des Nulldurchganges aus der die T_1-Relaxationszeit zu errechnen ist, wird ein $\frac{\pi}{2}$-Impuls eingestrahlt.

Die Entwicklung nueurer NMR—Methoden, wie z.B die Methode der Vielimpuls NMR—Festkorper-Hochauflosung (NMR—FKHA), ermoglicht die Messung der chemischen-und der Knight-Verschiebungen solcher Kerne, deren Messung mit der konventionellen Breitlinienmethoden nicht moglich ist Diese Methode zwingt dem Spinoperatorfaktor der Dipol-Dipol-Wechselwirkung (DDWW) $\mathcal{H}_d = b_{ij})I_iI_j - 3I_{zi}I_{zj})$ zwischen den in der Probe vorhandenen Kernen eine Zeitabhangigkeit auf, die durch impulsformige (oder auch kontibuierliche) Einstrahlung starker hochfrequenter Magnetfelder auf die Probe erreicht wird. Durch diese Impulse, die bestimmte Abstande und Hochfrequenzphasen gegeneinander haben, kann man erreichen, dass das Verhalten des Spinnsystems in einem Koordinatensystem, das mit der Frequenz der Einstrahlung rotiert, von einem effektiven Hamiltonoperator beschrieben wird. Durch eine bestimte Auswahl der Impulsabstande und Hochfrequenzphasen kann man in diesem Koordinatensystem die DDWW zum Verschwinden bringen und damit eine verschmalerte Resonanzlinie erreichen.

Es wurde gezeigt [1—3], dass die Quermagnetiesierung $M_{x'}(t)$ in dem rotierenden Koordinatensystem mit einem effektiven Zeitkonstanten T_{2e} gegen Null verschwindet. T_{2e} stellt die im allgemeinen gegenuber transversalen Relaxationszeit T_2 verlangerte effektive transversale Relaxationszeit T_{2e} dar. Das Verhaltnis T_{2e}/T_2 ist demzufolge als ein Mass fur die Wirksamkeit des Verschmalerungsexperiments anzusehen. ($T_{2e} \cong 10^2 T_2$).

---

* Teil der Dissertationsschrift von P. Maxim prasentiert 1977 an der Universitat Jena (D.D R)

** Sektion Physik der Friedrich-Schiller"—Universitat Jena

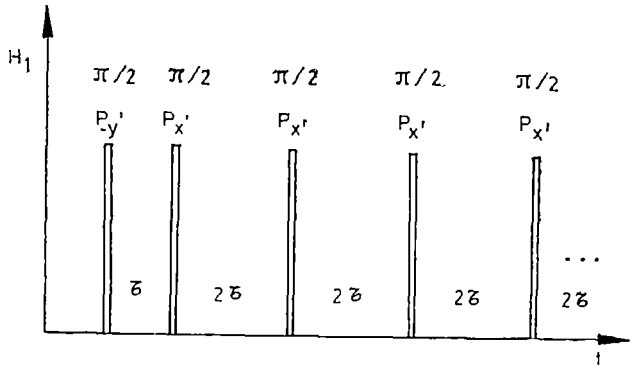

Abb 1 *MW* 4 — Impulsfolge.

Die T_{2e}-Relaxationszeit ist jeder verschmalernden Vielimpulsfolge charakteristisch. Sie ist aber direckt mit Hilfe der sogenannten *MW* 4-Impulsfolge (Abb.1) zu messen, die ausserdem den Vorteil hat, das sie eine einfache Auswertung der Parameter, die die Bewegung charakterisieren, ermoglichen.

Diese Impulssequenz bewirt die Bildung einer Folge von Festkorperechos, deren Amplituden mit der T_{2e}-Zeitkonstante abnehmen. Im Falle einer homonuklearen Spinsystems mit dem Spinwert 1/2 wie bei den Wasserstofkernen, ergibt sich auch fur T_{2e} eine dem T_1 ahnliche Temperaturabhangigkeit. So zeigt T_{2e} ein Minimum fur $\tau_c/\tau = \pi/2$ wo τ_c die Korrelationszeit der thermischen Bewegung ist; fur $\tau_c \ll \tau$ ist $T_{2e} \sim \tau_c^{-1}$ und fur $\tau_c \gg \tau$ ist $T_{2e} \sim \tau_c$. Die Relaxation wird am effektivsten wennn das Frequenszpektrum der betreffenden Bewegung ein Maximum in der Nahe der effektiven Resonanzfrequenz $\omega_e = \frac{2\pi}{4\tau}$ hat.

Aus dem Vergleich der zwei Methoden geht hervor, dass sie die Beobachtung der thermischen Bewegung in verschiedenen Frequenzbereichen ermoglichen und sich dadurch ergänzen.

Zum Unterschied von der oben erwähnten $\pi - \frac{\pi}{2}$ Impulsfolge fur dem Nachweis der zeitabhangigen z-Magnetisierung wird eine *MW* 4-Folge anstelle des $\frac{\pi}{2}$ — Impulses verwendet (π—MW 4-Verfahren). Der Nachweis erfolgt diesmal durch die Beobachtung der effektiven Relaxations-funcktion mit der Abfallszeitkonstanten T_{2e} Die Zeit zwischen π-Impuls und Beginn der *MW* 4-Folge ist anhand der Beobachtung der effektiven Relaxationsfunktion auf denjenigen Wert t_v justierbar, bei der die Magnetisierung gerade Null ist, und demzufolge auch die effektive Relaxationsfunktion wahrend der *MW* 4-Folge Null ist. Die einzige Bedingung fur die Anwendbarkeit ist $T_1 \gg T_{2e}$, eine Bedingung, die jedoch ohnehin bei der Anwendung der Linienverschmälerung erfüllt ist.

Die π-*MW* 4-Impulsfolge hat gegenuber der $\pi - \frac{\pi}{2}$ Methode die folgende Vorteile:

1. Da $T_{2e} \gg T_2$, kann man viel leichter t_v in Videobetrieb auf dem Oszillografischirm bestimmen.

2. Mit Hilfe dieser Methode ist es moglich, die gleichzeitige Messung von T_1 und T_{2e} durchzufuhren, da eine erhebliche Senkung der Messzeit bei der Messung in Abhangigkeit von der Temperatur entritt.

3. Es ist sehr leicht moglich, eine Erhohung der Genauigkeit der Messung von t_v und damit T_1 durch Akkumulation der MW 4-Signale zu erreichen. Damit wird eine sehr genaue Ausmessung des Verlaufs von $M_z(t)$ moglich, indem man die MW 4-Impulsfolge zu verschiedenen Zeiten einstrahlt und die MW 4-Anfangsamplitude misst.

4. Sollten es zwei Sorten von Kernen sein (Kerne mit demselben Spinwert, die jedoch, z.B , verschiedener Phasen gehoren), die unterschiedlich relaxieren, so wird der T_1-Relaxationsprozess durch

$$M_{T_1}(t) = \frac{A_1}{A_1 + A_2} \exp\left(-\frac{t}{T_1^{(1)}}\right) + \frac{A_2}{A_1 + A_2} \exp\left(-\frac{t}{T_1^{(2)}}\right) \tag{1}$$

beschrieben und der T_{2e}-Relaxationsprozess durch

$$M_{T_{2e}}(t) = \frac{A_1}{A_1 + A_2} \exp\left(-\frac{t}{T_{2e}^{(1)}}\right) + \frac{A_2}{A_1 + A_2} \exp\left(-\frac{t}{T_{2e}^{(2)}}\right) \tag{2}$$

wo A_1 und A_2 die Magnetisierungsamplituden der zwei Kernsorten zur Zeit Null sind. Wenn $T_1^{(1)}$ und $T_1^{(2)}$ unterschiedlich sind, so relaxieren dann die zwei Komponenten laut Abbildung 2.

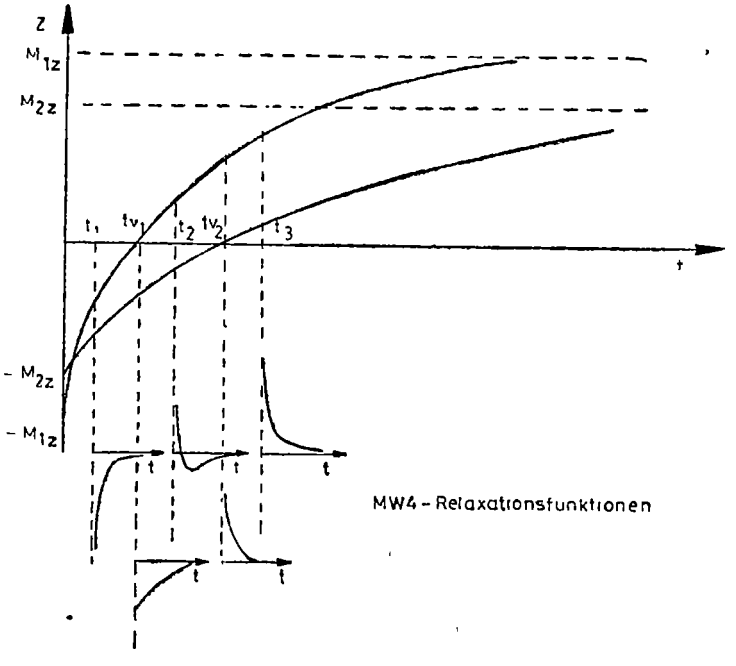

Abb. 2 Feststellung des Nulldurchganges der Relaxationsfunktionen zweier Komponenten einer Mischphase.

In Abb 2 wurde ohne Beschrankung der Allgemeinheit angenommen, dass $T_1^{(2)} > T_1^{(1)}$, $A_1 < A_2$ und $T_{2e}^{(2)} > T_{2e}^{(1)}$ gilt Strahlt man die *MW* 4-Impulsfolge nach der t_{v1}-Zeit ein, so bleibt nur die Komponente 2 ubrig, die dann mit der Zeitkonstanten T_{2e} relaxiert. In einem zweiten Experiment ist nach der Zeit t_{v2} die Magnetisierung der Komponente 2 Null, so dass dann nur die Komponente 1 weiter zu beobachten ist. In der Zeit t_1, t_2 oder t_3 beobachten wir die entsprechenden Bilder, je nachdem ob die zwei Komponenten gleiche Vorzeichen (negativ bei t_1, positiv bei t_3) oder umgekehrte Vorzeichen haben (bei t_2). Daraus folgt der Vorteil dieser Methode, dass mit Hilfe der *MW* 4-Impulsfolge die T_1-Relaxationszeit der zwei Komponenten unmittelbar und getrennt zu messen sind. Entsprechend Pkt. 2 kann in einem Messvorgang gleichzeitig $T_1^{(1)}$ und $T_{2e}^{(2)}$ bzw $T_1^{(2)}$ und $T_{2e}^{(1)}$ gemessen werden.

Mit Hilfe dieser Methode wurde die Temperaturabhängigkeit der T_1-Relaxationszeiten der Protonen in ThH_x mit $x = 1{,}90$; $2{,}19$; $2{,}50$; $2{,}90$, $3{,}26$; $3{,}54$; $3{,}61$. Sie ermoglichteuns die gleichzeitige und unmittelbare Messung der T_1-Relaxationszeiten der Protonen auch solcher Konzentrationen ($x = 2{,}19$; $2{,}50$; $2{,}90$; $2{,}90$, $3{,}26$), die eine Mischung zweier Phasen (Dihydrid und Th_4H_{15}) sind [4].

Die Messungen wurden an einem im Rahmen des Wissenschaftsbereiches Hochfrequenzspektroskopie der Sektion Physik der Universität Jena aufgebauten 60 *MHz* Protonenresonanzspektrometers fur FKHA — Vielimpuls- und Relaxationszeitmessungen durchgefuhrt Es wurde mit einer minimalen τ-Zeit der *MW* 4-Impulsfolge von 3 μs gearbeitet.

(Eingegangen am 23 Februar 1979)

LITERATUR

1 W Grunder, Dissertation, Leipzig, 1973
2 R. Willsch, Dissertation, Jena, 1975
3. R. Muller, R. Willsch, J Magn Res, **21**, 135 (1976)
4. W M. Mueler, J. P Blackledge, G. Libowitz, *Metall Hydrides*, Acad Press, New york—London, 1968

MĂSURAREA TIMPULUI DE RELAXARE T_1 A PROTONILOR ÎN DOMENIUL CONCENTRAŢIILOR BIFAZICE A TH_x CU AJUTORUL UNEI METODE DE MULTIPLE PULSURI

(Rezumat)

Prin aplicarea unei secvenţe de impulsuri MW 4 în urma unui impuls π s-a reuşit măsurarea directă şi concomitentă a timpilor de relaxare T_1 şi T_2 a protonilor în hidrura de toriu, precum şi a timpilor de relaxare T_1 a două componente, aparţinînd concentraţiilor de hidrogen corespunzătoare unui amestec de faze

STUDIA UNIV BABEŞ-BOLYAI, PHYSICA, XXIV, 2, 1979

CONSIDÉRATIONS SUR UNE LOI DE CONSERVATION DE LA TURBULENCE MAGNÉTOHYDRODYNAMIQUE ISOTROPE

STELIANA CODREANU

On sait que dans le cas spécifique du mouvement turbulent, entièrement homogène et isotrope, de vitesse moyenne nulle dans tout le volume du fluide, il y a la loi de conservation [1]

$$\int \overline{(\vec{v}\vec{v}')}r^2 \, dV = \text{const.} \tag{1}$$

déduite, pour la première fois, par L. Loytsianski, $\vec{v}$ et $\vec{v}'$ étant les vitesses du fluide en deux points voisins du flux, $\vec{r}$ — la distance entre ces deux points, l'intégrale étant prise dans tout le volume du fluide et la barre désignant la médiation

Des relations analogues à (1) ont été établies dans le cas de la turbulence magnétohydrodynamique par S. Chandraskhar [2]. Particulièrement, pour le cas du champ magnétique, on a déduit la relation :

$$\overline{(\vec{h}\vec{h}')}r^2 \, dV = \text{const.} \tag{2}$$

En s'appuyant sur la relation

$$\int \overline{(rot \ \vec{v} \ \text{rot} \ \vec{v}')}r^2 \, dV = 0 \tag{3}$$

pour une turbulence isotrope [3], et en faisant une analogie entre rot $\vec{v}$ et $\vec{h}$, on trouve que la constante de (2) est nulle.

En utilisant une méthode différente, A L. Tseskis [4] a montré que

$$\int \overline{(\vec{h}\vec{h}')}r^2 \, dV = 0 \tag{4}$$

Nous nous proposons de montrer, en utilisant la méthode [4], qu'il y a aussi la relation :

$$\int \overline{(rot \ \vec{h} \ \text{rot} \ \vec{h}')}r^2 \, dV = 0 \tag{5}$$

ou

$$\int \overline{(\vec{j}\vec{j}')}r^2 \, dV = 0 \tag{6}$$

$\vec{j}$ et $\vec{j}'$ étant la densité de courant en deux points voisins du fluide conducteur turbulent.

Soit l'intégrale

$$\vec{N} = \int (\vec{r} \times \vec{j})\ \mathrm{d}V \tag{7}$$

prise dans tout le volume du fluide.

Avec $\vec{j} = \nabla \times \vec{h}$, (7) dévient

$$\vec{N} = \int [\vec{r} \times (\nabla \times \vec{h})]\,\mathrm{d}V \tag{8}$$

En utilisant l'identité :

$$(\nabla \times \vec{h}) \times \vec{r} = -\vec{r} \times (\nabla \times \vec{h}) - (\vec{h} \times \nabla) \times \vec{r} \tag{9}$$

où ∇ agit sur toutes les variables situées à sa droite, on peut mettre (8) sous la forme :

$$\vec{N} = \int [\vec{r} \times (\nabla \times \vec{h})]\,\mathrm{d}V = -\int [(\Delta \times \vec{h}) \times \vec{r}]\,\mathrm{d}V - \int [(\vec{h} \times \nabla) \times \vec{r})\mathrm{d}V \tag{10}$$

On transforme la première intégrale du second membre dans une intégrale de surface. Ainsi, on a

$$\int [(\nabla \times \vec{h}) \times \vec{r}]\mathrm{d}v = \oint \vec{r} \times (\vec{h} \times \vec{ds}) \tag{11}$$

en sachant que [5] :

$$\int [(\vec{r}\nabla)\vec{h} + \vec{h}\ (\nabla\vec{r}) - \nabla(\vec{r}\vec{h})]\mathrm{d}V = \oint r \times (\vec{h} \times \vec{ds})$$

Donc (10) peut s'écrire comme :

$$\vec{N} = -\oint \vec{r} \times (\vec{h} \times \vec{ds}) - \int [(\vec{h} \times \nabla) \times \vec{r}]\mathrm{d}V \tag{12}$$

Si $\vec{h}$ s'anulle vers l'infini, l'intégrale de la surface disparaît. La deuxième intégrale donne :

$$-\int [(\vec{h} \times \nabla) \times \vec{r}]\mathrm{d}V = 2\int \vec{h}\,dV \tag{13}$$

en sachant que

$$(\vec{h} \times \nabla) \times \vec{r} = -\vec{h}(\nabla\vec{r}) + \vec{h} = -2\vec{h}$$

Mais, $\vec{h} = \nabla \times \vec{A}$, où $\vec{A}$ est le potentiel vecteur. Donc,

$$\int \vec{h}\,dV = \int (\nabla \times \vec{A})dV = -\oint \vec{A} \times \vec{ds} \tag{14}$$

Cette intégrale s'anulle elle aussi à cause du comportement de $\vec{A}$ à l'infini, ainsi que

$$\vec{N} = 0 \tag{15}$$

Soit maintenant l'expression suivante.

$$N_{ik} = \int (x_i j_k - x_k j_i) dV \tag{16}$$

Transformons cette intégrale comme suit:

$$\int x_k j_i \, dV = \int \frac{\partial}{\partial x_2} (x_i x_k j_v) \, dV - \int x_i x_k \frac{\partial j_v}{\partial x_2} dV - \int x_i j_k \, dV \tag{17}$$

Une fois transformée en intégrale de surface, la première intégrale du second membre disparaît, étant donne que, sur la surface délimitant le fluide, la composante normale de la densité de courant est nulle, de sorte que

$$j_k ds_k = (\vec{j}\,\vec{n}) ds = 0$$

La seconde intégrale disparaît en vertu de la loi de conservation de la charge électrique $\nabla \vec{j} = 0$

Ainsi on a:

$$\int x_k j_i \, dV = - \int x_i j_k dV \tag{18}$$

et on peut recopier N_{ik} sous la forme

$$N_{ik} = 2 \int x_i j_k dV \tag{19}$$

La somme des carrés des composantes N_{ik} est égale au double du carré de la valeur absolute du vecteur $\vec{N}$

$$|\vec{N}|^2 = 2 \left[\int x_i j_k dV \right]^2 = 2 \iint x_i x'_i j_k j'_k \, dV \, dV' \tag{20}$$

Cette expression peut se mettre sous la forme:

$$|\vec{N}|^2 = - \iint (x_i - x'_i)^2 j_k j'_k \, dV \, dV' \tag{21}$$

où les intégrales contenant les carrés x_i^2 et $x_i'^2$ disparaissent, étant donné que

$$\iint x_i'^2 j_k j'_k \, dV \, dV' = \int x'_i j'_k \, dV' \int j_k \, dV$$

et $\int j_k \, dV = 0$, puisque $\int \vec{j} \, dV = \int \nabla \times \vec{h} \, dV = - \oint \vec{h} \times \vec{ds} = 0$

Le produit $j_k j'_k = \vec{j}\vec{j}'$, sous l'intégrale (21), est le produit des densités de courant en deux points de coordonnées x_k et x'_k, de distance mutuelle $r = \sqrt{(x_k - x'_k)^2}$ Prenons la moyenne de ce produit sur toutes les positions des points x_k et x'_k, pour r donné, dans le volume envisagé.

On a $\overline{\vec{j}\vec{j}'}$

En effectuant sous l'intégrale (21) une telle médiation, on obtient

$$|\vec{N}|^2 = \int f dV$$

où

$$f = -\int \overline{(\vec{j}\vec{j}')} r^2 \, dV' \tag{22}$$

L'expression sous l'intégrale décroît rapidement lorsque r croît. Le mouvement étant isotrope, la quantite $\overline{\vec{j}\vec{j}'}$ n'est fonction que de r, et si r augmente, elle décroît rapidement, puisque les densités de courant en deux points très éloignés l'un de l'autre peuvent être considérées comme étant statistiquement indépendantes.

D'autre part, la turbulence étant homogène, la quantité f est constante dans tout le volume du fluide, et on peut donc écrire

$$N^2 = fV$$

Mais nous avons montré déjà que $\vec{N} = 0$, donc il en résulte que $f = 0$, c'est à dire

$$\int \overline{(\vec{j}\vec{j}')} r^2 dV = 0$$

Ainsi nous sommes conduits à la conclusion que dans le cas envisagé, d'un mouvement turbulent isotrope, la condition $\vec{N} = 0$, équivaut à

$$\int (\vec{j}\vec{j}') r^2 \, dV = 0$$

qui peut être considéré comme un invariant de type Loytsianski.

(Manuscrit reçu le 5 mars 1979)

BIBLIOGRAPHIE

1. L. Landau, L. Lifchitz, *Mécanique des fluides*, Ed. Mir, Moscou, 1971, p. 176
2. S Chandrasekhar, Proc. Roy Soc., **204, A,** 405 (1051)
3. G K Batchelor, *The theory of homogeneous turbulence*, Cambridge, Univ Press, 1953
4. A L. Tseskis, Magn ghidrodinamica, **2,** 133 (1974)
5 M. Gutmann, *Probleme de calcul vectorial*, Ed. tehnică, Bucureşti, 1961, p 220

CONSIDERAŢII PRIVIND O LEGE DE CONSERVARE A TURBULENŢEI MAGNETOHIDRODINAMICE IZOTROPE

(Rezumat)

În lucrare se demonstrează existenţa unui nou invariant de tip Loiţeanski

STUDIA UNIV. BABEŞ-BOLYAI, PHYSICA, XXIV, 2, 1979

STUDIUL NICHELULUI ÎN ZEOLIŢI SINTETICI PRIN SPECTROSCOPIA OPTICĂ

D. STRUGARU

Introducere. Proprietăţile zeoliţilor sintetici, în deosebi cele catalitice, sînt determinate de structura lor cristalină, de natura cationilor prezenţi, de tratamentul termic şi în mod special de mărimea cîmpului electrostatic în diferitele poziţii accesibile cationilor şi moleculelor adsorbite. Rezonanţa electronică de spin şi spectroscopia optică, alături de studiile prin raze X, dau informaţii asupra poziţiilor cationice şi a interacţiunii cationilor metalici cu moleculele adsorbite.

În această lucrare sînt prezentate rezultatele obţinute cu privire la interacţiunea cationilor de nichel în zeolit X, (NiX), cu moleculele de apă adsorbită şi modificările de valenţă a nichelului prin tratarea în hidrogen, folosind spectroscopia optică.

Spectrele de absorbţie ale complecşilor metalelor de tranziţie pun în evidenţă existenţa unor benzi, care sînt situate în domeniul vizibil şi infraroşul apropiat Aceste benzi apar în urma tranziţiilor $d-d$, caracteristice metalelor tranziţionale cu orbitali d incomplet ocupaţi.

Pentru interpretarea benzilor de absorbţie este necesar să avem în vedere termenii caracteristici configuraţiei electronice ale ionului de nichel, cît şi scindarea lor în cîmpuri de diferite simetrii [2]. Cunoscîndu-se diagrama scindării termenilor, se poate postula ordinea şi energia tranziţiilor dintre nivelele energetice rezultate.

Metoda experimentală. S-au folosit probe zeolit NiX preparate după metoda indicată în [1].

Spectrele optice au fost înregistrate cu ajutorul unui spectrofotometru Carl Zeiss Jena de tip VSU-2P în domeniul spectral 320—1900 nm, în reflexie pe substanţă în stare solidă. Spectrele au fost evaluate conform ecuaţiei Schuster-Kubelka-Munk [3]

$$\frac{\chi}{\sigma} = \frac{(1 - R_\infty)^2}{2F_\infty} = F(R_\infty)$$

unde χ este coeficientul de absorbţie, σ coeficientul de împrăştiere şi R_∞, reflectanţa absolută a unei probe de grosime infinită.

Rezultate experimentale şi discuţii. În figura 1 sînt indicate spectrele de absorbţie pentru probe NiX cu diferite concentraţii de Ni^{2+}, iar în figura 2 spectrul obţinut pentru probe NiX tratate în hidrogen la 400 °C.

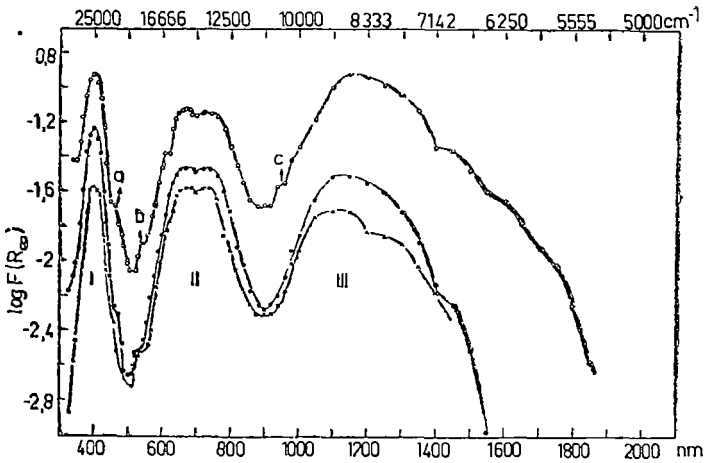

Fig. 1. Spectrul de absorbţie a zeolitului NiX hidratat
○ —32,2% Ni, ● — 27%Ni; × — 20%Ni

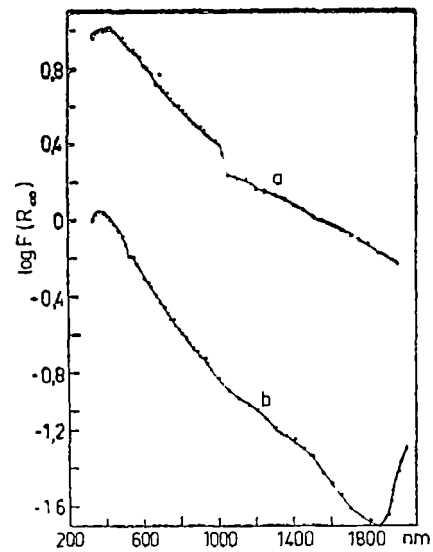

Fig 2 Spectrul de absorbţie a zeolitului NiX tratat în hidrogen la 400 °C
a — 29,3% Ni, *b* — 6,4% Ni.

În cazul probelor hidratate (fig. 1), se observă existenţa unor maxime de absorbţie a căror poziţie se modifică puţin în funcţie de concentraţia de nichel (tabelul 1).

Tabel 1

Proba	Maxime de absorbţie (cm^{-1})			Dq (cm^{-1})	B (cm^{-1})	
	ν_1	ν_2	ν_3			
NiX (20%)	9 090	14 492	25 000	909	814,8	0,78
NiX (27%)	8 888	14 285	24 813	888,8	828,9	0,79
NiX (32,2%)	8 695	13 986	24 390	869,5	819 4	0,78
$[Ni(H_2O_6)]^{2+}$	8 500	13 500	25 300	850	886,6	0,85

Ordinea şi poziţia benzilor de absorbţie datorată tranziţiilor $d-d$ deduse din diagrama nivelelor energetice ale termenului ^3F sînt:

$$^3A_{2g} \rightarrow {}^3T_{2g} \qquad (6\,500 - 11\,000)\ cm^{-1}$$

$$^3A_{2g} \rightarrow {}^3T_{1g}(F) \qquad (11\,000 - 20\,000)\ cm^{-1}$$

$$^3A_{2g} \rightarrow {}^3T_{1g}(P) \qquad (20\,000 - 28\,000)\ cm^{-1}$$

Maximele de absorbţie ale celor trei benzi sînt apropiate ca valoare cu cele găsite pentru $[Ni(H_2O)_6]^{2+}$ [4]. Astfel, putem considera că ionii de nichel în zeolitul hidratat se prezintă ca un complex octaedral, $[Ni(H_2O)_6]^{2+}$.

Tranziția la $^3T_{1g}(F)$ apare sub forma unui dublet, bine rezolvat în cazul $Dq/B \cong 1$, și poate fi consecința tranzițiilor de spin interzise

$$^3A_{2g} \rightarrow {}^1E_g \quad \text{și} \quad {}^3A_{2g} \rightarrow {}^1T_{1g}$$

Apariția acestui dublet poate fi interpretată prin interacțiunea de configurație cu nivelul $^3T_{1g}(F)$ [4] sau, după alți autori, prin termenul de cuplaj spin — orbită [5].

Umerele *a*, *b* și *c*, ar putea fi atribuite unor stări fundamentale distorsionate [5], sau unei despicări Jan-Teller a stării excitate [7].

După reducerea probelor Ni*X* în hidrogen [1], benzile de absorbție caracteristice complexului $[Ni(H_2O)_6]^2$ dispar (fig.2). Atomii metalici care apar în urma reducerii în hidrogen, cu configurația d^{10}, neavînd orbitali *d* liberi, nu prezintă complecși cu benzi de absorbție în vizibil și infraroșul apropiat, deoarece nu există posibilitata unor tranziții *d*—*d* sau a unui transfer de electroni de la ligand la metal.

Teoria cîmpului cristalin ne oferă o interpretare a spectrului Ni^{2+} în cîmp de simetrie O_h [8]. Termenii tripleți ^3F și ^3P provin de la configurația $3d^8$ a Ni^{2+} care au o energie de separare egală cu 15 *B*, sînt despicați în următoarele nivele:

$$^3A_{2g}(F)\,;\ E = -12\ Dq$$

$$^3T_{2g}(F)\,;\ E = -2\ Dq$$

$$^3T_{1g}(F)\,;\ E = +3\ Dq + \frac{15}{2}B - \frac{1}{2}\,[(15\,B - 6\,Dq)^2 + 64(Dq)^2]^{1/2}$$

$$^3T_{1g}(P)\,;\ E = 3\ Dq + \frac{15}{2}B + \frac{1}{2}\,[(15B - 6\,Dq)^2 + 64(Dq)^2]^{1/2}$$

unde *Dq* este a zecea parte din diferența de energie dintre orbitalii e_g și t_{2g}, ia *B* este parametrul Racah.

Tranzițiile de spin — permise corespund următoarelor energii:

$$^3A_{2g} \rightarrow {}^3T_{2g}(F)\,;\ \nu_1 = 10\ Dq$$

$$^3A_{2g} \rightarrow {}^3T_{1g}(F)\,;\ \nu_2 = \frac{15}{2}B + 15\,Dq - \frac{1}{2}\,[(15\,B - 6\,Dq)^2 + 64\,(Dq)^2]^{1/2}$$

$$^3A_{2g} \rightarrow {}^3T_{1g}(P)\,;\ \nu_3 = \frac{15}{2}B + 15\,Dq + \frac{1}{2}\,[(15\,B - 6\,Dq)^2 + 64\,(Dq)^2]^{1/2}$$

Folosind aceste ecuații putem obține valorile pentru *Dq* și *B*:

$$Dq = \frac{1}{10}\nu_1 \quad \text{iar} \quad B = \frac{1}{2}(\nu_2 + \nu_3 - 3\,\nu_1)$$

Valoarea parametrului Racah, *B*, obținut pentru complex este întotdeauna mai mică decît valoarea 1 041 cm^{-1} a ionului liber. Valoarea redusă este considerată a fi un indiciu asupra caracterului covalent în legătură și anume

$$\beta = \frac{B(\text{complex})}{B(\text{ion liber})}$$

Valorile obţinute din spectrele optice pentru B, Dq şi β sînt cuprinse în tabelul 1.

Rezultalele obţinute de Sendoda [9] asupra unor probe NiX (95% Ni şi 30% Ni) în funcţie de gradul de hidratare indică o modificare a maximelor de absorbţie la temperaturi cuprinse între 100—400 °C, sugerînd existenţa unei distorsiuni de la simetria octaedrică, sensibil dependentă de numărul de molecule de apă sau grupuri hidroxil. Valoarea obţinută pentru β de 0,30 (95% Ni) respectiv 0,47 (30% Ni) pentru probe evacuate la 500 °C, indică o vecinătate a cationilor de nichel diferită decît la probe evacuate la temperaturi mai joase, iar legăturile $Ni - O$ sînt mult mai covalente decît la complexul $[Ni(H_2O)^{2+}$. Prin scăderea gradului de hidratare o parte a cationilor de nichel migrează din poziţiile S_2 în poziţiile S_1 din prismele hexagonale. În acest caz ionii de nichel sînt complet coordinaţi la scheletul de aluminosilicat şi sînt localizaţi în coordinare hexagonală planară [10]. Această concluzie este sprijinită de spectrele RES obţinute pentru NiX [1], deoarece numai probele încălzite peste 400 °C furnizează semnal RES. Pentru ionii de nichel fixaţi pe locurile S_2 trebuie considerat un cîmp cristalin de simetrie mai joasă deoarece aceşti ioni sînt RES inactivi

Concluzii. Cationii Ni^{2+} în zeolit X hidratat formează complecşi octaedrali, $[Ni(H_2O)_6]^{2+}$. Energia stărilor Ni^{2+} sînt interpretate considerînd un cîmp de simetrie O_h.

Apare o distorsionare a cîmpului octaedric în funcţie de gradul de hidratare, sensibil dependentă de numărul de molecule de apă sau grupuri hidroxil.

Legăturile Ni — 0 sînt mult mai covalente decît legăturile în complexul $[Ni(H_2O)_6]^{2+}$.

Prin tratarea zeolitului NiX în hidrogen apare o reducere a Ni^{2+} la nichel atomic.

(Intrat în redacţie la 9 martie 1979)

BIBLIOGRAFIE

1. D. Strugaru, Al Nicula, Studia Univ Babeş-Bolyai, Physica, 1, 56 (1977)
2. A. B P. Lever, Inorganic Electronic Spectroscopy, New-York, 1968
3. P. Kubelka, J Opt Soc Ann, 38, 448 (1948)
4. C. K Jorgensen, Acta Chem. Scand., **9**, 1362 (1955).
5. A D Lieher, C J Ballhausen, Ann Phys, **6**, 134 (1959)
6. C. Furlani, G. Morpurgo, Z Physic, Chem (Frankfurt), **28**, 93 (1961).
7. H. A Weakleim, D S McClure, J. Appl Phys Suppl, **33**, 347 (1962)
8. L. Sacconi, in *Transition Metal Chemistry* (R L. Carlin, Ed), vol. 4, p 199, Dekker, New-York, 1968
9. Y. Sendoda, Y. Ono, T Keii, J. Catal., 357 (1975)
10. K. Klier, M. Ralek, J. Phys Chem Solid, **29**, 945 (1968).

fila 109

THE OPTICAL SPECTROSCOPY STUDY OF NICKEL IN X-ZEOLITE

(Summary)

Optical spectra of Ni^{2+} in syntetic zeolite X, have been recorded and interpreted. In hydrated zeolite Ni cations are in octahedral complexes $[Ni(H_2O)_6]^{2+}$ Upon dehydration, the coordination environment of Ni changes from the octahedral complex into a planar one After the hydrogen treatment, the transition from ionic state to metallic state appears.

STUDIA UNIV BABEŞ-BOLYAI, PHYSICA, XXIV, 2, 1979.

HYPERFINE SPLITTING OF THE g ~ 4,3 LINE IN A TeO_2—PbO·Mn^{2+} GLASS

AL. NICULA, M. PETEANU, I. ARDELEAN

It was reported in the literature [1] the possibility of obtaining vitreous compounds having as basic component the tellurium dioxide, TeO_2

Consequently we experimented the chances of preparing some TeO_2+ PbO glasses. The most suitable composition turned out to be $95TeO_2$ + 5PbO, which gave a stable matrix, having the specific properties of the vitreous state. We impurify then this matrix with paramagnetic transitional elements ions, in order to obtain glasses suitable for electron spin resonance (ESR) measurements. Being sensitive to the symmetry and the strength of bonds involving the impurity ion in the host diamagnetic matrix, the ESR spectra offer interesting information about the microstructure of the vicinity of these paramagnetic ions

Therefore, we prepared glasses having the composition xMnO (1—x) [$95TeO_2$ + 5PbO] for x = 0 5, 1, 3, 5; 10; 15, 20 mol %, by melting the oxide mixtures at 1200 °C and quenching them upon an inox steel plate, from the homogenizing temperature, to the room temperature The ESR spectra were recorded at room temperature and liquid nitrogen temperature, by using the JES—3B spectrometer, at X band.

Essentially, the spectra consist in an absorption signal centered at g~ 4.3 and another one having g ~ 2 (fig la) At small impurity ions concentrations, C_{Mn} = 0.5, 1, the first signal prevails in the spectra, much more intense than the second, and having the hyperfine structure (hfs) characteristic to Mn^{55}(I = 5/2) distinctly resolved. We point out the fact that it was not reported till now the hfs resolution on the g ~ 4 3 signal in oxidic glasses As C_{Mn} increases in the sample, the signal 1 hfs resolves more and more weakly, the signal 2 intensity increases, and after a certain limit of concentration, C_{Mn} = 10, 15, 20, this overlaps the signal 1 If initially the signal 2 was strongly assymetric, at high C_{Mn} it tends to symmetrise (fig 1b). Not even at small C_{Mn} values, the signal 2 did not show any hfs.

The measurements at liquid nitrogen temperature did not change the structure of the spectra. One observed only the signals intensity increasing and a best resolution of these (fig 1b)

Accidental impurifying of one of the oxidic components with Fe^{3+} ions, introduced the signals 1' in the spectra (fig. 1)

The characteristics of the ESR signals for the studied samples, are tabelated in Table 1.

As it is known [2, 3] the signal having g ~ 4 3 result from Mn^{2+} ions incorporated in the glass matrix, involved in strong bonds with the network forming ions, which give rise to a strong crystal field Theoretically, one obtains values of 4.3 for the isotropic *g* factor, considering the paramagnetic ion in an axially distorted cubic neighbourhood [4], or considering the rhombic crystal field [5]

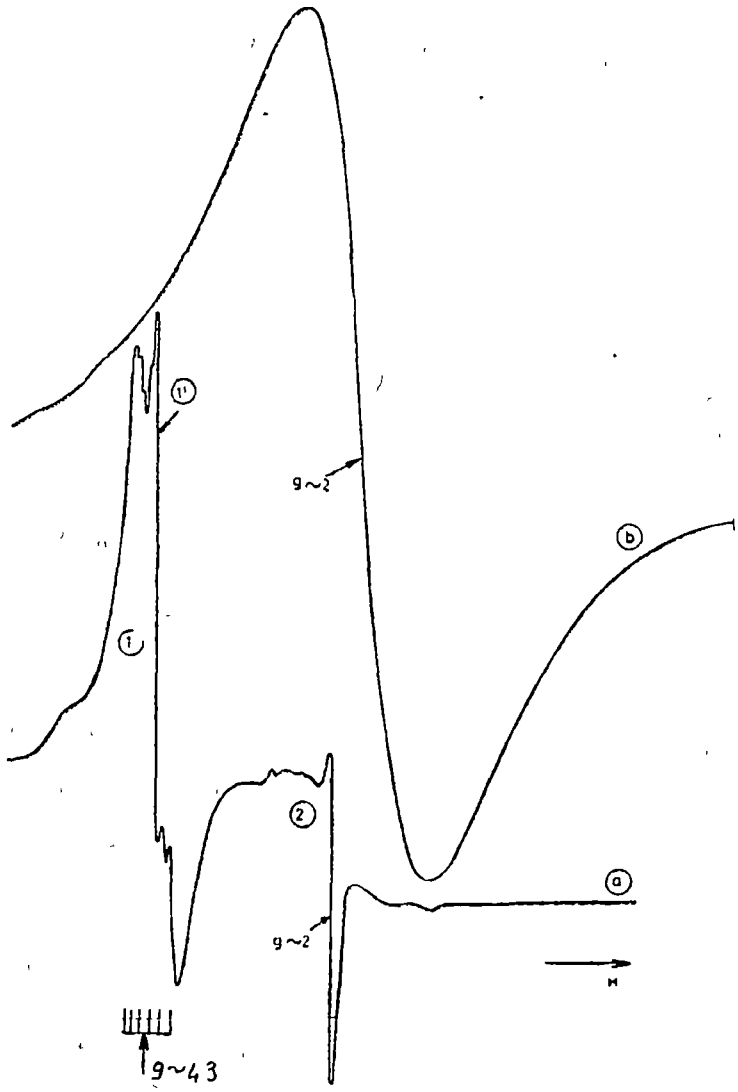

Fig. 1 The ESR spectra of the $95TeO_2 5PbO$ glasses for various MnO content a) 0·5 mol % MnO, b) 20 mol % MnO.

making option for one symmetry or the other, according to the studied vitreous matrix.

The hfs resolution for the g ~ 4.3 signal confirms the strong bonds, having a pronounced covalent character, for the Mn^{2+} ions with the nighbours from the first coordination sphere, as it has been certified by the ESR investigations on chalcogenide glasses [6]. The sextet width invariability as concentration

Table 1

Sample	I_1 (arb units)	I_2 (arb units)	ΔH_1 (gauss)	ΔH_2 (gauss)	g_1	g_2
0.5 Mn	3.78	1.35	491.2	85 95	4 3084	2 1295
1 Mn	7.56	1.43	497.3	98 24	4.2049	2 1385
3 Mn	6.56	8 56	504.7	1068.36	4.1549	2.0750
5 Mn	4.33	22 33	566.6	1069.58	4.1685	2.0792
10 Mn	54.25		1154 3		2.0792	
15 Mn	98.0		1295.5		2.0585	
20 Mn	169 0		1240·3		2.0585	

changes, indicates a high stability of the paramagnetic ion vicinity symmetry, in our glasses. The clearly resolved hfs denotes a sufficiently regular configuration. The hfs resolution degree dependence on the Mn^{2+} ions content, results as effect of the isolated components width dependence on the dipol. — dipol interaction. Being conditioned by isotropic dipolar interactions, the hfs components width is unique, but the g values dispersion results in the separation between these components increasing, as the magnetic field increases on the spectra. Consequently there are variety of Mn^{2+} ions subjected to crystal fields varying from one ion to another, because of the fluctuations in the second coordination sphere, typical for the impurity ions in the glass network.

The g ~ 2 signals, non having any hfs even at small Mn^{2+} concentration, may be attributed to formations involving more than one Mn^{2+} ion, randomly distributed in the glass matrix. At C_{Mn} rising, the Mn^{2+} ions number entering homogeneously in the network decreases, becoming preferable the above-mentioned groups formation, fact which is atested by the relative intensity decreasing of the g ~ 4.3 signal, and the signal 2 intensity increasing. The ESR signals symmetrisation at high C_{Mn} values, confirms the high degree of disorganisation of the matrix, as result of the excessive doping.

For the hfs calculation, at the g ~ 4.3 line, we start from the fact that this line corresponds to the transitions inside the Kramers doublets of the Mn^{2+} ion, subjected to strong crystal field, having the wave functions [7]:

$$\psi_{\pm} = \frac{1}{\sqrt{1+\alpha^2}} [| \pm 5/2 > + \alpha | \pm 3/2>], \quad \alpha = -\sqrt{5}/3. \tag{1}$$

For the hfs calculation it is not essential to specify the strong crystal field symmetry which gives rise to this doublet (axially distorted cubic crystal field, or rhombic field). It is important only the fact that in both cases the wave functions of the doublet have the expression (1) and therefore, it results a 4.3 isotropic g factor, independently of the magnetic field H_0 orientation, with respect to the Mn^{2+} center axis. Consequently, we may quantify the S = 5/2 spin of the ion along the H_0 direction.

We shall consider isotropic the hyperfine interaction operator $\mathcal{H}_{hfs} = A.I.S.$ between the spin S and the nuclear spin $I = 5/2$ of Mn^{55}. For obtaining the nonequidistant hfs sextet observed, it is sufficient to consider the

second order hyperfine interaction. The splitting for the doublet level (1), is [8]:

$$E_{\pm}^{m} = \mp g\beta H_0 \pm \frac{1}{4} gAm \pm \frac{gA^2}{16\beta H_0}(I^2 + I - m^2 \mp m) \tag{2}$$

where $g = 4.3$, and the H_0 indicate the center of the sextet.

The hfs transitions resolved for $\Delta m = 0$, will rise at values of the magnetic field, given by:

$$H_m = H_0 - \frac{A^2}{8\beta^2 H_0} I(I+1) - \frac{A}{2\beta} m + \left(\frac{A}{2\beta}\right)^2 \frac{m^2}{2H_0}. \tag{3}$$

Because in the investigated glasses the separation between adiacent components of the hfs increases as the magnetic field increases on the spectrum, it results from (3), that $A < 0$.

The nonequidistancy degree can be evaluated by using the ratio [9]:

$$k_0 = \frac{1}{\Delta H_{\text{aver}}} \left| \Delta H_{3/2}^{5/2} - \Delta H_{-5/2}^{-3/2} \right|. \tag{4}$$

where the splitting ΔH_{m-1}^{m} is determined from (3), while

$$H_{\text{aver}} = \frac{1}{5} \sum_{m} \Delta H_{m-1}^{m}$$

It results from (3) the separation $\Delta H_{1/2}^{1/2} = A/2\,\beta$, therefore A can be approximated by measuring the separation between the central lines of the sextet. From the recorded spectra we obtained $A/2\beta = 79.115$ gauss. Evaluating the separations between the hfs components and comparing them to the values estimated on the spectrum we obtain (Table 2) a suficient satisfactory agreement, in the limit of errors.

Table 2

ΔH_{exp}	71 25	75.18	79.115	83.04	87.96
ΔH_{teor}	70 757	74.936		83 294	87 473

The nonequidistancy degree, k_0, calculated from the ΔH_{m-1}^{m}, values experimentally estimated, has the value 0.163. A 16% nonequidistancy for the hfs components, agrees very well with the reported data [8].

The second order hyperfine interaction explains well enough the hyperfine structure of the $g \sim 4.3$ signals.

(Received March 10, 1979)

REFERENCES

1. G. Sperlich, P. Urban, Phys. Stat. Sol. (b), **61**, 475 (1974)
2. T. Castner, G. S Newell, W. C. Holton, C. P. Slichter, J Chem Phys, **32**, 668 (1960).
3. D. L. Griscom, R. E. Griscom, J. Chem Phys, **47**, 2711 (1967).
4 De Wijn, Van Balderen, J Chem. Phys., **46**, 1381 (1967)
5. D. Loveridge, S. Parke, Phys Chem. Glasses, **12**, 19 (1971)
6. I. V. Chepeleva, E. A. Zhilinskaia, V. N Lazukin, Phys Stat Sol. (b), **82**, 189 (1977).
7. Al. Nicula, M. Peteanu, Studia Univ Babeş-Bolyai, Phys, p 42 (1976).
8 Al Nicula, I Ursu, S Nistor, Rev. Roum. Phys, **10**, 229 (1965)
9. V. N Lazukin, I V Chepeleva, DAN SSSR, **214**, (4), 787 (1974)

DESPICAREA HIPERFINĂ A SEMNALULUI g ~ 4,3 ÎNTR-O STICLĂ TeO_2—PbO Mn^{2+}

(Rezumat)

Lucrarea reprezintă un studiu efectuat asupra sticlelor TeO_2—PbO dopate controlat cu ioni Mn^{2+}, prin metoda RES

Despicarea hiperfină a semnalelor avînd g~4,3 poate fi interpretată considerînd interacţiuni hiperfine în ordinul doi al teoriei perturbaţiilor.

STUDIA UNIV BABEŞ-BOLYAI, PHYSICA, XXIV, 2, 1979

LA DÉPENDANCE DU COEFFICIENT SEEBECK DU RUTILE DE LA PRESSION DU GAZ AMBIANT

VALER CRISTEA et VICTOR BABEŞ*

I. **Introduction.** Le rutile (TiO_2), ainsi que les autres oxydes des métaux de transition, comme par exemple CeO_2, Nb_2O_5, Ta_2O_5 etc. peuvent présenter des propriétés semiconductrices, soit de type p (par oxydation), soit de type n (par réduction), résultant de leur non-stoechiométrie.

Les semiconducteurs de type n, tels nos échantillons, sont ainsi caractérisés par un déficit global d'oxygène, qui entraîne l'existence de défauts dans le réseau comme les lacunes anionique ou les cations interstitiels, en faisant abstraction de la possibilité qu'il y existent aussi des cations hétérovalents, présents ou introduits en qualité d'impurétés dans le réseau du semiconducteur, lesquels peuvent augmenter ou diminuer la concentration des électrons de conduction [1].

Toujours dans le cas du rutile, on a obtenu un très grand nombre de résultats expérimentaux concernant la nature des défauts, mais qui sont loin d'être concordants. Pami les techniques expérimentales, la plus souvent utilisée est l'étude de la conductivité électrique, relativement facile à réaliser. En essayant d'imposer l'un des deux mécanismes responsables de la conductivité (lacunes d'oxygène ou ions de Ti interstitiels), Herrmann et ses collaborateurs [1] [2] discutent la loi de variation de la conductivité électrique σ avec la pression partielle de l'oxygène P_{O_2}, en équilibre avec le solide

$$\sigma = k \cdot P_{O_2}^{-1/a} \tag{1}$$

la valeur du paramètre a étant liée à la nature des défauts. Des informations supplémentaires sont obtenues en étudiant la dépendance du coefficient Seebeck (coefficient de p. t. é.) de la pression partielle d'oxygène [3]. Aux hautes températures (environ 1 000 °C), Baumard et Tani [4] [5] trouvent une bonne concordance des résultats des mesures du coefficient Seebeck et de la conductivité électrique pour le rutile pur ou dopé avec du Nb et montrent que l'utilisation du modèle classique des défauts ponctuels permet une bonne approximation dans l'étude quantitative des propriétés de transport, pour de faibles écarts à la stoechiométrie.

II. **Le dispositif expérimental.** Dans cet article les auteurs présentent leurs premiers résultats concernant l'étude de la dépendance du coefficient Seebeck de la pression, autour de 300 K, pour divers milieux gazeux (air, azote, argon), comme suite des recherches précédentes portant sur le mécanisme de conduction du rutile réduit ou dopé avec du Nb [6] [7].

On a mesuré la tension Seebeck sur un échantillon monocristallin de rutile avec 0,005% Nb, ayant la géométrie rectangulaire, à l'aide de la méthode et du cryostat déjà utilisés dans les travaux précédents [8] [9]. L'installation a du

* L'institut Polytechnique de Cluj-Napoca.

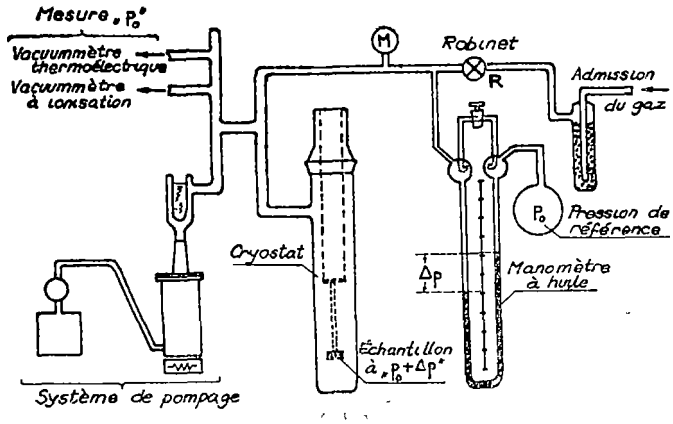

Fig. 1. Schéma de principe de l'installation de mesure.

être completée avec une partie de réglage et de mesure de la pression, dont le principe est illustré dans la figure 1.

Le réglage de l'admission du gaz se fait avec le robinet R. Pour la mesure de la pression dans l'installation,on choisit une pression de référence p_0 (obtenue avec les pompes de vacuum), qu'on mesure soit avec le manomètre à ionisation ($\sim 10^{-4}$ mm Hg), soit avec le manomètre à thermocouple ($\sim 10^{-3} \div \sim 10^{-2}$ mm Hg), et par rapport à laquelle on détermine le dénivellement Δp produit dans le manomètre à huile par le gaz admis. On couvre ainsi un domaine de pression jusqu'à environ 20 mm Hg. Pour des pressions plus grandes, allant jusqu'à la pression atmosphérique, on utilise le manomètre métallique M (fig. 1) en montage de vacuummètre. On note enfin que l'admission du gaz se fait lentement, afin de ne pas troubler l'équilibre thermique de l'échantillon.

La mesure de la tension Seebeck est réalisée avec un microvoltmètre électronique TR—1452, vérifié par comparaison avec un compensateur de classe 0,015.

La mesure et le réglage des températures des extrémités froide et chaude de l'échantillon ont été décrits dans les articles précédents [8] [9].

III. **Résultats expérimentaux.** La variation du coefficient Seebeck fonction de la pression (variable de $\sim 10^{-2}$ à $\sim 7 \cdot 10^2$ mm Hg), à la température moyenne d'environ 310 K, pour un gradient moyen de 25 K, est présentée dans la figure 2, le gaz admis étant successivement l'air, l'azote et l'argon.

Dans tous les cas présentés en fig. 2, on peut observer que la variation maximale du coefficient Seebeck apparaît pour des pressions allant de 0,1 à 80 mm Hg, et représente une augmentation d'environ 25—35% par rapport à la valeur mesurée en vide, fonction du gaz ambiant.

IV. **Discussions et conclusions.** Les valeurs du coefficient Seebeck à la pression normale (atmosphérique), α_n, sont toujours plus grandes que celles correspondant aux pressions réduites (vide), α_v, permettant ainsi d'expliquer la variation ci-dessus par le changement de la concentration des porteurs de charge, fonction de la pression du gaz ambiant. Le gaz adsorbé forme des liai-

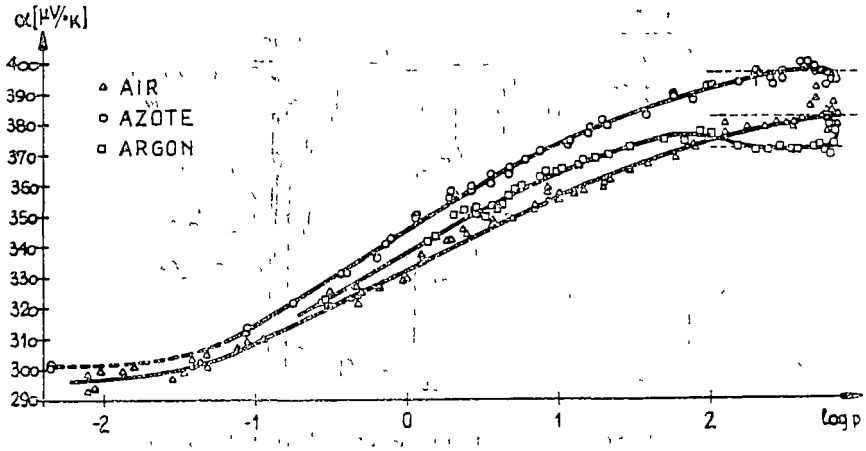

Fig 2 La variation du coefficient Seebeck fonction de la pression

sons de chémosorption, avec capture d'électrons du volume de l'échantillon. Par la suite, la concentration des électrons libres se réduit et la tension thermoélectrique augmente quand la pression du gaz devient plus grande.

Cette observation doit nous permettre d'évaluer la variation de la concentration d'électrons à partir de la variation du coefficient Seebeck fonction de la pression du gaz. Vu que, pour cet échantillon, nous avons trouvé antérieurement [7] la valabilité de la formule de Pisarenko

$$\alpha = \frac{k}{e}\left[(r+2) + \ln\frac{N_c}{n}\right] \tag{2}$$

où le paramètre r est déterminé par le mécanisme de „scattering" des électrons, N_c représente la densité effective d'états et n est la concentration des électrons libres.

En supposant que N_c est constant, on déduit à partir de (2)

$$\alpha_n - \alpha_v = \frac{k}{e}\ln\frac{n_v}{n_n} \tag{3}$$

d'où on obtient le rapport des concentrations d'électrons en vide, n_v, respectivement à la pression normale, n_n,

$$\frac{n_v}{n_n} = \exp\left(\frac{\alpha_n - \alpha_v}{k} \cdot e\right) \tag{4}$$

Connaissant la valeur de n_v, obtenue par mesures d'effet Hall [10], $n_v = 6 \cdot 10^{18}$ cm^{-3}, on peut calculer immédiatement la valeur n_n correspondant au milieu gazeux.

Toujours dans le cas de l'hypothèse de N_c constant, on peut calculer le déplacement ΔW_F du niveau Fermi produit par l'interaction de l'échantillon

avec le gaz ambiant, à partir de la relation

$$n = N_c \exp \frac{W_F}{kT} \tag{5}$$

d'où

$$\Delta W_F = k\,T \ln \frac{n_v}{n_n} \tag{6}$$

Les valeurs ainsi calculées, pour la température $T = 310$ K, sont groupées dans le tableau 1. Les mesures à basse pression pour le cas de l'argon n'étant pas complètes, le tableau 1 ne comprend pas les valeurs correspondant à ce cas.

Tableau 1

Valeurs de n_n, n_v/n_n et ΔW_F en air et en azote

Gaz ambiant	n_v/n_n	n_n[cm^{-3}]	ΔW_F[eV]
Air	2,72	$2{,}21 \cdot 10^{18}$	$7{,}26 \cdot 10^{-2}$
Azote	3,05	$1{,}96 \cdot 10^{18}$	$8{,}15 \cdot 10^{-2}$

On note que les valeurs de ΔW_F comprises dans le tableau ci-dessus, completées avec la valeur de W_{Fv}, correspondant au vide pour l'échantillon 1 de l'article [6], sont en accord qualitatif avec la valeur obtenue en air, à la pression normale, pour le même échantillon 1 [7].

Le grand nombre d'états de surface, apparus comme suite de la chémosorption du gaz, peut être motivé partiellement par la faible épaisseur de l'échantillon et le grade réduit d'usinage de la surface (polissage mécanique). À part ça, la variation du coefficient Seebeck, fonction de la nature et de la pression du gaz ambiant, peut être influencée par le changement du potentiel d'extraction des électrons et, par la suite, la modification de la hauteur de la barrière de potentiel aux contacts [11]. Le sens observé de la variation est en accord qualitatif avec les résultats obtenus par Baumard [4] pour les échantillons de rutile impurifiés avec du Nb, dans le domaine des hautes températures.

(Manuscrit reçu le 10 mars 1979)

BIBLIOGRAPHIE

1. J. M Herrmann, Journal de Chimie Physique, **73**, 5, 474 (1976)
2. J. M. Herrmann, P. Montgolfier, P. Vergnon, Journal de Chimie Physique, **73**, 5, 479 (1976).
3. P Godè, J P. Pelegrin, J J. Oehlig, C R Acad Sci Paris, **C 281**, 171 (1975).
4. J F Baumard, E. Tani, The Journal of Chemical Physics, **67**, 3, 857 (1977)
5. J. F. Baumard, E Tani, Phys. Stat. Sol. (a), **39**, 373 (1977).
6. V. Cristea, V. Babeş, Phys Stat. Sol. (a), **45**, 617 (1978).

7. V. Cristea, Rev. Roum. Phys., 23, 6, 587 (1978).
8. V. Cristea, Studia Univ. Babeş-Bolyai, Phys., 2, 45 (1973).
9. V. Babeş, V. Cristea, Bul. Şt. Inst. Polit. Cluj-Napoca, 20 (in print).
10. N. P. Bogoroditski, V. Cristea, Ya. I. Panova, Fiz. Tverd. Tela, 9, 253 (1967).
11. V. I. Liachenko, *Elektronnie iavlenia na poverhnosti poluprovodnikov*, Izd. Naukova Dumka Kiev 1968, p. 100.

DEPENDENŢA COEFICIENTULUI SEEBECK AL RUTILULUI DE PRESIUNEA GAZULUI AMBIANT

(Rezumat)

Lucrarea cuprinde studiul dependenţei coeficientului Seebeck de presiunea gazului ambiant (aer, azot, argon) în limitele 0,01 — 740 mm col. Hg, pentru o probă monocristalină de rutil impurificat cu 0,005% Nb. Este descrisă sumar instalaţia experimentală şi metodica măsurării. Datele experimentale sînt interpretate în aproximaţia gazului electronic nedegenerat. Creşterea coeficientului Seebeck cu 25 — 35% la admisia gazului în instalaţie este pusă pe seama chemisorbţiei ce are loc la suprafaţa probei şi a variaţiei potenţialului de contact Se evaluează variaţia concentraţiei purtătorilor liberi şi deplasarea nivelului Fermi.

STUDIA UNIV BABEŞ-BOLYAI, PHYSICA, XXIV, 2, 1979

EFECTUL SOLVENTULUI ASUPRA SPECTRULUI ELECTRONIC AL NAFTALINELOR MONOSUBSTITUITE (I)

IRIMIE MILEA

Efectul solventului asupra modificărilor care apar în spectrul unei substanţe solvate prezintă importanţă deoarece o parte din analizele spectrofotometrice curente se fac la astfel de soluţii binare. În general, poziţia bandelor de absorbţie şi fluorescenţă se modifică în funcţie de solvent. Explicarea teoretică a acestui fenomen a fost încercată în multe studii [1], [2], [3] în care se ţine cont de teoria polarizării dielectricilor lichizi a lui Onsager [4] şi de teoria asupra solvenţilor polari a lui Ooshika, [5] care consideră influenţa dipolilor permanenţi existenţi în solvent asupra moleculelor solvate. Formulele deduse pentru deplasarea frecvenţelor sînt complexe dar cercetările experimentale arată că în spectrele de absorbţie [6] şi emisie [7] într-o bună aproximaţie pentru solvenţi şi molecule nepolare acestea sînt egale cu

$$\Delta\nu = \frac{e^2M^2}{a^3hc} \cdot \frac{n^2-1}{2n^2+1} = 10{,}71 \times 10^9 \frac{f}{\nu a^3} \cdot \frac{n^2-1}{2n^2+1}$$

unde: $\Delta\nu$ — mărimea deplasării bathocromice exprimată în numere de undă; ν — numărul de undă pentru maximul de absorbţie; f — puterea oscilatorului în banda de absorbţie; M — mărimea momentului de dipol al tranziţiei electronice respective; n — indicele de refracţie al solventului în regiunea de absorbţie studiată, a — raza în Å a cavităţii presupusă sferică în care se găseşte molecula solvată; e — sarcina electronică [8].

În prezenta lucrare am urmărit verificarea dependenţei aproximativ liniare a deplasării bandei intense de absorbţie care apare la naftalinele monosubstituite în regiunea din jurul valorii de 31 000 cm^1 de funcţia $\frac{n^2-1}{2n^2+1}$, în şase solvenţi la temperatura camerei. Spectrele au fost efectuate cu un spectrofotometru UV VIS, Zeiss-Jena. Concentraţia de $8 \cdot 10^{-3}$ Mol. şi grosimea cuvei de 1 cm, au permis punerea în evidenţă a tranziţiei de absorbţie amintită. S-a lucrat la scara de extensie maximă, iar precizia determinărilor poziţiei bandei a fost de ± 25 cm^{-1}. Indicii de refracţie ai solvenţilor în regiunea de la 31 000 cm^{-1} s-au obţinut prin extrapolare din curba de dispersie. Substanţele, α şi β fluor, clor, brom şi metil naftaline au fost purificate prin distilare repetată în vid, respectiv prin recristalizări repetate, iar solvenţii pentan, hexan, heptan, ciclohexan, metilciclohexan şi decalină prin metodele cunoscute de purificare a hidrocarburilor aromatice [9].

Din figura care ilustrează rezultatele experimentale obţinute se observă că în general, în limitele preciziei determinărilor, există o dependenţă liniară a poziţiei bandei de absorbţie de funcţia $f\left(\frac{n^2-1}{2n^2+1}\right)$. Unele abateri mai mari ~ 50 cm^{-1} se datoresc şi lărgimii bandei, ceea ce a făcut dificilă poziţionarea. Din figura 1 se poate observa şi că pe măsură ce greutatea moleculară a mole-

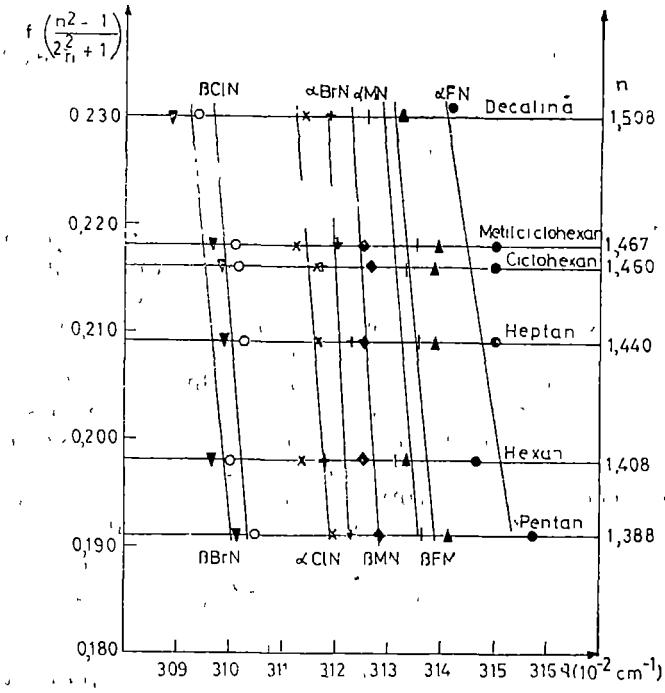

Fig. 1.

culei solvate creşte deplasarea bandei de absorbţie spre lungimi de undă lungi odată cu creşterea lui n devine mai constantă. Din înclinarea dreptelor caracteristice se poate de asemenea observa că pentru moleculele studiate raportul $\frac{f}{\nu a^3}$ rămîne aproximativ constant. Deci interacţiunea cu solvenţii respectivi este în mare măsură aceeaşi pentru moleculele de naftalină monosubstituite.

(Intrat în redacţie la 13 martie 1979)

BIBLIOGRAFIE

1. E. G. Mc Rae, J. Phys. Chem., **61**, 562 (1957).
2. N. G. Bahsiev, Opt. i. spectr., **7**, 52 (1959).
3. N. G. Bahsiev, Opt. i. spectr., **10**, 717 (1961)
4. L. Onsager, J. Amer. Chem. Soc., **58**, 1485 (1936).
5. Y. Ooshika, J. Phys. Soc. Japan, **9**, 594 (1954).
6. O. V. Sverdlova, Opt. i spectr., **6**, 349 (1959).
7. C. Mihul, V. Pop şi M. Haba, Studii de cercet. ştiinţ. Fizică şi şt. tehnice, Acad. R. P. R. Iaşi, **2**, 175 (1960)
8. N. S. Bayliss, J. Chem. Phys., **18**, 292 (1950).
9. L. Gattermann, *Die Praxis Des Organischen Chemikers*, Walter de Gruyter, Berlin und Leipzig, 1936.

STUDIA UNIV. BABEŞ-BOLYAI, PHYSICA, XXIV, 2, 1979

NOTE

EPR OF CHROMIUM IN B_2O_3—Li_2O—Al_2O_3—Cr_2O_3 GLASSES

LAVINIA COCIU, LUMINIŢA TRIF, AL. NICULA

Introduction. Electron paramagnetic resonance spectra of chromium have been investigated in various glasses [1]. Landry, Fournier and Young [3] have studied the EPR spectra of Cr^{3+} in a phosphate glass as a function of Cr_2O_3 concentration up to 8,65 wt% Cr_2O_3 and found two paramagnetic species: isolated, octahedrally coordinated Cr^{3+} and antiferomagnetically coupled pairs of Cr^{3+}

We have investigated EPR spectra of chromium in lithiumborate glasses with $1 \div 10$ mole $\%Cr_2O_3$.

Experimental. The glasses were prepared by supercooling after firing of appropriate mixture of H_3BO_3, Li_2CO_3, γ-phase Al_2O_3 and Cr_2O_3 for 1 hour at 1250 °C in corundum crucibles. The composition of some of the investigated samples are listed in table 1.

Table 1

B_2O_3	Li_2O	Al_2O	Cr_2O_3	$\Delta H^* \pm 6$ gauss
79	15	5	1	
70	24	5	1	
70	20	5	5	1010
70	15	5	10	1140
59	35	5	1	351
55	35	5	5	390
50	35	5	10	516

* Linewidth of the broad resonance

The EPR spectra were recorded using 9 GHz spectrometers (JES—3B and ART—6) at the room temperature.

Results. The EPR spectra of chromium are pronounced dependent on the composition of the glasses. Figure 1 shows the EPR spectra of the samples with up to 24 mol % concentration of Li_2O, and figure 2 shows the EPR spectra of the samples containing 35 mol % Li_2O, for the same concentration of Cr_2O_3.

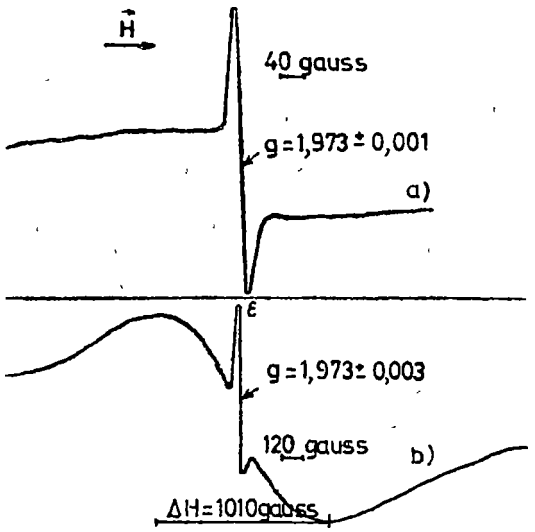

Fig. 1 Electronic paramagnetic spectra for glasses of composition
a) 70 mol % B_2O_3 24 mol % $LiO_2$5 mol % Al_2O_3 1 mol Cr_2O_3
b) 70 mol % B_2O_3 20 mol % Li_2O_3 5 mol% Al_2O_3 5 mol % Cr_2O_3

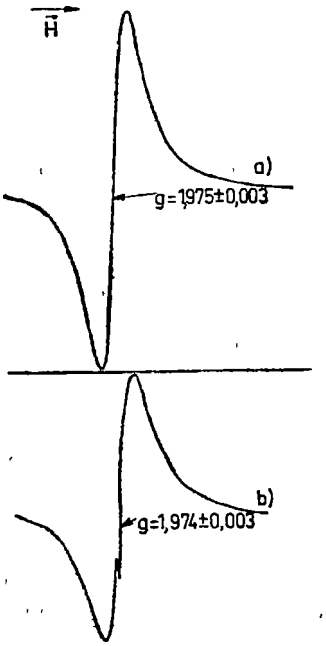

Fig. 2 Electronic paramagnetic resonance spectra for glasses of composition.
a) 59 mol % B_2O_3 35 mol % Li_2O 5 mol % Al_2O_3 1 mol % Cr_2O_3
b) 55 mol % B_2O_3 35 mol % Li_2O 5 mol % Al_2O_3 5 mol % Cr_2O_3

Let g_{eff} be defined through the relationship $h\nu = g_{eff}\ \beta H$ where H is the magnetic field strength at which the absorption line lies. The line width, ΔH, is measured between the extrema of the first derivative line.

The spectrum la consists of a resonance with a g_{eff} value of 1.971 $\pm$ 0,001 and $\Delta H = 32 \pm 2$ gauss.

The sample with a higher content (5 mol% or 10 mol %) of Cr_2O_3 exhibits EPR spectra with two resonances: a broad line ($\Delta H = 1010$ gauss) and a narrow signal, with $g = 1 \cdot 973 \pm 0.003$ and $\Delta H = 25 \pm 6$ gauss, denoted ε in the figure 2 b.

In the EPR spectra of the high alkali glasses (35 mol % Li_2O), the ε line is not well resolved (Fig. 2) and the broad line is more narrow relative to that of the samples with a lower Li_2O concentration, for the same Cr_2O_3 content.

Discussion. The change in aspect of the spin resonance spectrum with the composition of the investigated glasses, implies the presence of two paramagnetic centers in samples.

The broad, symmetric signal is given by isolated Cr^{3+} ions. Because of the large concentration of Cr_2O_3 in glasses, the Cr^{3+} spectrum does not exhi-

bit resolved structure which enables us to draw conclusions about the local symmetries.

The narrow signal, ε, may be attributed [1, 2] to Cr^{5+} ions. It is well resolved for the samples with up to 25 mol % Li_2O, that means in such glasses the 5-valence state is more probable than in higher alkali content glasses which give a poor ε signal.

The exchange interaction between Cr^{3+} ions might be the reason for the narrowing of the Cr^{3+} line. It has been shown [3] by Landry, Fournier and Young that when isotropic exchange interaction, JS_1S_2, is larger than the Zeeman term, a single ERS line at $g = 2.0$, appears in the spectum of phosphate glasses. No such a line was detected in spectrum of the borrate glasses investigated by us.

(Received March 30, 1979)

REFERENCES

1. J. Wong and C. A. Angell, Appl. Spectroscopy Revs., 4, (2), 155 – 232 (1971).
2. J. Bohandy, J. of Solid State Chemistry, 3, 467 – 472 (1971).
3. R. Y. Landry, J. T. Fournier and C. G. Young, J. Chem. Phys., 46, 4. 1285 (1967).

RPE A CROMULUI ÎN SISTEMUL STICLOS $B_2O_3-Li_2O-Al_2O_3-Cr_2O_3$

(Rezumat)

S-au studiat spectrele de rezonanță paramagnetică electronică a cromului în sticle cu bor urmărindu-se dependența lor de compoziția probelor. S-a pus în evidență existența a două tipuri de centri paramagnetici asociați ionilor Cr^{3+} și Cr^{5+}.

RECENZII

T. Mayer – Kuckuk, **Atomphysik** Editura Teubner, Stuttgart, 1977, 233 pagini, 112 figuri.

Cartea este o introducere în fizica atomică şi se adresează studenţilor dornici să se ocupe cu fizica cuantică Autorul a scris deja în anul 1970 volumul de fizică nucleară Fiind elevul lui W Bothe, desigur i-a fost mai aproape de preocupările sale ştiinţifice să prezinte întîi nucleul atomic Acest lucru se oglindeşte şi în volumul de fizică atomică mai ales prin faptul că aranjarea capitolelor s-a făcut după ordinea crescîndă a gradelor de libertate ale sistemelor tratate, prin prezentarea structurii în pături electronice

Cartea se împarte în zece capitole cu două anexe Autorul introduce noţiunile în mod obişnuit pentru ca să înlesnească cititorului consultarea altor cărţi. După capitolul introductiv despre concepţiile de bază în fizica atomică în cap 2 se prezintă ecuaţia lui Schrödinger În cap 3 se analizează atomul de hidrogen cu discuţia funcţiilor de undă Capitolul patru tratează spinul şi momentul magnetic al dipolului în cîmp magnetic În cap. 5 se reîntoarce la atomul de hidrogen cu discuţia structurii fine, structurii hiperfine şi a efectelor din electrodinamica cuantică, În capitolul 6 se descrie emisia fotonilor, regulile de selecţie, efectul Zeeman şi emisia stimulată Capitolul 7 se ocupă de proprietăţile sistemelor cu particule identice Relativ scurt se prezintă în cap 8 atomii cu mai mulţi electroni evitîndu-se tratarea unor amănunte din spectroscopia optică În cap 9 se prezintă interacţiunea dintre învelişul electronic cu cîmpurile electrice şi magnetice Ultimul capitol este consacrat surselor de radiaţii coerente şi necoerente

Cartea recenzată ţine cont de interesul reînviat pentru fizica atomică, mai ales pentru cei ce folosesc rezultatele fizicii atomice în electronica cuantică, geofizică, fizica plasmei, protecţia mediului, astrofizică, biofizică şi din acest motiv incontestabil s-a redactat oarecum modern

Se poate discuta în ce măsură prezentarea mecanicii cuantice aşa de detaliat la început este utilă. Este adevărat că din fizica atomică s-a desprins mecanica cuantică şi aceste două discipline se pot despărţi greu, dar pentru înţelegerea multor fenomene, legi din fizica atomică nu este nevoie de rezolvarea unor ecuaţii din mecanica cuantică

Experienţele sînt descrise ţinînd cont de înţelegerea esenţei, deci sînt fără detalii, excepţie făcînd doar experienţa lui Millikan. Cartea este în mare parte mai teoretică. Cele două anexe atestă de asemenea acest fapt Anexa 1 se ocupă cu numere complexe, iar anexa 2, cu compararea diferitelor reprezentări din mecanica cuantică

Cartea este utilă mai ales pentru cei care vor să studieze bazele teoretice ale fizicii atomice. Autorul foloseşte în mare parte sistemul de unităţi SI, dar atrage atenţie că cei care nu cunosc unităţile mai vechi vor avea greutăţi în orientarea în literatura de specialitate Pentru învingerea acestor greutăţi este prezentat la începutul volumului un tabel cu transformarea unităţilor în alte sisteme

FRANCISC KOCH

În cel de al XXIV-lea an (1979) *Studia Universitatis Babeş-Bolyai* apare semestrial în specialităţile :

matematică

fizică

chimie

geologie-geografie

biologie

filozofie

ştiinţe economice

ştiinţe juridice

istorie

filologie

На XXIV году издания (1979) *Studia Universitatis Babeş-Bolyai* выходит два раза в год со следующими специальностями:

математика

физика

химия

геология-география

биология

философия

экономические науки

юридические науки

история

филология

Dans sa XXIV-e année (1979) *Studia Universitatis Babeş-Bolyai* parait semestriellement dans les spécialités :

mathématiques

physique

chimie

géologie-géographie

biologie

philosophie

sciences économiques

sciences juridiques

historie

philologie

743 904

Abonamentele se fac la oficiile poştale, prin factorii poştali şi prin difuzorii de presă, iar pentru străinătate prin ILEXIM Departamentul export—import presă, P. O. Box 136—137, telex 11226, Bucureşti, str. 13 Decembrie nr. 3.

Lei 10